

CAP ROCK INTEGRITY IN CO₂ STORAGE

A THESIS SUBMITTED TO
THE GRADUATE SCHOOL OF NATURAL AND APPLIED SCIENCES
OF
MIDDLE EAST TECHNICAL UNIVERSITY

BY

CHANTSALMAA DALKHAA

IN PARTIAL FULFILLMENT OF THE REQUIREMENTS
FOR
THE DEGREE OF DOCTOR OF PHILOSOPHY
IN
PETROLEUM AND NATURAL GAS ENGINEERING

AUGUST 2010

Approval of the thesis:

CAP ROCK INTEGRITY IN CO₂ STORAGE

submitted by **CHANTSALMAA DALKHAA** in partial fulfillment of the requirements for the degree of **Doctor of Philosophy in Petroleum and Natural Gas Engineering Department, Middle East Technical University** by,

Prof. Dr. Canan Özgen
Dean, Graduate School of **Natural and Applied Sciences**

Prof. Dr. Mahmut Parlaktuna
Head of Department, **Petroleum and Natural Gas Engineering**

Prof. Dr. Ender Okandan
Supervisor, **Petroleum and Natural Gas Engineering Dept., METU**

Examining Committee Members:

Prof. Dr. Nurkan Karahanoglu
Geological Engineering Dept., METU

Prof. Dr. Ender Okandan
Petroleum and Natural Gas Engineering Dept., METU

Prof. Dr. Mahmut Parlaktuna
Petroleum and Natural Gas Engineering Dept., METU

Prof. Dr. Nilgun Gulec
Geological Engineering Dept., METU

Prof. Dr. Halim Mutlu
Geological Engineering Dept., OGU

Date: 11/08/2010

I hereby declare that all information in this document has been obtained and presented in accordance with academic rules and ethical conduct. I also declare that, as required by these rules and conduct, I have fully cited and referenced all material and results that are not original to this work.

Name, Last name : Chantsalmaa DALKHAA

Signature :

ABSTRACT

CAP ROCK INTEGRITY IN CO₂ STORAGE

Dalkhaa, Chantsalmaa

Ph.D., Department of Petroleum and Natural Gas Engineering

Supervisor: Prof. Dr. Ender Okandan

August 2010, 163 pages

One way to reduce the amount of CO₂ in the atmosphere for the mitigation of climate change is to capture the CO₂ and inject it into geological formations. The most important public concern about carbon capture and storage (CCS) is whether stored CO₂ will leak into groundwater sources and finally into the atmosphere.

To prevent the leakage, the possible leakage paths and the mechanisms triggering the paths must be examined and identified. It is known that the leakage paths can be due to CO₂ - rock interaction and CO₂ – well interaction.

The objective of this research is to identify the geochemical reactions of the dissolved CO₂ in the synthetic formation water with the rock minerals of the Sayindere cap rock by laboratory experiments. It is also aimed to model and simulate the experiments using ToughReact software. Sayindere formation is the cap rock of the Caylarbasi, a southeastern petroleum field in Turkey.

The mineralogical investigation and fluid chemistry analysis of the experiments show that calcite was dissolved from the cap rock core as a result of CO₂- water- rock interaction.

Using the reactive transport code TOUGHREACT, the modeling of the dynamic experiment is performed. Calcite, the main primary mineral in the Sayindere is dissolved first and then re-precipitated during the simulation process. The decreases of 0.01 % in the porosity and 0.03% in permeability of the packed core of the Sayindere cap rock are observed in the simulation.

The simulation was continued for 25 years without CO₂ injection. However, the results of this simulation show that the porosity and permeability are increased by 0.001 % and 0.004 %, respectively due to the CO₂-water-rock mineral interaction. This shows that the Sayindere cap rock integrity must be monitored in the field if application is planned.

Keywords: CO₂ storage, cap rock integrity, CO₂- water- rock interaction, geochemical modeling and simulation

ÖZ

CO₂ DEPOLAMADA ÖRTÜ KAYAÇ BÜTÜNLÜĞÜ

Dalkhaa, Chantsalmaa

Ph.D., Petrol ve Doğal Gaz Mühendisliği Bölümü

Tez Yöneticisi: Prof. Dr. Ender Okandan

Ağustos 2010, 163 sayfa

İklim değişikliğinin önemli faktörlerinden biri olan, atmosferdeki CO₂ miktarını azaltmanın yollarından biri, CO₂'i tutmak ve jeolojik formasyonlara enjekte etmektir. Karbonu tutma ve depolama ile ilgili olarak en önemli husus, yüksek konsantrasyondaki CO₂'nin teklikeli olması nedeniyle, depolanan CO₂'nin geri atmosfere ve yer altı su kaynaklarına karışıp karışmayacağıdır.

Bu kaybı önlemek için, olası kaçak çıkışları ve bunu tetikleyen mekanizmalar belirlenmeli ve çalışılmalıdır. Kaçakların nedeninin, CO₂- kayaç etkileşimi ve CO₂-kuyu çimentosu etkileşimi olduğu bilinmektedir.

Bu çalışmada, CO₂ depolama sırasında, Sayındere formasyonunda gerçekleşebilecek çözünme ve çökme reaksiyonlarının belirlenmesi için deneysel bir çalışma yürütülmüştür. Ayrıca, ToughReact yazılımı kullanılarak, yapılan deneyin modellenmesi amaçlanmıştır. Sayındere formasyonu Türkiye'nin güneydoğusunda yer alan Çaylarbaşı petrol sahasının örtü kayacıdır.

İnce kesit, elektron taramalı mikroskop analizleri ile ve sıvı analizleri sonuçları , CO₂-örtü kayaç- su etkileşimi sonucunda örtü kayaçta bol miktarda bulunan kalsitin çözüldüğünü göstermektedir.

TOUGHREACT kodu kullanılarak dinamik deneyin simülasyonu yapılmıştır. Simülasyon sonucunda, Sayındere formasyonun ana minerali olan kalsit önce suda çözülmüş ve daha sonra geri çökelme oluştuğu görülmektedir. Simülasyonda örtü kayaçtaki gözenekte % 0.01 ve geçirgenlikte % 0.03 düşüş görülmüştür.

CO₂ ile doymuş su basıldıktan sonra, 25 yıl içinde Sayındere örtü kayaç mineral değişikliğinin simülasyonu da yapılmıştır. Ancak, bu simülasyon sonucunda, gözenek ve geçirgenlikte 0.001 % ve 0.004 % artış göstermektedir ki bu da eğer sahada CO₂ depolanması planlanacak ise, Sayındere örtü kayaç bütünlüğü takip edilmelidir.

Anahtar kelimesi: CO₂ depolama, örtü kayaç bütünlüğü, , CO₂- kayaç- su etkileşimi, jeokimyasal modellemesi ve simülasyonu.

To my beloved ones...

ACKNOWLEDGMENTS

This dissertation would not have been possible without the support from mentors, friends, family, the Department of Petroleum and Natural Gas Engineering and Petroleum Research Laboratory, METU.

Firstly and foremost, I would like to express my deepest and sincere thankfulness to my thesis supervisor Prof. Dr. Ender Okandan not only for her guidance, advice, criticism, encouragement, support and precious insight throughout the research but also her unforgettable and valuable contributions to my career. She was beyond being the advisor and professor for these years.

I also thank Prof. Dr. Mahmut Parlaktuna, the chairperson of Department of Petroleum and Natural Gas Engineering, for his endless support and valuable advice. Also, my special thanks go to my thesis committee members for their valuable suggestions and comments.

As well as, the humorous approaches and lively support of my dear friends are gratefully acknowledged. I am so lucky to have your friendship, understanding, support and love. Especially, I wish to say “thank you very much” to my dear friend, Sevtac Bulbul for her endless support, encouragement and love.

Naci Dođru is also deeply acknowledged for constructing and helping during the experimental set-up. Can Polat also deserves special thanks for helping me with the software PETRASIM.

Turkish Petroleum Corporation is greatly appreciated for providing the cores from Sayındere formation and water analysis of the Caylarbasi field.

The staffs of the Water laboratory of Petroleum Research Center and Plasma Laboratory of Central Laboratory of METU are appreciated for their analysis and support.

I wish to thank the Departments of Geological Engineering and Metallurgical Engineering for the mineralogical analyses.

I would like to thank The Scientific and Technological Research Council of Turkey for awarding me the PhD Fellowship for Foreign Citizens during my doctoral study.

At last, but not the least, I would like to thank my family for their never ending support, trust, love and encouragement.

TABLE OF CONTENTS

ABSTRACT	iv
ÖZ	vi
ACKNOWLEDGMENTS	ix
TABLE OF CONTENTS.....	xi
LIST OF FIGURES	xiv
LIST OF TABLES.....	xx
CHAPTERS	
1. INTRODUCTION	1
1.1 What is global warming and climate change?	1
1.2 CO ₂ Emission.....	2
1.3 Carbon Capture and Storage.....	5
1.3.1 CO ₂ Capture	6
1.3.2 CO ₂ Storage	7
1.3.3 CO ₂ Storage Sites	8
1.4. CO ₂ Trapping Mechanisms	11
1.5 Safety of Carbon Storage	11
2. LITERATURE SURVEY	13
2.1 CO ₂ - Water Interaction.....	13
2.2 CO ₂ -Water-Rock Interaction	16
2.3 Laboratory investigations on CO ₂ -brine-rock interaction.....	17
2.4 Numerical modeling of CO ₂ - rock interaction.....	20
3. STATEMENT OF THE PROBLEM.....	23
4. MATERIALS FOR THE EXPERIMENTS.....	24
4.1 Fluid Chemistry of Sayındere Formation.....	25
4.2 Mineral Investigation of Sayındere Formation.....	27

4.2.1 Thin Section Analysis of Sayindere Cores	27
5. EXPERIMENTAL INVESTIGATION	29
5.1 Static Experiment	29
5.1.1 Static experimental set-up.....	29
5.1.2 Static experiment procedure	32
5.1.3 Results and Discussion of the Static Experiment.....	36
5.2 Dynamic Experiment	45
5.2.1 Carbonate Removal	45
5.2.2 Clay type determination by XRD Analysis	46
5.2.3 Mineral Composition of Sayindere core.....	47
5.2.4 Dynamic Experimental set-up.....	48
5.2.5 Dynamic Experimental procedure.....	53
5.2.6 Results and Discussion of the Dynamic Experiment	57
6. NUMERICAL MODELING OF CO ₂ -FLUID-ROCK INTERACTION	59
6.1 Reactive transport code TOUGHREACT	60
6.2 PETRASIM	62
7. REACTIVE TRANSPORT MODELING OF THE DYNAMIC EXPERIMENT ...	63
7.1 Geometric model and the cap rock properties	63
7.2 Formation mineralogy	65
7.3 Formation water of Sayindere cap rock	68
7.4 CO ₂ Injection into the Sayindere packed core.....	69
7.4.1 CO ₂ Injection simulation scenario.....	69
7.4.2 CO ₂ Injection simulation results and discussion.....	70
7.4.3 CO ₂ Injection stop and investigating the CO ₂ -saturated water- cap rock mineral interaction in longer time period, 25 years	73
8. RESULTS AND DISCUSSION.....	75
9. CONCLUSION	79
REFERENCE	82
APPENDICES	
A. ALKALINITY MEASUREMENT	86

B. THIN SECTION ANALYSIS PHOTOS	89
C. PHOTOS OF THE STATIC EXPERIMENT.....	93
D. SEM/EDX ANALYSIS RESULTS OF THE 30 DAY-STATIC EXPERIMENT.	96
E. SEM PHOTOS OF THE 30 DAY-STATIC EXPERIMENT.....	101
F. SEM/EDX ANALYSIS RESULTS OF THE 100 DAY-STATIC EXPERIMENT	104
G. SEM PHOTOS OF THE 100 DAY-STATIC EXPERIMENT	113
H. XRD ANALYSIS RESULTS (DYNAMIC EXPERIMENT).....	118
I. DETERMINATION OF THE POROSITY AND PERMEABILITY.....	124
J. KINETICS OF MINERAL DISSOLUTION AND PRECIPITATION.....	126
K. RESULTS OF THE CO ₂ EQUILIBRATION WITH THE FORMATION WATER	128
L. RESULTS OF THE SIMULATION OF THE DYNAMIC EXPERIMENT	136
M. FORMULAS FOR POROSITY AND PERMEABILITY CALCULATIONS IN SIMULATION	148
N. RESULTS OF THE SIMULATION OF 25 YEARS WITHOUT CO ₂ INJECTION	149
CURRICULUM VITAE.....	161

LIST OF FIGURES

Figure 1. 1 World Map of CO ₂ Emissions (IEAGHG, 2002)	3
Figure 1. 2 Main CO ₂ emission sites in Turkey (TUBITAK KAMAG, 2009)	4
Figure 1. 3 CO ₂ Capture Processes.....	7
Figure 2. 1 Speciation of the dissolved CO ₂ as a function of pH, in a 1 M NaCl solution at 60° C (closed system) (Lagneau et al., 2005).....	14
Figure 2. 2 Speciation of the dissolved CO ₂ as a function of pH, in a 1 M NaCl solution at 60 °C (open system) (Lagneau et al., 2005).....	15
Figure 2. 3 Solubility of CO ₂ in pure water: influence of the pressure and temperature (Duan and Sun, 2002)	15
Figure 2. 4 Solubility of CO ₂ at 60 c: influence of the pressure and salinity (Duan and Sun, 2002)	16
Figure 4. 1 Cores taken from Sayindere cap rock	27
Figure 5. 1 The schematic diagram of the experimental set-up.	30
Figure 5. 2 Pressure and Temperature recordings of the static experiment.....	35
Figure 5. 3 Schematic representation of the SEM analysis.....	36
Figure 5. 4 The scheme of the dynamic experiment.....	49
Figure 5. 5 CO ₂ solubility (Dodds et al, 1956).....	54
Figure 5. 6 Pressure stabilization during dissolution of CO ₂ in the brine	55
Figure 5. 7 Pressure and temperature recordings of the dynamic experiment	56
Figure 7. 1 Schematic representation of the model	64
Figure 7. 2 Z-X cross section of the grid system.....	70
Figure B. 1 Calcite grains	89
Figure B. 2 Calcite veins.....	89
Figure B. 3 Fossils	90
Figure B. 4 Glauconite.....	90
Figure B. 5 Laminations.....	91

Figure B. 6 Hematite.....	91
Figure B. 7 Quartz	92
Figure C. 1 Mixing cylinder and core holders inside the oven	93
Figure C. 2 Side view of experimental set-up.....	94
Figure C. 3 Whole part of the experimental set-up	95
Figure D. 1 In-Depth SEM/EDX Micrograph (inner part)-after the 30 day-experiment	96
Figure D. 2 In-Depth SEM/EDX Micrograph (near to surface_1) -after the 30 day- experiment.....	97
Figure D. 3 In-Depth SEM/EDX Micrograph (near to surface_2) -after the 30 day- experiment.....	97
Figure D. 4 In-Depth SEM/EDX Micrograph (near to surface_3) -after the 30 day- experiment.....	98
Figure D. 5 In-Depth SEM/EDX Micrograph (near to surface_1) -prior to the 30 day- experiment.....	98
Figure D. 6 In-Depth SEM/EDX Micrograph (inner part)-prior to the 30 day-experiment	99
Figure D. 7 Top Surface SEM/EDX Micrograph_1-after the 30 day-experiment	99
Figure D. 8 Top Surface SEM/EDX Micrograph_2-after the 30 day-experiment	100
Figure D. 9 Top Surface SEM/EDX Micrograph_1-prior to the 30 day-experiment....	100
Figure E. 1 Near to surface view of in depth SEM Analysis -prior to the 30 day- experiment.....	101
Figure E. 2 Inner view of in depth SEM Analysis -prior to the 30 day-experiment	101
Figure E. 3 Near to surface view of in depth SEM Analysis_1- after the 30 day- experiment.....	102
Figure E. 4 Near to surface view of in depth SEM Analysis_2- after the 30 day- experiment.....	102
Figure E. 5 Top surface SEM Analysis_1- after the 30 day-experiment.....	103
Figure E. 6 Top surface SEM Analysis_2- after the 30 day-experiment.....	103

Figure F. 1 In -Depth SEM/EDX Micrograph (inner part)-prior to the 100 day- experiment.....	104
Figure F. 2 In-Depth SEM/EDX Micrograph (near to surface_1) –prior to the 100 day- experiment.....	105
Figure F. 3 In-Depth SEM/EDX Micrograph (near to surface_2) –prior to the 100 day- experiment.....	105
Figure F. 4 Top Surface SEM/EDX Micrograph_1-prior to the 100 day-experiment ..	106
Figure F. 5 Top Surface SEM/EDX Micrograph_2-prior to the 100 day-experiment ..	106
Figure F. 6 Top Surface SEM/EDX Micrograph_3-prior to the 100 day-experiment ..	107
Figure F. 7 Top Surface SEM/EDX Micrograph_4-prior to the 100 day-experiment ..	107
Figure F. 8 In-Depth SEM/EDX Micrograph (near to surface_1) –after the 100 day- experiment.....	108
Figure F. 9 In-Depth SEM/EDX Micrograph (near to surface_2) –after the 100 day- experiment.....	108
Figure F. 10 In-Depth SEM/EDX Micrograph (near to surface_3) –after the 100 day- experiment.....	109
Figure F. 11 In-Depth SEM/EDX Micrograph (near to surface_4) –after the 100 day- experiment.....	110
Figure F. 12 In-Depth SEM/EDX Micrograph (near to surface_5) –after the 100 day- experiment.....	110
Figure F. 13 In -Depth SEM/EDX Micrograph (inner part)-after to the 100 day- experiment.....	111
Figure F. 14 Top Surface SEM/EDX Micrograph_1-after the 100 day-experiment.....	111
Figure F. 15 Top Surface SEM/EDX Micrograph_2-after the e100 day-xperiment.....	112
Figure F. 16 Top Surface SEM/EDX Micrograph_3-after the 100 day-experiment.....	112
Figure G. 1 Near to surface view of in depth SEM Analysis -prior to the 100 day- experiment.....	113
Figure G. 2 Inner view of in depth SEM Analysis -prior to the 100 day-experiment...	113
Figure G. 3 Top surface SEM Analysis -prior the 100 day-experiment.....	114

Figure G. 4 Near to surface view of in depth SEM Analysis _1-after the 100 day-experiment.....	114
Figure G. 5 Near to surface view of in depth SEM Analysis_2-1 after the 100 day-experiment.....	115
Figure G. 6 Near to surface view of in depth SEM Analysis_3- after the 100 day-experiment.....	115
Figure G. 7 Near to surface view of in depth SEM Analysis-4-after the 100 day-experiment.....	116
Figure G. 8 Top Surface SEM Analysis_1- after the 100 day-experiment.....	116
Figure G. 9 Top Surface SEM Analysis_2- after the 100 day-experiment (wormholes)	117
Figure H. 1 XRD Analysis of the original grinded core.....	118
Figure H. 2 XRD Analysis after the acid treatment	119
Figure H. 3 Analysis of the sample waited in ethylene glycol.....	120
Figure H. 4 Analysis of the air dried sample	121
Figure H. 5 Analysis of the sample dried at 300 °C	122
Figure H. 6 XRD Analysis of the sample dried at 550 °C.....	123
Figure L. 1 Time evolution of pressure during the 99 day-simulation.....	136
Figure L. 2 Time evolution of pH during the 99 day-simulation.....	136
Figure L. 3 Time evolution of AlO_2^- during the 99 day-simulation.....	137
Figure L. 4 Time evolution of Ca^{+2} during the 99 day-simulation.....	137
Figure L. 5 Time evolution of Cl^- during the 99 day-simulation	138
Figure L. 6 Time evolution of Fe^{+2} during the 99 day-simulation	138
Figure L. 7 Time evolution of H^+ during the 99 day-simulation.....	139
Figure L. 8 Time evolution of H_2O during the 99 day-simulation.....	139
Figure L. 9 Time evolution of HCO_3^- during the 99 day-simulation	140
Figure L. 10 Time evolution of Mg^{+2} during the 99 day-simulation.....	140
Figure L. 11 Time evolution of Na^+ during the 99 day-simulation	141
Figure L. 12 Time evolution of $\text{O}_2(\text{aq})$ during the 99 day-simulation.....	141
Figure L. 13 Time evolution of $\text{SiO}_2(\text{aq})$ during the 99 day-simulation	142

Figure L. 14 Time evolution of SO_4^{-2} during the 99 day-simulation	142
Figure L. 15 Variation in volume fraction of calcite during the 99 day-simulation	143
Figure L. 16 Variation in volume fraction of hematite during the 99 day-simulation ..	143
Figure L. 17 Variation in volume fraction of kaolinite during the 99 day-simulation ..	144
Figure L. 18 Variation in volume fraction of magnesite during the 99 day-simulation	144
Figure L. 19 Variation in volume fraction of quartz during the 99 day-simulation	145
Figure L. 20 Variation in volume fraction of siderite during the 99 day-simulation	145
Figure L. 21 Variation in volume fraction of dolomite during the 99 day-simulation ..	146
Figure L. 22 Time evolution of porosity during the 99 day-simulation	146
Figure L. 23 Time evolution of permeability during the 99 day-simulation	147
Figure N. 1 Time evolution of pressure during the 25 year-simulation	149
Figure N. 2 Time evolution of pH during the 25 year-simulation	150
Figure N. 3 Time evolution of AlO_2^- during the 25 year-simulation	150
Figure N. 4 Time evolution of Ca^{+2} during the 25 year-simulation	151
Figure N. 5 Time evolution of Cl during the 25 year-simulation.....	151
Figure N. 6 Time evolution of Fe^{+2} during the 25 year-simulation.....	152
Figure N. 7 Time evolution of H^+ during the 25 year-simulation	152
Figure N. 8 Time evolution of H_2O during the 25 year-simulation	153
Figure N. 9 Time evolution of HCO_3^- during the 25 year-simulation	153
Figure N. 10 Time evolution of Mg^{+2} during the 25 year-simulation	154
Figure N. 11 Time evolution of Na^+ during the 25 year-simulation	154
Figure N. 12 Time evolution of $\text{O}_2(\text{aq})$ during the 25 year-simulation	155
Figure N. 13 Time evolution of $\text{SiO}_2(\text{aq})$ during the 25 year-simulation	155
Figure N. 14 Time evolution of SO_4^{-2} during the 25 year-simulation	156
Figure N. 15 Variation in volume fraction of calcite during the 25 year-simulation	156
Figure N. 16 Variation in volume fraction of hematite during the 25 year-simulation.	157
Figure N. 17 Variation in volume fraction of kaolinite during the 25 year-simulation.	157
Figure N. 18 Variation in volume fraction of magnesite during the 25 year-simulation	158
Figure N. 19 Variation in volume fraction of quartz during the 25 year-simulation	158

Figure N. 20 Variation in volume fraction of siderite during the 25 year-simulation...	159
Figure N. 21 Variation in volume fraction of dolomite during the 25 year-simulation	159
Figure N. 22 Time evolution of porosity during the 25 year-simulation.....	160
Figure N. 23 Time evolution of permeability during the 25 year-simulation.....	160

LIST OF TABLES

Table 4. 1 Reservoir formation water analysis from Caylarbasi-1 (TPAO)	25
Table 4. 2 Analysis of the synthetic formation water	26
Table 5. 1 Technical specification of experimental apparatus.....	31
Table 5. 2 Core holder dimension	31
Table 5. 3 Mixing cylinder dimension.....	31
Table 5. 4 In-depth SEM Analysis of Core #5 (Inner part)	37
Table 5. 5 In depth SEM Analysis of Core #5 (Near to Surface).....	38
Table 5. 6 Top Surface SEM Analysis of Core #5	39
Table 5. 7 Water Analysis of the 30 day experiment	40
Table 5. 8 In-depth SEM Analysis of Core #4 (Inner part)	41
Table 5. 9 In depth SEM Analysis of Core #4 (Near to Surface).....	42
Table 5. 10 Top Surface SEM Analysis of Core #5	42
Table 5. 11 Water Analysis of the 100 day experiment.....	43
Table 5. 12 Comparison of water analyses of 30- and 100- day experiments	44
Table 5. 13 Mineral composition of Sayindere cap rock.....	47
Table 5. 14 Technical specifications of the dynamic experimental equipments.....	50
Table 5. 15 Core holder dimension	50
Table 5. 16 Mixing cylinder dimension.....	50
Table 5. 17 Fluid Analysis of the Discharged Water	57
Table D. 1 In-Depth SEM element analysis (inner part) -after the 30 day-experiment ...	96
Table D. 2 In-Depth SEM element analysis (near to surface_1) -after the 30 day- experiment.....	97
Table D. 3 In-Depth SEM element analysis (near to surface_2) -after the 30 day- experiment.....	97

Table D. 4 In-Depth SEM element analysis (near to surface_3) -after the 30 day-experiment.....	98
Table D. 5 In-Depth SEM element analysis (near to surface_1) -prior to the 30 day-experiment.....	98
Table D. 6 In-Depth SEM element analysis (inner part) -prior to the 30 day-experiment	99
Table D. 7 Top Surface SEM element analysis_1-after the 30 day-experiment.....	99
Table D. 8 Top Surface SEM element analysis_2-after the 30 day-experiment.....	100
Table D. 9 Top Surface SEM element analysis_1-prior to the 30 day-experiment	100
Table F. 1 In-Depth SEM element analysis (inner part) –prior to the 100 day-experiment	104
Table F. 2 In-Depth SEM element analysis (near to surface_1) - prior to the 100 day-experiment.....	105
Table F. 3 In-Depth SEM element analysis (near to surface_2) - prior to the 100 day-experiment.....	105
Table F. 4 Top Surface SEM element analysis_1-prior to the 100 day-experiment	106
Table F. 5 Top Surface SEM element analysis_2-prior to the 100 day-experiment	106
Table F. 6 Top Surface SEM element analysis_3-prior to the 100 day-experiment	107
Table F. 7 Top Surface SEM element analysis_4-prior to the 100 day-experiment	107
Table F. 8 In-Depth SEM element analysis (near to surface_1) - after the 100 day-experiment.....	108
Table F. 9 In-Depth SEM element analysis (near to surface_2) - after the 100 day-experiment.....	109
Table F. 10 In-Depth SEM element analysis (near to surface_3) - after the 100 day-experiment.....	109
Table F. 11 In-Depth SEM element analysis (near to surface_4) - after the 100 day-experiment.....	110
Table F. 12 In-Depth SEM element analysis (near to surface_5) - after the 100 day-experiment.....	110

Table F. 13 In -Depth SEM element analysis (inner part)-after to the 100 day- experiment.....	111
Table F. 14 Top Surface SEM element analysis_1-after the 100 day-experiment.....	111
Table F. 15 Top Surface SEM element analysis_2-after the 100 day-experiment.....	112
Table F. 16 Top Surface SEM element analysis_3-after the 100 day-experiment.....	112
Table I. 1 Porosity calculation.....	124
Table I. 2 Recordings of the experiment with the packed core of L=5.5 cm, D=2.54 .	125

CHAPTER 1

INTRODUCTION

1.1 What is global warming and climate change?

The greenhouse effect is a natural phenomenon. Most of the solar radiation hitting the earth is reflected from the surface and the atmosphere and then lost into the space. However, the greenhouse gases in the atmosphere catch and then quickly emit back the heat radiation. When too many greenhouse gases are collected, they trap the heat in the atmosphere, not letting them escape into the space. This causes an increase in the average temperature of the world. This process is called the global warming. The global warming can change the climate, resulting in warmer and warmer temperatures, an increased number of floods, hurricanes, droughts, storms and thus, it will have huge adverse impacts on human and the ecological system.

CO₂ is the main greenhouse gas emitted into the atmosphere, causing the global warming. The CO₂ sources responsible for its increased emission are thermal power generation, refineries, cement plants, petrochemical plants and growing large industrial complexes.

1.2 CO₂ Emission

Over the past several decades worldwide the burning fossil fuels has lead to a substantial rise in CO₂ emission. These increased CO₂ are the cause of warmer temperature, increased rainfall and raising sea level.

A global database of large stationary point sources of CO₂ emissions has been developed by IEAGHG (International Energy Agency Greenhouse Gas). The database was developed and published in 2002. Since 2002, IEAGHG has progressively improved the emission source data by updating the information contained in the database. The database contains longitude and latitude information for the main emission sites which allows it to be used to produce a geographical map of the emission sources. Figure 1.1 shows the world map of emissions produced by using the CO₂ Emission Database (IEAGHG). As seen from Figure 1.1, the places of most emission sites are in the regions where the developed countries, especially the North American countries and European countries are located. Figure 1.2 gives the industrial CO₂ emission sites in Turkey from data collected for the TUBITAK KAMAG project (TUBITAK KAMAG, 2009).

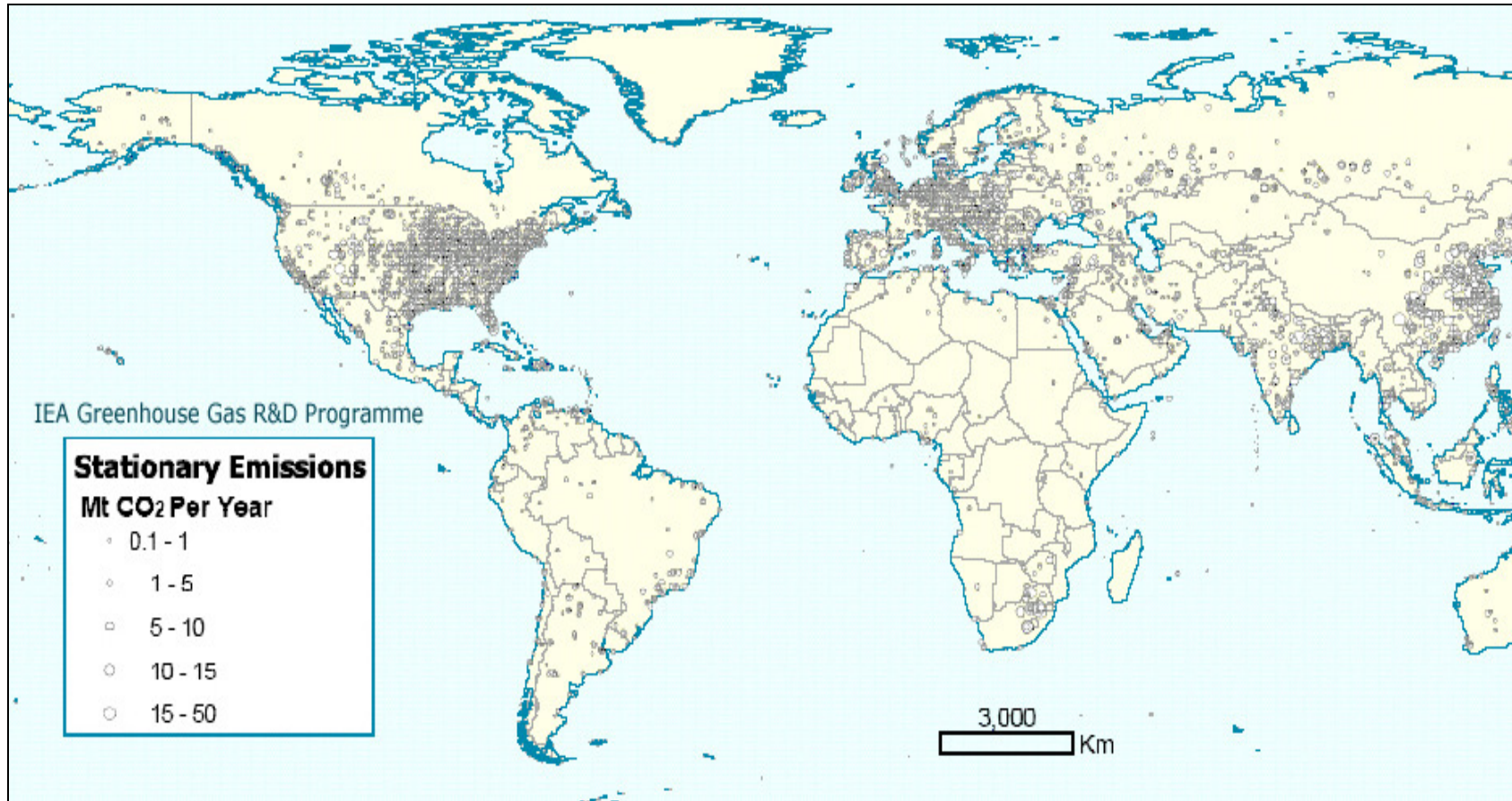


Figure 1. 1 World Map of CO₂ Emissions (IEAGHG, 2002)

Power Plants, Refineries and Sugar, Cement and Steel Factories in Turkey

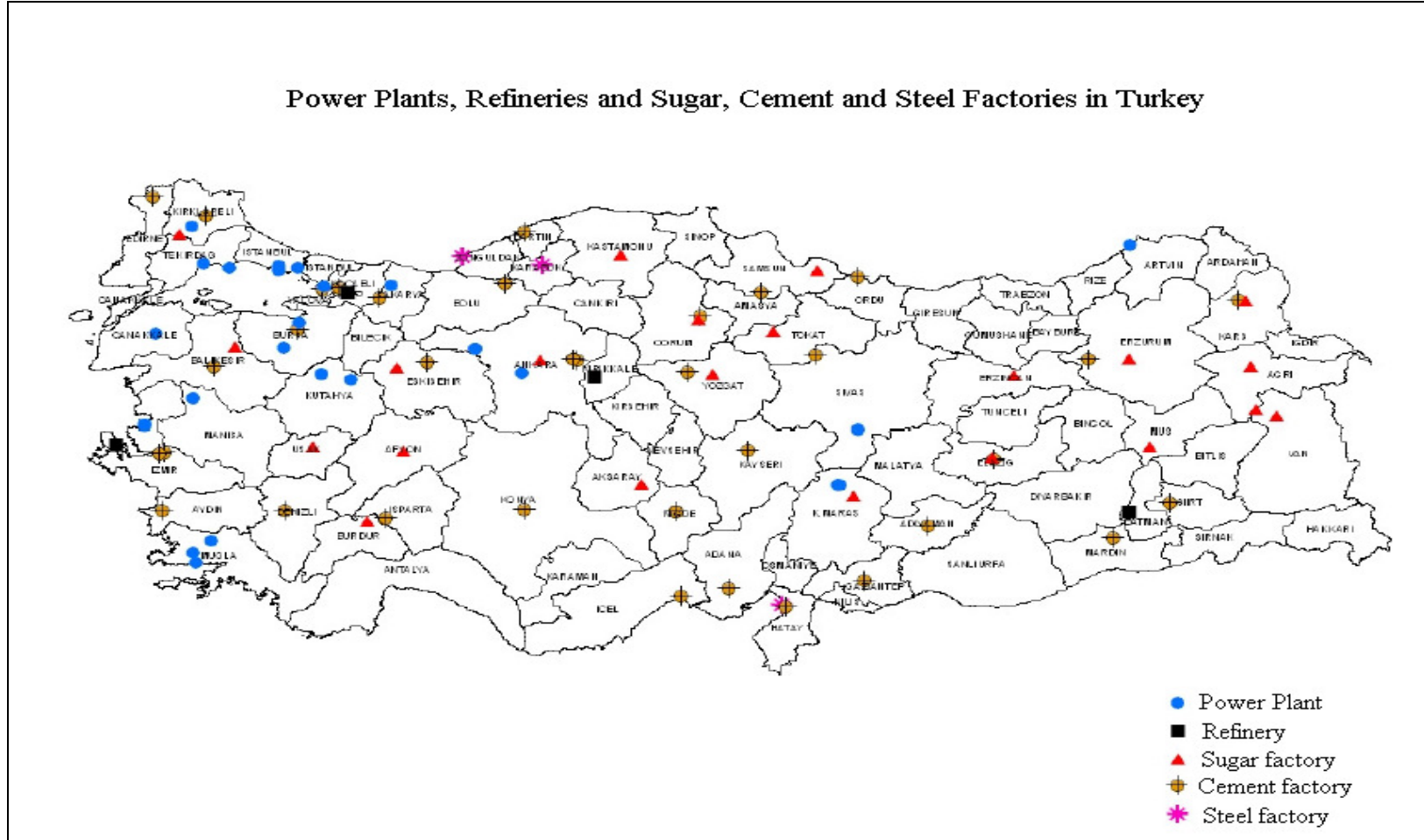


Figure 1. 2 Main CO₂ emission sites in Turkey (TUBITAK KAMAG, 2009)

There are several means to reduce the amount of CO₂ emission into the atmosphere such as increasing the energy efficiency of energy production, reducing the carbon intensity by substituting lower carbon or carbon free energy sources such as renewable sources for the current fossil fuels, nuclear energy an enhancement of biological sinks and finally carbon dioxide capture and storage (CCS) (IPCC Special Report, 2005).

1.3 Carbon Capture and Storage

CCS is a process consisting of the separation of CO₂ from industrial and energy-related sources, transport to a storage location and long-term isolation from the atmosphere (IPCC Special Report, 2005). CCS has been under consideration for more than ten years and initial test of CO₂ injection into a saline aquifer has been successfully in operation since 1996 in the Sleipner Field in the North Sea (Baklid, A. et al, 1996). Carbon storage into geological formation is an attractive option for the long term sequestration of the greenhouse gas. The injection technology required is a well proven one in petroleum industry for enhanced oil recovery operations.

The National Energy Technology Laboratory (NETL), part of DOE's national laboratory system provides Carbon Capture and Storage database including both active and proposed Carbon Capture and Storage (CCS) projects world-wide. Information in the database regarding technologies being developed for capture, evaluation of sites for sequestration of carbon dioxide (CO₂), estimation of project costs and anticipated dates of completion for projects are sourced from publically available information. This database provides the public with information regarding efforts by various industries, public groups, and governments towards development and eventual deployment of CCS technology. This is an active database that will be updated as information regarding these or new projects are released to the public.

It is available in Ms-Excel format at the http://www.netl.doe.gov/technologies/carbon_seq/database/index.html (U.S Department of Energy (DOE)).

1.3.1 CO₂ Capture

CO₂ capture is aimed to produce a concentrated stream of CO₂ at high pressure that can be transported to a storage location. Today, applications separating CO₂ in large industrial plants, including natural gas treatment plants and ammonia production facilities, are already underway. Capture processes also have been used to obtain commercially useful amounts of CO₂ from flue gas streams generated by the combustion of coal or natural gas. There are 3 main ways to separate the CO₂, depending on the process or power plant application of interest. Figure 1.3 shows the process flow diagram of each separation system (Wright, L. W. et al, 2004).

Post-combustion systems separate CO₂ from the flue gases produced by burning fossil fuels in air. These systems normally use a liquid solvent to capture the small fraction of CO₂ available in a flue gas stream in which the main constituent is nitrogen.

Pre-combustion systems process the fossil fuel in a reactor with steam and air or oxygen to obtain a mixture consisting mainly of carbon monoxide and hydrogen. Additionally, hydrogen and along with CO₂, is produced by reacting the carbon monoxide with steam in a second reactor. The resulting mixture of hydrogen and CO₂ can then be separated into a CO₂ gas stream, and a stream of hydrogen.

Oxyfuel combustion systems use oxygen or oxygen enriched air instead of air for combustion of the fossil fuels to produce a flue gas that is composed mainly water vapor and CO₂. This results in a flue gas with high CO₂ concentrations (greater than 80% by volume). The water vapor is then removed by cooling and compressing the gas stream.

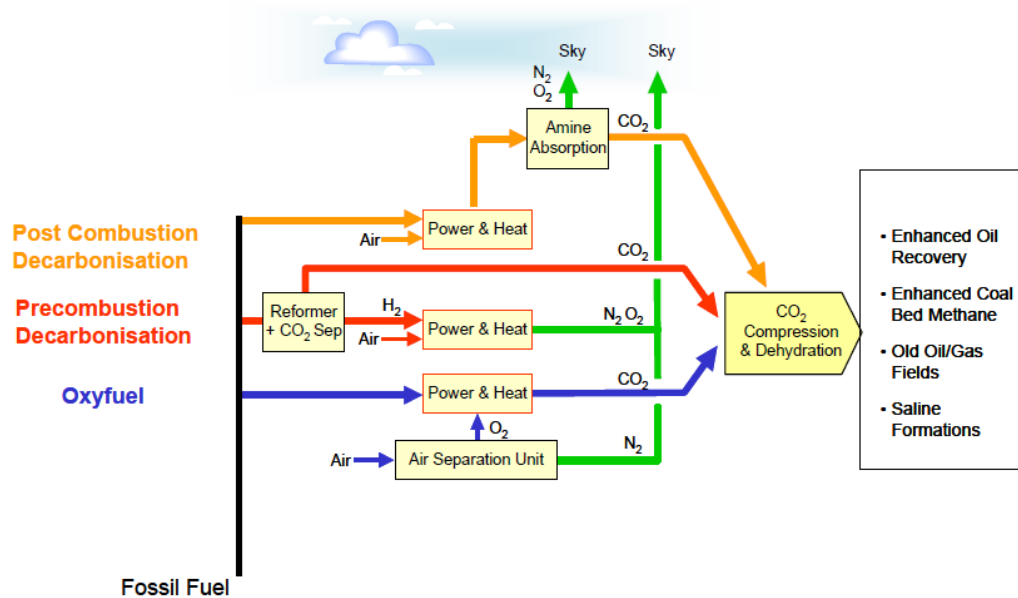


Figure 1. 3 CO₂ Capture Processes

1.3.2 CO₂ Storage

CO₂ can be stored into geological formation such as deep saline aquifers, depleted gas and oil reservoirs, oceans and unmined coal beds.

Using a depleted oil reservoir for CO₂ storage has several advantages among the other options. The reservoir is already dynamically and geologically well characterized. The abrupt leakage of stored CO₂ into the atmosphere would not be much considered since the reservoir has already contained hydrocarbons over long periods of time. Moreover, some existing wells may be converted to CO₂ injection wells at low cost. Others may be used to monitor the behavior of CO₂ within the reservoir after the injection process. Besides, the CO₂ injection is well known and proven technology for 25 years in oil industry to enhance the oil production. Additional oil may be produced from the depleted oil reservoir as a result of the CO₂ injection.

Among the geological storage options, CO₂ disposal in deep saline aquifers offers the largest storage capacity and being more abundant in the subsurface. This capacity was estimated to be between 1000 and 10,000 billion tones of CO₂ (IPCC Special Report, 2005). However, its drawback is that these systems are usually poorly characterized (Lagneau et al, 2005).

1.3.3 CO₂ Storage Sites

There are several worldwide CO₂ storage sites where CO₂ is currently being injected. The four main storage sites are In Salah in Algeria, Snohvit and Sleipner in Norway and Ketzin in Germany. Other storage sites are Weyburn in Canada, K12-B in Netherlands and Kaniow in Poland (CO₂ReMoVe, EU-FP 6 Project).

In Salah-Algeria

This is jointly operated by BP, Statoil and Sonatrach. CO₂ injection started in 2004, at a rate of about 0.9 Mt per year. The cost of the developments taking place in Algeria's In Salah gas fields is calculated to be \$2,300 million. In Salah Gas finally aims to supply 9 billion m³/year of natural gas to the southern European market. The natural gas contains up to 10% CO₂, which has to be reduced to 0.3% before the gas is supplied (Wright, I.W., 2007). Throughout the project, the anticipated peak in CO₂ production is likely to be around 60 MMscf/day, with an overall total of around 450 bscf. Re-injection of the CO₂ from the produced gas is expected to result in a net emissions reduction of approximately 900,000 tones of CO₂ per year (CO₂ReMoVe, EU-FP 6 Project).

Sleipner- Norway

It is operated by StatoilHydro. In 1995, the Norwegian government implemented a tax on CO₂ emissions and this was an incentive for Norwegian energy company Statoil to start experimenting with CCS on this offshore gas rig. The CO₂ content of the Sleipner gas varies 4-9.5 %. The Sleipner CO₂ storage operation commenced in 1996, and remains the world's most mature large-scale demonstration of storage technology with more than 7 Mt of CO₂ injected currently in situ. Current time-lapse seismic surveys provide a unique, world-leading reference dataset applicable to the general understanding of large-scale storage in saline aquifers (CO2ReMoVe, EU-FP 6 Project).

Snohvit- Norway

CO₂ storage began on Snohvit field in April 2008. Statoil is reinjecting CO₂ produced from the field into the ground beneath the gas-bearing formation on the field. The produced gas contains 5-8 mole % of CO₂. Before the liquefaction process, the mole content of CO₂ must be reduced to 50 ppm. The reinjection will reduce CO₂ emissions by 700,000 ton/ year when Snohvit is at full capacity (CO2ReMoVe, EU-FP 6 Project).

Ketzin-Germany

The GFZ German Research Center for Geosciences started CO₂ storage in Ketzin in June 2008. Within the framework of the European CO₂-SINK project, approximately 60.000 tons of CO₂ will be stored between 2008 and 2010 at a depth of more than 600 m. An injection well and two observation wells have been successfully completed to depths of 800 m, equipped with modern sensor technology and successfully tested. (CO2ReMoVe, EU-FP 6 Project).

K12-B- Netherlands

Since 1987, The K12-B gas field has been producing natural gas with a relatively high CO₂ content. The CO₂ is separated from the natural gas before it is transported. Until recently the CO₂ was vented, but it is now injected into the gas field, at a depth of approximately 4000 m. K12-B is the first CO₂ storage site in the world where CO₂ is being injected into the same reservoir from which it was, together with methane, produced. The feasibility of CO₂ injection and storage in depleted natural gas fields and the corresponding monitoring and verification are being investigated (CO2ReMoVe, EU-FP 6 Project).

Weyburn- Canada

A Canadian oil and gas corporation EnCana Corporation announced to implement a large scale EOR project in an oilfield near Weyburn, Saskatchewan, using CO₂ captured from Dakota Gasification Company's Synfuels Plant in 1998. The main goal of the Weyburn project is to predict and verify the ability of an oil reservoir to store CO₂. The work has focused on understanding the mechanisms of CO₂ distribution and containment within the reservoir and the degree to which CO₂ can be permanently stored. The expertise obtained can be used when selecting other storage sites (CO2ReMoVe, EU-FP 6 Project,).

Kainov- Poland

A pilot site for CO₂ storage in coal seams was set-up at Kaniow, Poland. This site consisted of one injection and one production well. About 760 ton of CO₂ has been injected into the reservoir from August 2004 to June 2005. A follow-up EC project, MOVECBM, aimed at assessing the storage performance of the reservoir, i.e. whether the injected CO₂ was adsorbed onto the coal or whether it was still present as free gas in the pore space. The site now provides a valuable opportunity to monitor the post-injection phase of storage evolution (CO2ReMoVe, EU-FP 6 Project).

1.4. CO₂ Trapping Mechanisms

CO₂ storage into geological formation is achieved by a combination of processes: displacement of the in situ fluids by CO₂, dissolution of CO₂ in the formation water, and geochemical reaction of CO₂ with rock minerals to form stable, solid compounds such as carbonates. When CO₂ is injected into subsurface, at first displacement of in situ fluids by CO₂ dominates, however, over time scales of decades and centuries, the dissolution of CO₂ into brine and geochemical reactions become more important (Sengul, 2006).

In Fact, during CO₂ storage, four CO₂ trapping mechanisms exist to retain the injected CO₂ in geological formations (Gaus et al, 2008): structural, residual, solubility, or mineral trapping. Structural trapping involves the storage of CO₂ as supercritical fluid beneath a low permeability cap rock. Residual trapping represents the supercritical CO₂ that is trapped in small pores and can not be mobilized anymore. Solubility trapping involves the dissolution of CO₂ into brine or oil. Mineral trapping involves CO₂ rich reservoir brine reaction with the reservoir rock minerals to precipitate as carbonate minerals. Permanent sequestration of CO₂ can be achieved by third mechanism, mineral trapping.

1.5 Safety of Carbon Storage

It is crucial to prove the long term reliability and safety of CO₂ geological storage. The risks involved in the pipeline transport of CO₂ and with surface injection facilities are reasonably well understood and are already borne by the enhanced oil recovery industry. However, the injected and stored CO₂ may migrate into groundwater sources and contaminate them and may even reach the surface and leak back to the atmosphere. If it is the case, then it means the process is not working as a climate change mitigation method. Therefore, the assessment of CO₂ sequestration needs to be carried out on the basis of a better understanding of in situ physical and chemical processes induced by

CO₂ injection and storage, of improved numerical modeling of CO₂ fate and a detailed knowledge of relevant site characterization (Bachu, 2002). There are many risks associated with CO₂ storage. One of the risks is the dissolution of cap rock by acidic CO₂-rich fluids resulting from CO₂ injection. During underground CO₂ storage, the containment of CO₂ will be crucially dependent on the cap rock integrity above the CO₂. Thus, it is necessary to evaluate how the CO₂ might impact cap rocks, since this could control the ultimate longevity of CO₂ storage.

CHAPTER 2

LITERATURE SURVEY

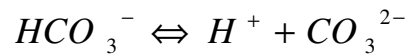
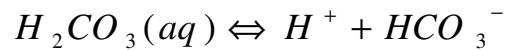
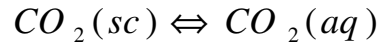
The chemistry of geological formation water is the result of different hydrogeochemical processes such as mixing, dissolution/precipitation of minerals, bacterial activity and interactions with organic materials. The injection of CO₂ into the geological formations creates an extra process affecting the chemistry of the brine and increasing the chemical reactivity of the system. This is why the success of CO₂ storage and its worldwide development depends largely on the understanding of CO₂ interaction with formation water and minerals in the long term (Gaus et al, 2008).

2.1 CO₂- Water Interaction

It is known that the injected supercritical CO₂ moves upward with favorable vertical permeability and the buoyancy effects, from the injection point and accumulates under the overlying cap rock after a few years of injection (Gaus et al, 2005).

Once the CO₂ has reached the base of the cap rock it will dissolve into the cap rock formation water and then diffuse vertically upward into the cap rock. The cap rock formation water is acidized as the CO₂ dissolves in it (Lagneau et al, 2005).

The following equations are homogeneous reactions since they involve only aqueous components.



The above speciation of dissolved CO_2 is highly dependent on the pH.

From Figure 2.1, it is seen that, for the closed system, the speciation evolves from dominant $CO_2(aq)$ at low pH to HCO_3^- and finally CO_3^{2-} at intermediate and high pH. For the open system (Figure 2.2), the concentration of $CO_2(aq)$ stays constant and the higher the pH values, higher the concentration of HCO_3^- and CO_3^{2-} .

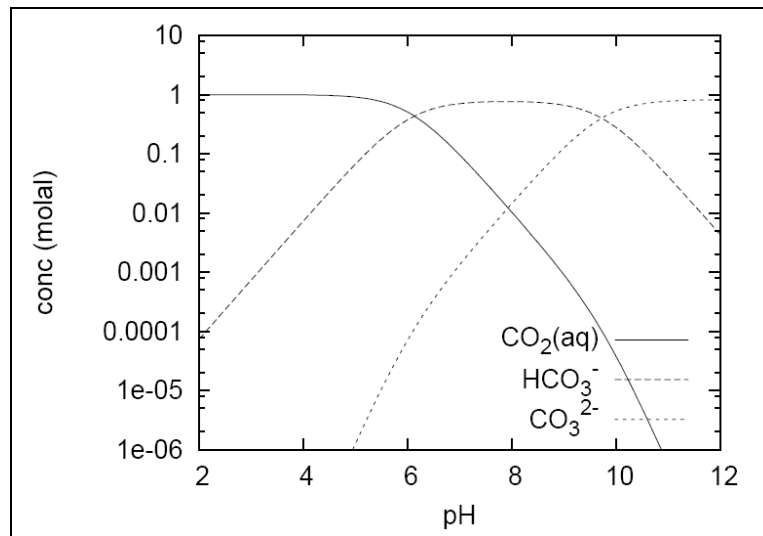


Figure 2. 1 Speciation of the dissolved CO_2 as a function of pH, in a 1 M NaCl solution at $60^\circ C$ (closed system) (Lagneau et al., 2005)

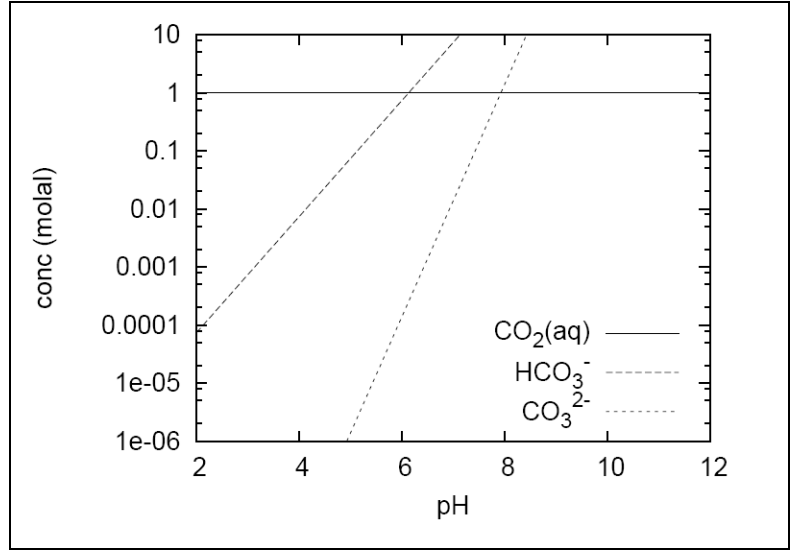


Figure 2. 2 Speciation of the dissolved CO₂ as a function of pH, in a 1 M NaCl solution at 60 °C (open system) (Lagneau et al., 2005)

The solubility of CO₂ depends on several factors such as pressure, temperature and salinity. Duan and Sun (2002) also investigated this. The solubility increases with pressure, but decreases with temperature and the salinity (Figure 2.3 and Figure 2.4). The salinity effect is known as the salting-out effect.

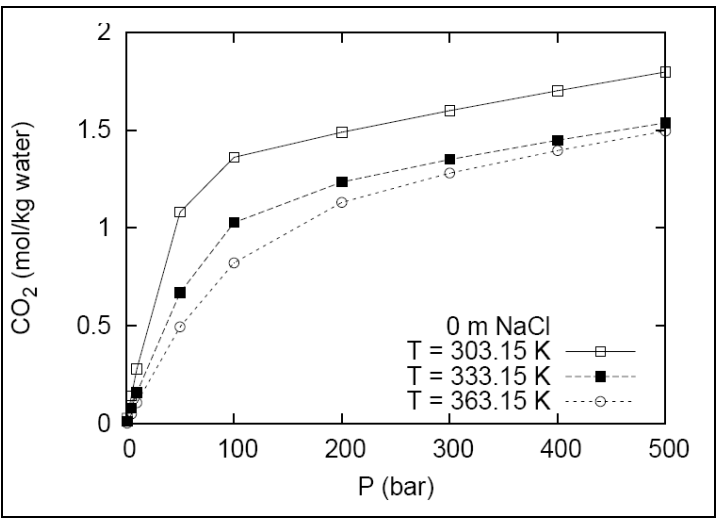


Figure 2. 3 Solubility of CO₂ in pure water: influence of the pressure and temperature (Duan and Sun, 2002)

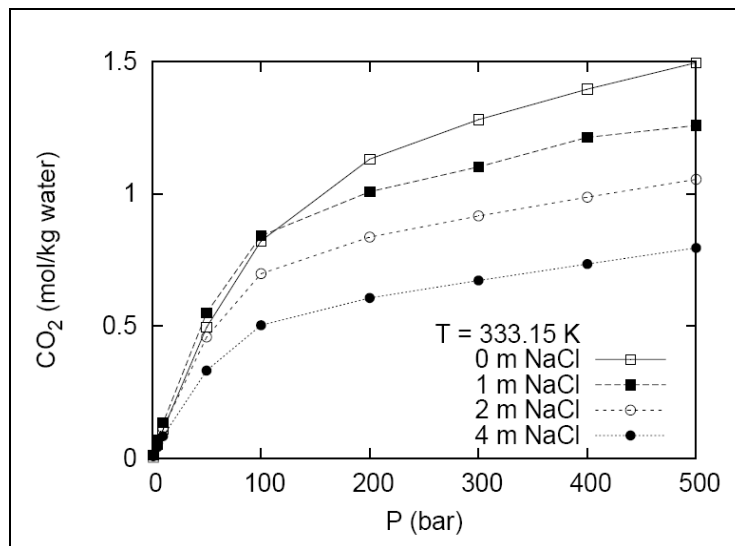


Figure 2. 4 Solubility of CO₂ at 60 °C: influence of the pressure and salinity (Duan and Sun, 2002)

2.2 CO₂-Water-Rock Interaction

The acidification due to the solubility of CO₂ into brine results in geochemical reactions with the rock minerals present in the cap rock. In other words, the carbonate ion CO_3^{2-} will eventually react with the cations present in the reservoir to precipitate carbonate minerals. In this case, the reactions that take place depend on the mineral composition of the reservoir rock.

The most common of these reactions are:



Geochemical reactions between dissolved CO₂ and the minerals present in the cap rock lead to porosity and thus permeability changes. Porosity can be increased due the dissolution of initial cap rock minerals in the acidized formation water whereas it can be decreased as a result of the precipitation of secondary minerals (minerals which are not available at the beginning of the reaction). A porosity increase would be undesirable since this would make the injected CO₂ leak through the cap rock while this is good for the reservoir rock regarding the higher storage capacity. However, a porosity decrease is an advantage, which would further increase the sealing capacity of the cap rock. In fact, the porosity decrease due to new mineral precipitations would usually be around 1% of total volume. But such a small decrease would lead to much a significant decrease of permeability almost 20% (Calabrese and Masserano, 2006).

Carbonate formations are found to be limited in the quantity of CO₂ that can be trapped by geochemical reactions. Siliciclastic formation are expected to have the best potential for trapping CO₂, by precipitating carbonate minerals, when they contain an assemblage of basic aluminosilicate minerals such as feldspars, zeolite, illite, chlorite and smectites (Gunter et al., 1997). When these aluminosilicate minerals react with aqueous CO₂, they dissociate to form a kaolinite and the CO₂ is trapped in this form. The protons (H⁺) in the aqueous solution are replaced with the cations from the dissolution of initial aluminosilicate minerals. Dissolution of most minerals consumes H⁺ thus increasing the pH of the brine (becomes more basic). Precipitation of mineral releases H⁺ thus decreasing pH of the brine (becomes more acidic).

2.3 Laboratory investigations on CO₂-brine-rock interaction

Laboratory experiments are rarely conducted since prediction of the long-term reactions between CO₂ dissolved formation water and rock minerals is difficult by short term experiments. Moreover, complete reactions and mineral trapping of CO₂ would require

minimum time scales in the order of years once injected CO₂ had dissolved in the formation water. Increasing the temperature to 100-150°C is expected to increase the kinetic rates sufficiently to observe significant reactions. While the higher temperature and increased salinity tend to increase reaction rates, they are also responsible for significantly reduced dissolved CO₂ in solution.

Gunter *et al* (1997) carried out experiments on potential CO₂ trapping reactions in the Glauconite Sandstone aquifer at 105 °C and 90 bars for one month. The main aluminosilicate minerals of this aquifer, which would contribute to the trapping capacity of the aquifer, were feldspar and glauconite. However, very little reaction was observed during this experiment period. The geochemical code PATHARC.94 was used to predict the CO₂ trapping reactions. The results of the experiments and the modeling show that these reactions are slow- at least on the order of tens to hundreds of years.

Kaszuba *et al* (2005) conducted experiments in a flexible cell hydrothermal apparatus to determine the extent of fluid-rock interactions. The system was held at 200 °C and 200 bars for 59 days to approach steady state, then CO₂ was injected and allowed to react another 80 days. The results show significant reactions occurred such as magnesite precipitation. Moreover, the fluid analysis shows increase in Cl ion, which is partly due to supercritical CO₂ desiccation of brine.

Egermann *et al* (2005) performed experiments in which coinjection of supercritical CO₂ and brine to limestone. The results show that the flow rate and the initial fluid composition in the core played important role in the CO₂-brine-rock interaction causing various heterogeneous dissolution patterns and in some cases to re-precipitation and reduction in permeability.

Bateman *et al* (2005) conducted a well-constrained long term (7.5 months) laboratory work reacting known amounts of minerals with CO₂ rich-fluids to represent situations where CO₂ is being injected into deep geological formations. Using BGS coupled code,

modeling the experimental systems was performed. It was concluded that the model results tend to overestimate the reaction degree compared with those of experimental works.

Lin *et al* (2007) carried out experiments consisting of four different systems (supercritical CO₂-rock, water-rock, supercritical CO₂-vapour-rock and supercritical CO₂-water-rock). The experiments were conducted in hydrothermal autoclave at 100° C. Rock minerals were quartz, biotite and granite. In all the scCO₂-rock system, without water, no evident chemical alternation occurred contributing to the dissolution of rock minerals. In the case of introduction of water or vapor, elements dissolved from both quartz and biotite were too low to be responsible for the occurrence of high concentration elements dissolved in the residual solution in the granite system.

While reviewing the literature surveys on geochemical aspects of CO₂ sequestration as a means of reducing its amount in the atmosphere, there is almost no study on *cap rock* integrity. However, there are several experimental studies conducted with CO₂-saturated formation water on *reservoir rock* under various temperature and pressure conditions in the consideration of mineral trapping of CO₂ in the reservoir rock after the injection.

Indeed, the subjects of cap rock and reservoir rock studies are similar. What is different here is the rock composition. Moreover, formation water composition of cap rock, which must be one of the parameters to be known in the geochemical investigation of cap rock integrity, is not usually analyzed in the field. But this problem can be solved by assuming the cap rock formation water is similar to the reservoir formation water (Xu *et al*, 2005).

2.4 Numerical modeling of CO₂- rock interaction

Experimental data are needed, but they are limited in time, space, and conditions. Numerical simulation techniques thus provide a useful tool to extend the experimental results, and to predict the fate of the injected CO₂ in geological formations (Lagneau et al, 2005).

There are several commercial numerical modeling codes such as PHREEQC, HYTEC, GEM-GHG and TOUGHREACT to predict long term geochemical evolution of the rock after massive amount of CO₂ sequestration.

Xu *et al* (2005) developed a conceptual model of CO₂ injection in sandstone-shale formation using common hydrogeologic properties and mineral compositions of Gulf Coast sediments. The reactive transport code TOUGHREACT was used to investigate the mass transfer between the beds and CO₂ trapping through carbonate precipitations. Simulation results show that most CO₂ sequestration occurs in the sandstone bed. The main CO₂ trapping minerals are dawsonite and ankerite. The CO₂ mineral trapping capacity reaches about 90 kg/m³ after 100,000 years.

The study of Gaus *et al* (2005) focuses on the geochemical aspects of the Sleipner injection project, with special attention to the long term integrity of the Nordland Shale cap rock preventing upward migration of the injected CO₂. Reactive transport modeling combining reaction kinetics and diffusive transport is used to qualify and quantify the effects of geochemical reactions on the porosity of the cap rock at the Sleipner site, using the code PHREEQC (V2.6). The simulation results show that some carbonate dissolution occurs at first, but in long term, feldspar alteration is the dominant reaction and also the exact mineralogical composition of the plagioclase fraction in the cap rock plays an important role. These reactions may result in a little decrease in porosity and

therefore also a decrease permeability which might locally improve the cap rock integrity is expected.

Lagneau *et al* (2005) performed simulations using the code HYTEC. Two deep saline aquifers were the areas of interest of CO₂ injection: Dogger- the carbonated aquifer in Paris Basin and Bunter- the sandstone aquifer in North Sea. It was expected that CO₂ dissolution in the carbonated one and carbonate mineral precipitation in the sandstone one. The simulation results show that, in the carbonated Dogger aquifer, transport controlled the dispersion of the dissolved CO₂ in the flow direction. For the sandstone Bunter aquifer, the evolution is controlled by the reactivity of the dissolved CO₂ with the reservoir rock minerals. The dissolution of silicate minerals enables the precipitation of secondary new carbonates.

Calabrese and Messarano (2006) performed simulations using GEM-GHG to investigate the influence of physical and chemical process occurring during CO₂ sequestration in a depleted gas field located in north of Italy on the total storage capacity. The simulation results indicate that the storage capacity decreases as the rate of injection decreases. At high rates, the CO₂ channeled through high permeability paths and the maximum bottomhole pressure imposed to the system will be reached more rapidly than the cases at low injection rate, and the injection well will be shut sooner, giving a lower total injected capacity. Also it is observed that CO₂ impurity affects adversely the storage capacity.

Andre *et al* (2007) studied the physical and chemical impact of CO₂ injection on the properties of the carbonate Dogger aquifer (Paris Basin- France), through 1 D radial numerical simulation using the multiphase reactive transport code TOUGHREACT. Two injection cases were investigated. The first one considers injection of CO₂-saturated water. The continuous injection of acid solution involves continuous dissolution of all carbonates. A large porosity increase up to 90 % was predicted after an injection period of 10 years. The second case is the injection of supercritical CO₂. The

overall geochemical activity is much lower than that of CO₂ saturated water case. Also, the injected supercritical CO₂ causes the vaporization of the water leading to the formation water with higher ionic strength, which is known as desiccation process.

The paper of Gherard *et al* (2007) focuses on the study of the reactive mechanism which may occur as a consequence of CO₂ geological disposal at depth in a potentially highly-reactive cap rock, consisting of carbonate-rich shale. Gas- water- rock interactions resulting from CO₂ migration into the cap rock have been simulated using TOUGHREACT under two alternative mass transport conditions; diffusion in the aqueous phase and gas and / or liquid advection. In case of transport by molecular diffusion in the aqueous phase, CO₂-leakage becomes self-limiting and pores become clogged with newly precipitated minerals after very short time. On the other hand, when transport of chemical is dominated by advection, CO₂ leakage through cap rock enhances both porosity and permeability.

In this study, geochemical reactions are investigated through experimental work on the core on the Sayindere cap rock formation. Experimental works consists of the static and dynamic experiments. Moreover, using ToughReact, reactive transport modeling simulator, the long term evolution of the cap rock minerals under CO₂ injection is simulated.

CHAPTER 3

STATEMENT OF THE PROBLEM

One way to reduce the amount of CO₂ in the atmosphere is to capture the CO₂ and inject it into geological formations. The key to the success of CO₂ sequestration process is to prove that the leakage of injected CO₂ is insignificant. It is known that the leakage paths can be due to CO₂ - rock interaction and CO₂ – well interaction after massive injection of CO₂. This study focuses on the former interaction. Although supercritical CO₂ is normally inert, when it dissolves in water or brine, it makes formation water acidic. This acidized water can react with the cap rock minerals and thus geochemical reactions can take place. These reactions can change the porosity and therefore, the permeability and furthermore affect the sealing capacity of cap rocks.

The aim of this research is to identify the geochemical reactions of the CO₂ saturated in the synthetic formation water with the rock minerals of the Sayındere cap by laboratory investigations. It is also aimed to assess the potential impacts of geochemical processes on the integrity of the Sayındere cap rock core by using the reactive transport code TOUGHREACT and compare the both results. The Sayındere formation is the cap rock of the Caylarbasi, a southeastern petroleum field in Turkey. In a previous study (TUBITAK KAMAG, 2009), the Caylarbasi field has been selected as one of the sites for the possible CO₂ storage in Turkey.

CHAPTER 4

MATERIALS FOR THE EXPERIMENTS

For this work, 6 core plugs were provided by TPAO from Sayıdere formation which is the cap rock for many oil fields in southeastern Turkey. Specifically, it is the caprock of Caylarbasi oil field which was selected for a prefeasibility study on CO₂ storage project (TUBITAK-KAMAG, 2009). Although Sayıdere is a cap rock overlying the oil reservoirs in the southeastern part of Turkey, in some fields like Karakus, oil was produced from fractured layers of Sayıdere formation. The top and bottom of Sayıdere formation are Kastel and Karabogaz formations. The average thickness of Sayıdere is around 100 m and it exhibits homogenous lithology: clayey carbonate. It was deposited in a deep ocean environment during the late Campanian, which is the fifth of six stages in the Upper Cretaceous series. The Campanian period is between 83.5 ± 0.7 Ma to 70.6 ± 0.6 Ma (million years ago). Thin section analysis of the core sample from the Sayıdere cap rock reveals that the formation is mostly composed of calcite (85%), clay (13%) and small amounts of quartz, hematite and glauconite.

The types of chemical reactions taking places between rock minerals and formation water in the presence of dissolved CO₂, obviously depend on initial mineral composition and dissolved metal species within formation water. Therefore, before an experiment or a simulation, the initial rock mineral composition and formation chemistry must be known to evaluate the geochemical aspects of underground CO₂ storage.

4.1 Fluid Chemistry of Sayindere Formation

The formation water analysis of Sayindere cap rock of Caylarbasi field is not available since the reservoir is important for petroleum engineering than the cap rock. The reservoir formation water analysis from the Caylarbasi -1 well was carried out in TPAO Research Center. The composition of this water is given in Table 1 (where $MEQ = (\text{mg/lt}) / MW * \text{charge number}$, $MEQ (\%) = MEQ / \text{Total MEQ} * 100$).

Table 4. 1 Reservoir formation water analysis from Caylarbasi-1 (TPAO)

	mg/lt	ppm	MEQ	MEQ (%)
Sodium	641.04	640.84	27.89	36.76
Calcium	120.54	120.5	6.01	7.93
Magnesium	48.7	48.69	4	5.28
Iron	0.38	0.38	0.02	0.03
Sulfate	14.4	14.4	0.3	0.39
Chloride	761.2	760.97	21.47	28.3
Carbonate	0	0	0	0
Bicarbonate	985.26	984.96	16.16	21.3
Total	2571.52	2570.74	75.85	100

Assuming reservoir and cap rock formation waters are similar; Sayindere cap rock formation water was synthetically prepared. For the preparation of 1 L formation water, 1.83 mg of $\text{FeCl}_3 \times 6\text{H}_2\text{O}$, 36.83 mg of $\text{MgSO}_4 \times 7\text{H}_2\text{O}$, 333 mg of CaCl_2 , 375.64 mg of $\text{MgCl}_2 \times 6\text{H}_2\text{O}$, 1,356 g of NaHCO_3 and 688 mg of NaCl are calculated to give the above composition. So these chemical substances at the calculated amounts are mixed and dissolved in 1 L deionized water to prepare the synthetic formation water at the given composition.

After synthetically being prepared, the formation water was sent to the laboratory to check if the formation water had the same composition with the reference composition. The anions available in the water are measured by Ion Chromatography (IP) and the cations present in the water are measured by inductively coupled plasma-optical emission spectroscopy (ICP-OES) at the Petroleum Research Laboratory, METU. Alkalinity is determined by titration. For alkalinity, there is no direct measuring equipment. There are 3 kinds of alkalinity, hydroxide (OH⁻), normal carbonate (CO₃⁻²), bicarbonate (HCO₃⁻). In order to distinguish between the kinds of alkalinity present in a sample and determine the quantities of each, a titration is made with a standard acid using two indicators successively. The standard solution is 0.02 N H₂SO₄ and the indicators are phenolphthalein and methyl orange test solutions. The procedure of this analysis is given in Apendix A The chemistry analysis of synthetically prepared water is given in Table 4.2.

Table 4. 2 Analysis of the synthetic formation water

	ppm
Sodium	693.2
Calcium	41.92
Magnesium	47.36
Iron	1.190
Sulfate	15
Chloride	725
Bicarbonate	613
pH	7.453

4.2 Mineral Investigation of Sayindere Formation

6 core samples shown in Figure 4.1 were taken from TPAO for the experimental investigations. As seen from Figure 4.1, the cores are approximately 1 in. in diameter and 1.5 in. in length. The cores belong to Well Besni-1 and were taken from the Sayindere formation, the same cap rock with the cap rock of Caylarbasi Field. No cores were available from the Sayindere formation of Caylarbasi Field. Thus, the same cap rock cores were used in this thesis study. It is known that Sayindere cap rock is generally homogeneous, whose lower part is limestone and upper part is clay.

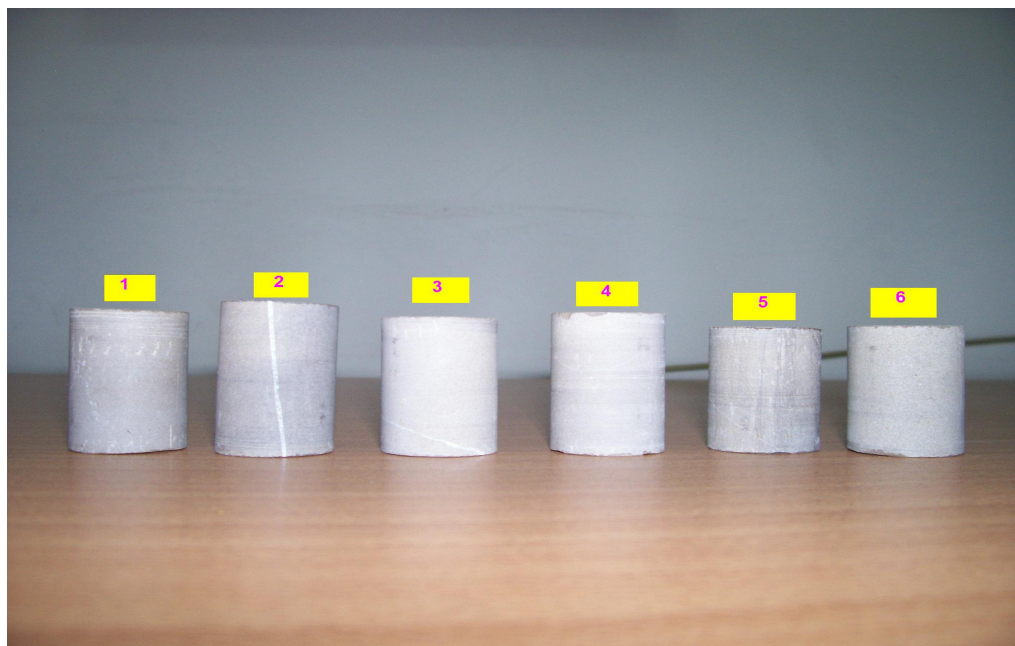


Figure 4. 1 Cores taken from Sayindere cap rock

4.2.1 Thin Section Analysis of Sayindere Cores

The purpose of this analysis is to investigate the composition of Sayindere cores. Sayindere is already known to be homogeneous and mainly composed of clayey carbonate. A Thin Section analysis can not give the type of the clay and clay composition, but can reveal other minerals the Sayindere formation is composed of. The

thin section analysis was done on the core # 4 by Nikon Eclipse E200 Optical Microscope at Geological Engineering Department, METU. As shown in Figure 4.1, the core is gray colored. The core represents a matrix of very fine grained calcite and clay minerals. From the optical microscope, it was seen there are many lighter and darker laminations with thickness of 0.1-0.8 mm. Tiny cracks parallel to these laminations are filled or stained with iron oxide. A lot of fossils and calcite grains are found. Calcite was formed by chemical processes and transported from other places. Moreover, a few rounded quartz, a small number of hematites and glauconites are found. It can be said that the rock is roughly composed of 85 % calcite, 1 % quartz, 0.5 % hematite and the remaining 13.5% percent clay (Göncüoğlu, 2010). Photos taken during thin section analysis are illustrated in Appendix B.

CHAPTER 5

EXPERIMENTAL INVESTIGATION

5.1 Static Experiment

5.1.1 Static experimental set-up

The experimental set up for the static (batch) experiment is shown in Figure 5.1. Some photos (Fig.C1, C2, C3) of the experimental apparatus are given in Appendix C. Technical specifications of the experimental equipment are listed in Table 5.1. As seen from Figure 5.1, there are two core holders to run the test on two cores simultaneously. The two holders are same in size (Table 5.2). The dimensions of the mixing cylinder for CO₂ and synthetic formation water are given in Table 5.3. Two core holders, the mixing cylinder are all made of stainless steel, except that the covers of the mixing cylinder are made of brass. Normally brass is resistant to corrosion; however, it was degraded due to long contact with acidic water during the experiment and caused corrosion problem, which is observed in the water sampling and SEM analyses.

Two original cores are used. It was aimed that after one month, the experiment in the 2nd core holder would be terminated and the SEM analysis of the core and the fluid chemistry analysis would be made to see any changes due to the CO₂-brine-rock interaction. If no change was observed from this experiment, the experiment in the 1st core holder would be kept for longer period than 1 month.

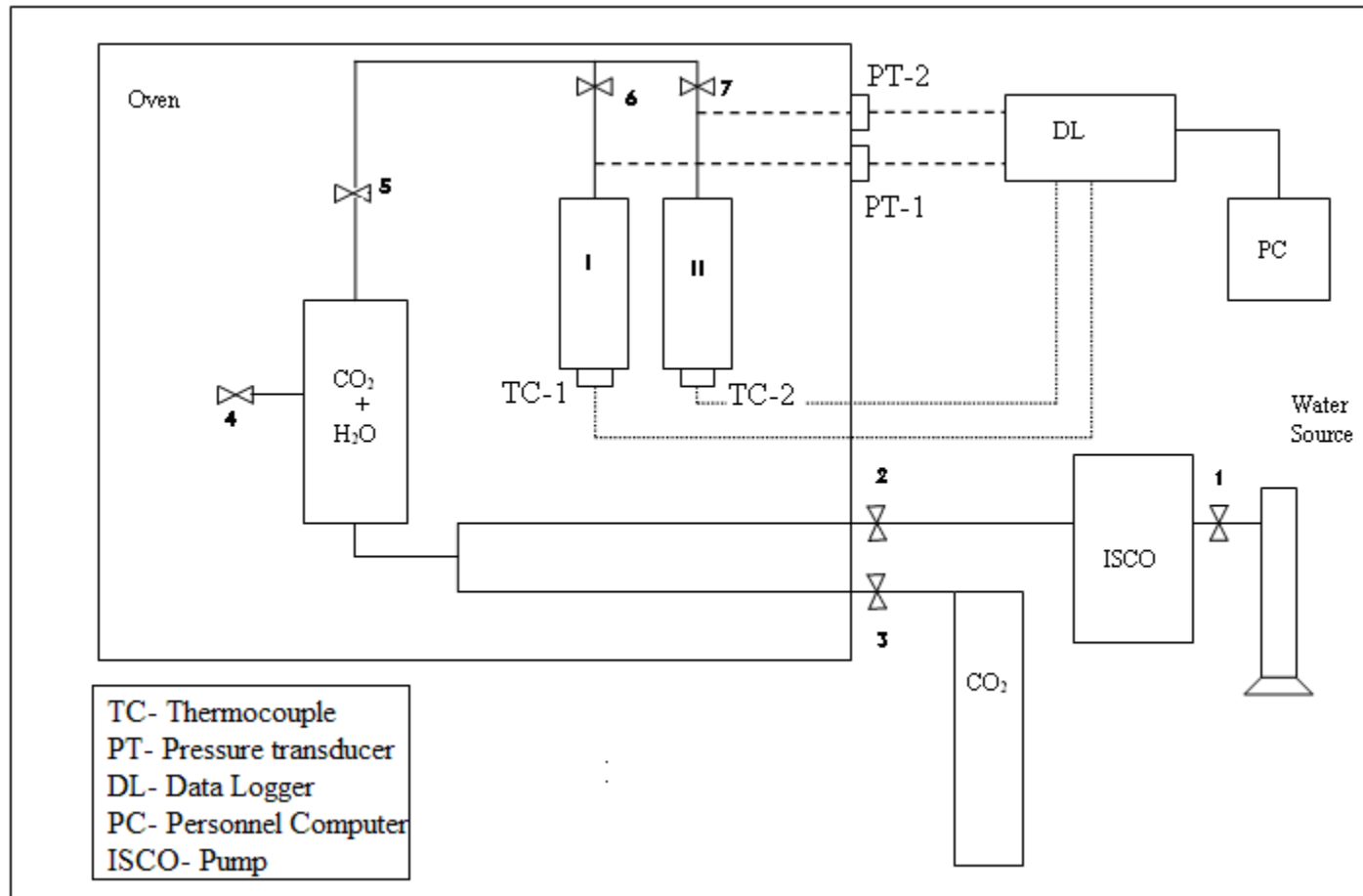


Figure 5. 1 The schematic diagram of the experimental set-up.

Table 5. 1 Technical specification of experimental apparatus

Experimental Apparatus	Specification
Pressure Transducer	0-3000 psia 4-20 mA
Thermocouple(PT-100)	-20 °C - +150 °C
ISCO 500D Pump	Cylinder Capacity: 507.38 ml Pressure Range: 10psi-3750 psia Refill or Depressurization rate: 1µl/min-204 ml/min at any pressure 0-3750 psi
CO2 Cylinder	40 lt, 65.8 kg, 250 bar
Core Holders	High pressure Steel
Mixing Cylinder	High pressure Steel
Dispatch Oven	10-400 °C
Elimko 680 Data Logger	Input types: Thermocouple, resistance Thermocouple, Voltage, Current Operating Temperature: -10°C - +55°C Memory: EEPROM max. 10 ⁵ writing

Table 5. 2 Core holder dimension

Diameter (cm)	3
Length (cm)	21
Volume (cm ³)	148.44

Table 5. 3 Mixing cylinder dimension

Diameter (cm)	4.7
Length (cm)	15.8
Volume (cm ³)	274.12

5.1.2 Static experiment procedure

Before the experiment, the thin section of core #4 and SEM analysis of the core #5 were made. The core 4 and 5 were put in the core colder-I and the core holder-II respectively. The experiment is conducted under the reservoir condition of a temperature of 90°C and a pressure of around 100 bar. This is the situation where CO₂ is in supercritical state.

Before the experiment started, the temperature of the oven was raised to a temperature of 90 °C. Firstly, valve #3 was opened and CO₂ was sent to the mixing cylinder at 400 psia. Then synthetic formation water was pumped by using ISCO pump at previously determined constant pressure of 1430 psia. In the mixing cylinder, CO₂ and water was left for 4 hours to equilibrate. Afterwards, valves #5 and #7 were opened and let the core holder-II be filled with mixture of CO₂ and synthetic water from the mixing cylinder. The core holder-II pressure was raised finally to around a pressure of 1550 psi by pumping water through ISCO pump and the valves #5 and #7 were closed.

Then, the mixing cylinder was cleaned and vacuumed and CO₂ was again sent into the mixing cylinder by CO₂ cylinder regulator at a pressure of 400 psia. Immediately after this, water was pumped by ISCO at 1550 psia. Having been kept for 4 hours for equilibration, the mixture of water and CO₂ were sent to the core holder-I through opening the valves #5 and #6. Its pressure was raised again by ISCO pump at 1550 psia. Afterwards, the valves #5 and #6 were closed.

The pressure of the 2nd core holder and the temperatures of both core holders were recorded. As shown in Figure 5.2, the pressure and temperatures are kept all constant.

Calculation of CO₂ amount used in the static experiment

Since CO₂ was sent into the mixing cylinder of volume 274.12 cm³ at pressure of 400 psia and temperature of 90 °C, the CO₂ amount sent can be calculated as follows:

$$\text{Mixing cylinder : } v = \pi r^2 h = \pi \left(\frac{4.7}{2} \right)^2 * 15,8 = 274.12 \text{ cm}^3$$

$$PV = znRT$$

$$n = \frac{PV}{zRT}$$

For CO₂, the critical temperature and pressure are:

$$T_c = 31.1 \text{ } ^\circ\text{C}$$

$$P_c = 73 \text{ atm}$$

So the reduced critical temperature and pressure:

$$T_r = \frac{T}{T_c} = \frac{90 + 273}{31.1 + 273} = 1.19$$

$$P_r = \frac{P}{P_c} = \frac{27.21}{73} = 0.373$$

At these conditions

$$z \approx 0.94$$

Given that,

$$R = 8.314472 \text{ cm}^3 \text{ MPa K}^{-1} \text{ mol}$$

$$P = 400 \text{ psia} = 2.758 \text{ MPa}$$

$$T = 90^\circ \text{C} = 363.15^\circ \text{K}$$

$$n = \frac{2.758 * 274.12}{0.94 * 8.314472 * 363.15} = 0.266 \text{ mol}$$

So, 0.266 mol of CO₂ dissolved in the water was in contact with the core in each core holders in the static experiments.

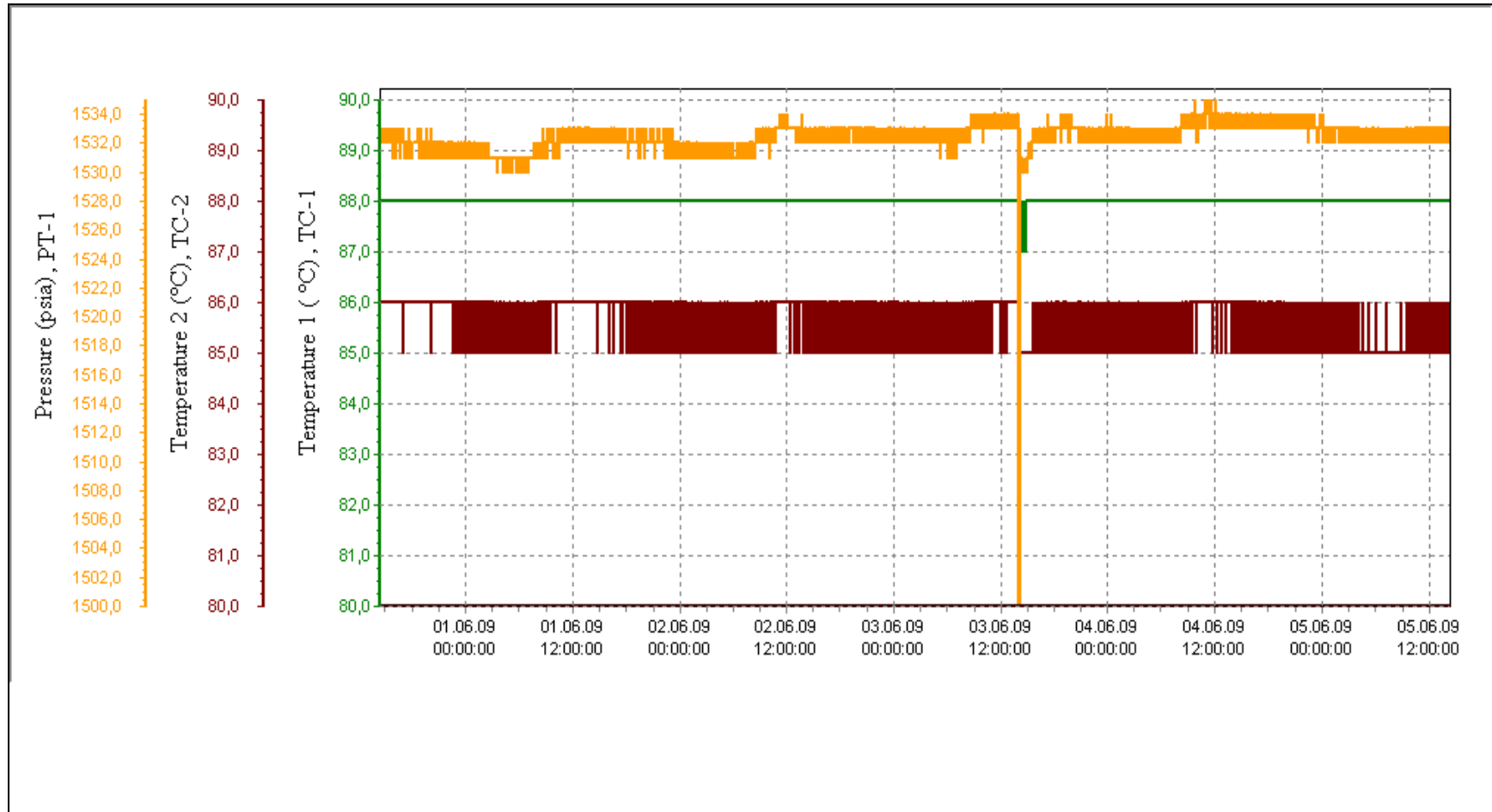


Figure 5. 2 Pressure and Temperature recordings of the static experiment (final 5 days)

5.1.3 Results and Discussion of the Static Experiment

After 30 and 100 days, the experiments in the 2nd and 1st core holders were terminated, respectively. SEM analyses of the cores were made to see any mineralogical changes on the core surfaces. Moreover, the fluid chemistry analyses of the mixtures in the core holders were made to investigate the possible geochemical reactions induced by CO₂ – formation water.

5.1.3.1 The 30 day-experiment

Sample Preparation for SEM/EDX Analysis

A thin layer of 5 mm is taken from the top of the core and it is divided into two parts to carry out top surface SEM/EDX of the one part and in-depth SEM/EDX of the other part (Figure 5.3). Both the in-depth and top surface SEM analyses of the core are carried out prior to and after the experiment. In depth SEM analysis, near to surface and inner part of the core are examined separately.

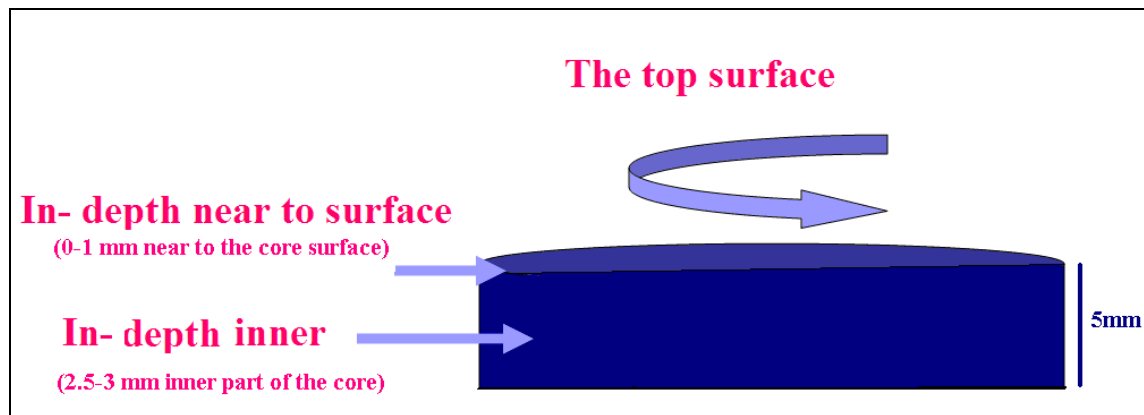


Figure 5. 3 Schematic representation of the SEM analysis

SEM/EDX analysis results of the 30 day experiment are given in Appendix D. SEM photos are illustrated in Appendix E. SEM analyses were carried out at the Department of Metallurgical Engineering. From the photos taken in SEM analysis (Figure E.3), it is seen that the near to surface appears to become looser than the inner part of the core, which is interpreted as being due to CO₂ diffusion into the core. The following tables give the concentrations of each element concentration revealed during the SEM/EDX analysis.

Table 5.4 shows the inner part in-depth SEM analysis of the core #5, prior to after the experiment for comparison. From Table 5.4, as expected the reaction occur at the surface, there is no difference in the element concentrations of inner part of the core sample. This explains that the inner part of the core is not affected as a result of the CO₂ saturated water. Oxygen, element concentration is around 52 %. Si and Ca element concentrations are approximately 5 % and 42 %, respectively.

Table 5. 4 In-depth SEM Analysis of Core #5 (Inner part)

	prior to experiment inner part	after experiment inner part
	Element Concentration (%)	
O	52.36	52.71
Si	4.72	5.42
Ca	42.93	41.88

Table 5. 5 In depth SEM Analysis of Core #5 (Near to Surface)

	prior to experiment near to surface	after experiment near to surface (site_1)	after experiment near to surface (site_2)	after experiment near to surface (site_3)
	Element Concentration (%)			
O	53.86	56.34	55.14	56.87
Al			0.50	0.30
Si	7.72	11.17	8.50	9.63
Ca	38.41	29.48	32.81	25.30
Fe		3.01	3.06	7.90

Table 5.5 illustrates the near to surface in depth SEM analyses of the core sample to see any change in element concentration by comparing the prior to and after the experiment concentrations. As seen in Table 5.5, after the 30-day experiment, three different sites of the near to surface SEM/EDX analyses are performed on the core #5. Different from the inner part, there are Al and Fe element available near to surface of the core. Moreover, prior to experiment, there are no Al and Fe ions near to surface of the core sample. The source of Fe ion seen on the near to surface of the core #5 after the experiment may be explained as the result of the corrosion in the experiment. All equipment in the experiment is made from high quality steel. However, the long time contact with acidic water may have caused degradation of the steel and resulted in corrosion.

However, the Ca element concentration is obviously decreased when the prior to and after the experiment Ca element are compared. It may explain that the Ca bearing minerals are dissolved into the CO₂ saturated formation water because, from the water

analysis given in Table 5.7, the Ca ion concentrations increased from 41.92 ppm to 382.2 ppm throughout the experiment.

The Al element seen on the near to surface may be due to the polishing core surfaces where Al₂O₃ was used before the SEM analysis. The upper top surface of the core before putting it into experiment was also polished.

Table 5. 6 Top Surface SEM Analysis of Core #5

	before the experiment	after the experiment (site_1)	after experiment (site_2)
	Element Concentration (%)		
O	53.13	54.39	54.14
Mg	0.91	0.98	0.71
Al	0.47		
Si	6.03		
Ca	39.45	27.07	28.62
Fe		17.57	16.54

Table 5.6 shows the top surface SEM analyses of the core sample prior to and after the static experiment. As seen in Table 5.6, after the experiment, two different sites of top surface SEM/EDX analyses are carried out on the core #5. Here, again, the Ca element concentration decrease is observed and it supports the explanation of dissolution of Ca bearing minerals into CO₂ saturated formation water. Also, from Table 5.6, there was Si element on the top surface of the core sample before the experiment. However, there is no Si element seen on the top surface after the experiment. Moreover, from water analysis (Table 5.7), there is Si ion in the formation water discharged after the experiment and there was no Si ion available in synthetically prepared formation water

prior to experiment. Thus, this may give the explanation for the dissolution of Si-bearing minerals, which is the quartz in the Sayindere core from the core in the experiment.

For the Fe seen on the top surface of the core after experiment, it may be due to the corrosion of the steel core holders.

Table 5.7 Water Analysis of the 30 day experiment

	Prior to experiment	After the experiment
	(ppm)	
Sodium	693.2	752.7
Calcium	41.92	382.2
Magnesium	47.36	152.1
Iron	1.19	0.443
Sulfate	15	117.18
Chloride	725	903.26
Bicarbonate	613	619
Silicon		16.14

Table 5.7 gives initial and final compositions of formation water of 30 day experiment. Cations available in water were analyzed by Inductively Coupled Plasma-Optical Emission Spectroscopy (ICP-OES) and anions were analyzed by Ion Chromatography (IC). The ICP-OES and IC analyses were carried out at the Water Laboratory of Petroleum Research Center, METU.

Bicarbonate ion concentrations were determined by titration technique. Apart from the initial ions available in the synthetically prepared formation water, there is new ion Si present in the final water after the experiment. SEM analysis of the core supports the presence of Si ion. Some Si-bearing minerals are dissolved as a result of CO₂- water-rock interaction. Also, some Ca and Mg bearing minerals are dissolved. Final concentrations of Ca and Mg ions are increased by 340.28 and 140.74 ppm respectively.

The sulfate and chloride ion concentrations are increased too. But SEM analyses of the core does not give any explanation to these increases.

5.1.3.2 The 100 day-experiment

SEM/EDX analysis results are given in Appendix H. Appendix G illustrates the photos of SEM Analysis of the 100 day-experiment. From the photos of SEM analyses (Figure G.7), there is a deposition layer on the surface, which appear a light coloured layer. Since there was no flow in the experiment, there was no transport of the reactant and reaction products. Thus, the formation of deposition layer can be explained in that way that the dissolved particles were deposited back on the core surfaces. Moreover, in Figure G.9, it is observed that there are wormholes created due to the heterogeneous pattern of calcite dissolution induced by the CO₂-formation water.

Table 5.8 shows the inner part in-depth SEM analysis of the core #4, prior to and after the experiment for comparison. From Table 5.8, there is no significant difference in the atom concentration of inner part of the core sample. In other words, the inner part of the core is not affected as a result of the experiment. This is also observed in the 30 day-experiment.

Table 5. 8 In-depth SEM Analysis of Core #4 (Inner part)

	Prior to experiment (inner part)	After experiment (inner part)
	Element Concentration (%)	
Al	2.48	6.79
Si	15.05	18.76
K		1.91
Ca	80.68	70.12
Fe		2.42
Mg	1.79	

Table 5. 9 In depth SEM Analysis of Core #4 (Near to Surface)

	Prior to the experiment	after the experiment (site_1)	after the experiment (site_2)	after experiment (site_3)
	Element Concentration (%)			
Al	1.45		1.64	
Si	5.76	7.94	13.33	3.52
S	15.35			
Ca	60.14	20.69	22.83	19.7
Fe	14.76	51.84	45.16	55.33
Mg		3.06	2.2	3.53

Table 5. 10 Top Surface SEM Analysis of Core #5

	Prior to the experiment	after the experiment (site_1)	after the experiment (site_2)
	Element Concentration (%)		
Al	0.35	1.03	1.79
Si	14.44	6.9	22.81
Ca	84.67	23.56	22.69
Fe	0.54	63.85	48.9
Mg		2.1	1.94

Table 5.9 illustrates the near to surface in depth SEM analysis of the core #5 to see any change in element concentration by comparing the prior to and after the experiment concentrations. Three different sites of the near to surface SEM/EDX analyses are performed on the core #4. Table 5.10 shows the top surface SEM analyses of the core #5 prior to and after the static experiment. Two different sites of the top surface SEM/EDX analyses are performed on the core #4. From the both tables above, there is large increase in Fe element concentration. It may be explained due to the corrosion of the core holder equipment subject to acid fluid for long time. Moreover, it is seen in Table 5.9 and Table 5.9, Ca element is significantly reduced, which shows calcite dissolution.

Table 5. 11 Water Analysis of the 100 day experiment

	Prior to the experiment	After the experiment
	(ppm)	
Sodium	693.2	616.7
Calcium	41.92	335.2
Magnesium	47.36	52.94
Iron	1.19	0.591
Sulfate	15	202.58
Chloride	725	642.75
Bicarbonate	613	628

Table 5.11 shows initial and final compositions of formation water of the 100 day-experiment. Ca ion increase is seen here again showing that calcite was again dissolved. Sulfate amount in water is increased from 15 ppm to 202.58 ppm during the experiment. However, there is no reasonable explanation for this sulfate increase.

Table 5. 12 Comparison of water analyses of 30- and 100- day experiments

	Prior to the 30-day experiment	After the 30-day experiment	Prior to the 100-day experiment	After the 100-day experiment
	(ppm)		(ppm)	
Sodium	693.2	752.7	693.2	616.7
Calcium	41.92	382.2	41.92	335.2
Magnesium	47.36	152.1	47.36	52.94
Iron	1.19	0.443	1.19	0.591
Sulfate	15	117.18	15	202.58
Chloride	725	903.26	725	642.75
Bicarbonate	613	619	613	628
Silicon		16.14		

According to Table 5.12, Ca^{+2} ion concentration is increased up to 340.28 ppm from its initial concentration of 41.92 ppm after 30 day experiment. In the 100-day experiment, the Ca^{+2} ion concentration is 335.2, which is increased compared to its concentration of prior to the experiment. However, when the Ca^{+2} concentration of 335.2 is compared to that of Ca^{+2} concentration in the 30- day experiment, it is lower in amount by 47 ppm. However, this is interpreted that it does not explain that calcite was re-precipitated in the 100- day experiment. On the other hand, calcite is effectively dissolved in earlier time of the experiment as in 30- day experiment and it no longer dissolves after that period.

There is no Si ion detected in the water after the 100-day experiment. Na^+ and Cl^- ion concentrations are decreased, which may be due to their coating on the core surface in 100 day experiment while their concentrations in the 30- day experiment are increased.

5.2 Dynamic Experiment

Before carrying out the dynamic (flow) experiment, the remaining cores (#1, #2, #3 and #6) from Sayindere formation were ground to a powder of less than 60 mesh (i.e 250 micron). The reason of grinding is that the original Sayindere cores were very impermeable and it is impossible to maintain flow through them.

Moreover, grinding of solid cores increases the rate of reaction in three ways. The first effect is to increase the surface area of the grains which allows a larger interface for reaction; the second is that the creation of fresh surfaces often results in high energy sites being exposed; and the third effect is that grains which were previously armoured by other grains, now have surfaces which would be in direct contact with the aqueous phase (Gunter et al., 1997).

Before the dynamic experiment, XRD analysis was planned to carry out for the exact mineral identification and mineral composition. To carry out the XRD analysis, acid treatment was previously performed to remove all carbonate out of the sample. The carbonate was removed by acid treatment technique. 10 g of grinded core sample was chosen for the XRD analysis as representative of the core mineral using Coning and Quartering method.

5.2.1 Carbonate Removal

10 g of the grinded cap rock sample was put in a 500 mL beaker and 100 mL of NaOAc buffer was added into the beaker. To bring the clay into suspension, the sample was stirred by a glass rod. The suspension was digested in near boiling water bath for 30 minutes with occasional stirring. The suspension was centrifuged for 10 minutes at 6000 rpm. The total 4 washings with NaOAc were done to remove all the carbonate content in 10 g cap rock sample. After the remaining part of the sample was air-dried, it weighed. The weight of this sample was 2.4 g, which is the weight of the non carbonate

sample, assuming all the carbonate content of the sample was washed out during the acid treatment. Therefore it was assumed that all the removed 7.6 g was carbonate.

5.2.2 Clay type determination by XRD Analysis

XRD Analysis was carried out at the Department of Geological Engineering, METU. The Thin Section analysis was previously done to for mineral identification and its composition. However, Thin Section analysis can not reveal the type of clay and its composition. Therefore, XRD analysis was carried out to determine the type of the clay and composition.

After the carbonate removal, 2.4 g out of 10 g of grinded sample was available for XRD analysis. 2.4 g of sample was put into a beaker and filled with pure water and then a small amount of acid was added to make sure that the cemented particles are separated from each other. Afterwards, mixture was stirred for some time and left for 8 hours, which is the start time of clay deposition and end of all other minerals deposition. That's why, after 8 hours, the clay suspended in the upper 10 cm part of the beaker was separated by a special pipette and collected into a smaller beaker.

The collected clay particles were sent into XRD Laboratory to determine the type of clay. The XRD analysis of the original powder is firstly carried out (Figure H.1). After the acid treatment is performed to remove the calcite, the XRD analysis is again carried out. Also, 4 XRD analyses of the air dried, waited in ethylene glycol, dried at the 300 °C and dried at 550 °C of the collected clay sample are separately done. It is found that the clay type is kaolinite since the clay was not observed in the sample after drying it at 550 °C by XRD Analysis (Türkmenoğlu, 2010). Results of XRD analysis are given Appendix H.

5.2.3 Mineral Composition of Sayindere core

During the XRD Analyses, there was still calcite revealed. From Figure H.2, it is seen that there is calcite peak at the value of 3.031. Therefore, this shows that all carbonate could not be removed by acid treatment although the acid treatment was repeated four times. This results in that the amount of calcite is more than 7.6 g in 10 g of representative sample. However during the simulation study it is assumed calcite composition is 76 % in the Sayindere core.

To find the amount of kaolinite, every 8 hours, the suspended clay was collected from the beaker by a special rod and the beaker was again filled with water and stirred for a few seconds. For a whole week, this procedure was repeated to collect all clay from the beaker until no more clay suspension was observed. Afterwards, the water was removed from the beaker, leaving the remaining minerals except for clay (kaolinite) and calcite. The remaining mineral is found as quartz since, from the XRD analysis, quartz was observed in the sample powder. Thin Section Analysis supports that the remaining mineral is quartz.

The remaining mineral, quartz, after the water removal, was air dried and weighed. Its weight was 2.27 g. So it was calculated that remaining 0.13 g was kaolinite removed by the suspension method. The final mass composition of Sayindere core by XRD Analysis is given in Table 6.1

Table 5. 13 Mineral composition of Sayindere cap rock

Mineral Composition	(mass percentage)
calcite	76 %
quartz	22.7%
kaolinite	1.3%

5.2.4 Dynamic Experimental set-up

As mentioned earlier, in dynamic experiment, the remaining cores were ground into 60 mesh size (250 micron) and packed into a core holder and CO₂ saturated- synthetically prepared water was injected through the packed core. Since the cores were very impermeable, they were ground so that a flow could be maintained throughout the experiment. The experimental condition was at a temperature of 90 °C and an injection pressure of 75 bar, representing the field condition.

The scheme of the dynamic experiment is shown in Figure 5.4. Technical specifications of the experimental equipments are listed in Table 5.14. The core holder's and mixing cylinder's dimensions are given Tables 5.15 and Table 5.16, respectively.

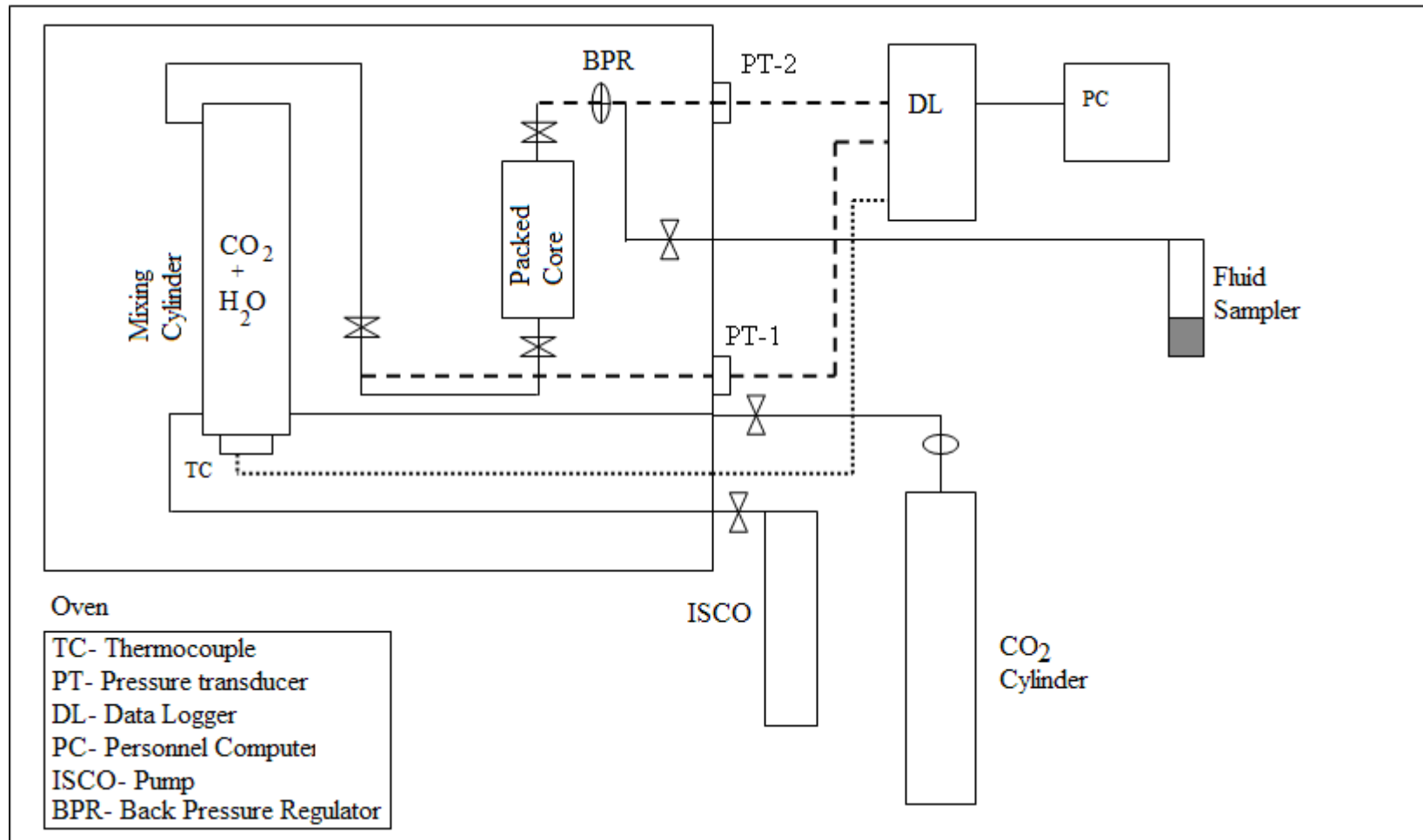


Figure 5. 4 The scheme of the dynamic experiment

Table 5. 14 Technical specifications of the dynamic experimental equipments

Experimental Apparatus	Specification
Pressure Transducers	0-3000 psia 4-20 mA
Thermocouple(PT-100)	-20 °C - +150 °C
ISCO 500D Pump	Cylinder Capacity: 507.38 ml Pressure Range: 10psi-3750 psia Refill or Depressurization rate: 1μl/min-204 ml/min at any pressure 0-3750 psi
CO2 Cylinder	40 lt, 65.8 kg 250 bar
Core Holder	High pressure Steel
Mixing Cylinder	High pressure Steel
Dispatch Oven	10-400 °C
Elimko 680 Data Logger	Input types: Thermocouple, resistance Thermocouple, Voltage, Current Operating Temperature: -10°C - +55°C Memory: EEPROM max. 10 ⁵ writing

Table 5. 15 Core holder dimension

Diameter (cm)	2.54
Length (cm)	5.5
Volume (cm ³)	27.85

Table 5. 16 Mixing cylinder dimension

Diameter (cm)	6.5
Length (cm)	41
Volume (cm ³)	1360

CO₂ was sent into the mixing cylinder at a pressure of 200 psia after the temperature oven was raised to a temperature of 90 °C. So the amount of CO₂ can be calculated as follows.

Calculation of CO₂ amount sent to the mixing cylinder

$$\text{Mixing cylinder : } v = \pi r^2 h = \pi \left(\frac{6,5}{2} \right)^2 * 41 = 1360 \text{ cm}^3$$

$$PV = znRT$$

$$n = \frac{PV}{zRT}$$

For CO₂, the critical temperature and pressure are:

$$T_c = 31.1 \text{ } ^\circ\text{C}$$

$$P_c = 73 \text{ atm}$$

So the reduced critical temperature and pressure:

$$T_r = \frac{T}{T_c} = \frac{90 + 273}{31.1 + 273} = 1.19$$

$$P_r = \frac{P}{P_c} = \frac{13.8}{73} = 0.186$$

$$z \approx 0.965$$

Given that,

$$R = 8.314472 \text{ cm}^3 \text{ MPa K}^{-1} \text{ mol}$$

$$P = 200 \text{ psia} = 1,379 \text{ MPa} = 13.58 \text{ bar}$$

$$T = 90^\circ \text{C} = 363.15^\circ \text{K}$$

$$n = \frac{1379 * 1360}{0965 * 8.314472 * 363.15} = 0,642 \text{ mol}$$

The amount of CO₂ sent to the mixing cylinder is 0.642 mol.

Assuming as pure water,

1kg of water= 1000cc

density of water= 1g/cc

From the Figure 5.5,

At 90°C and 75 bar,

CO₂ solubility= 3.0 lb. CO₂ /100lb. H₂O

1 lb = 0,45359 kg

3 lb. CO₂ = 1,36077kg = 1360.77 g

44g of CO₂ = 1mol of CO₂

Therefore,

3 lb. CO₂ / 100 lb. H₂O = 30,9266mol of CO₂ / 45359 cc of H₂O

So in 1360 cc of water, 0, 9273 mol of CO₂ will dissolve. So the injected 0.642 of mole CO₂ will be completely dissolved in the water.

5.2.5 Dynamic Experimental procedure

CO₂ was sent into mixing cylinder and then the synthetic formation water was injected into the mixing cylinder. CO₂ saturated water was intended to be used in this flow through experiment. It was waited until maximum of the sent CO₂ was dissolved into formation water at the pressure of 75 bar. The reason why it was waited for the CO₂ to dissolve is that maximizing aqueous CO₂ concentration will maximize the degree of fluid-rock reaction. It was observed that the pressure of the experiment system was decreasing as CO₂ dissolved into the formation water. The pressure decrease is the indicative of a decrease in the volume of the system due to the phase change of injected gas CO₂ into dissolved aqueous species. So, the system pressure was raised to the pressure of 75 bar, by slowly injecting the formation water into the mixing cylinder. Then, once it was made sure that no more CO₂ was dissolving into the formation water by observing the pressure recording of the system (Figure 5.6). After a week waiting, the system pressure came into stability around 75 bar.

Afterwards, the fluid was injected into the packed core by opening the valve. The formation water was being injected from the syringe pump at the pressure of 75 bar to maintain the 75 bar -system pressure. There is Backup Pressure Regulator (BPR) fitted at the top of the core holder and the BPR was set at the pressure of 74 bar. So, once the outlet pressure reached the pressure of 74 bar, the BPR automatically was opened and the fluid started discharging out of the core holder and it was collected into a beaker. When the amount of the discharging fluid reached 80 cc, it was taken into another beaker in order to make the fluid analyses. The amount of 80 cc was the minimum amount to be able to carry out the fluid chemistry analyses: ICP-OES, IC and titration. The temperature, the inlet and outlet pressures of the core holder were recorded. As shown in Figure 5.7, the pressures and temperature are all constant throughout the dynamic experiment.

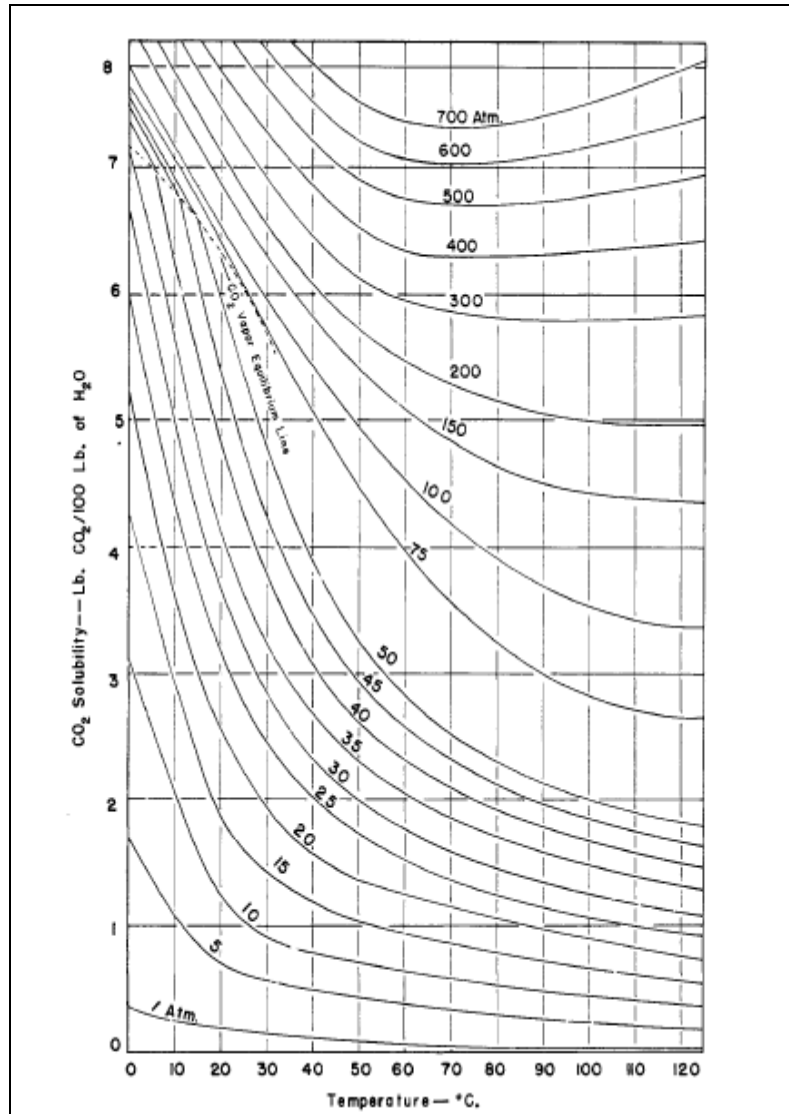


Figure 5.5 CO₂ solubility (Dodds et al, 1956)

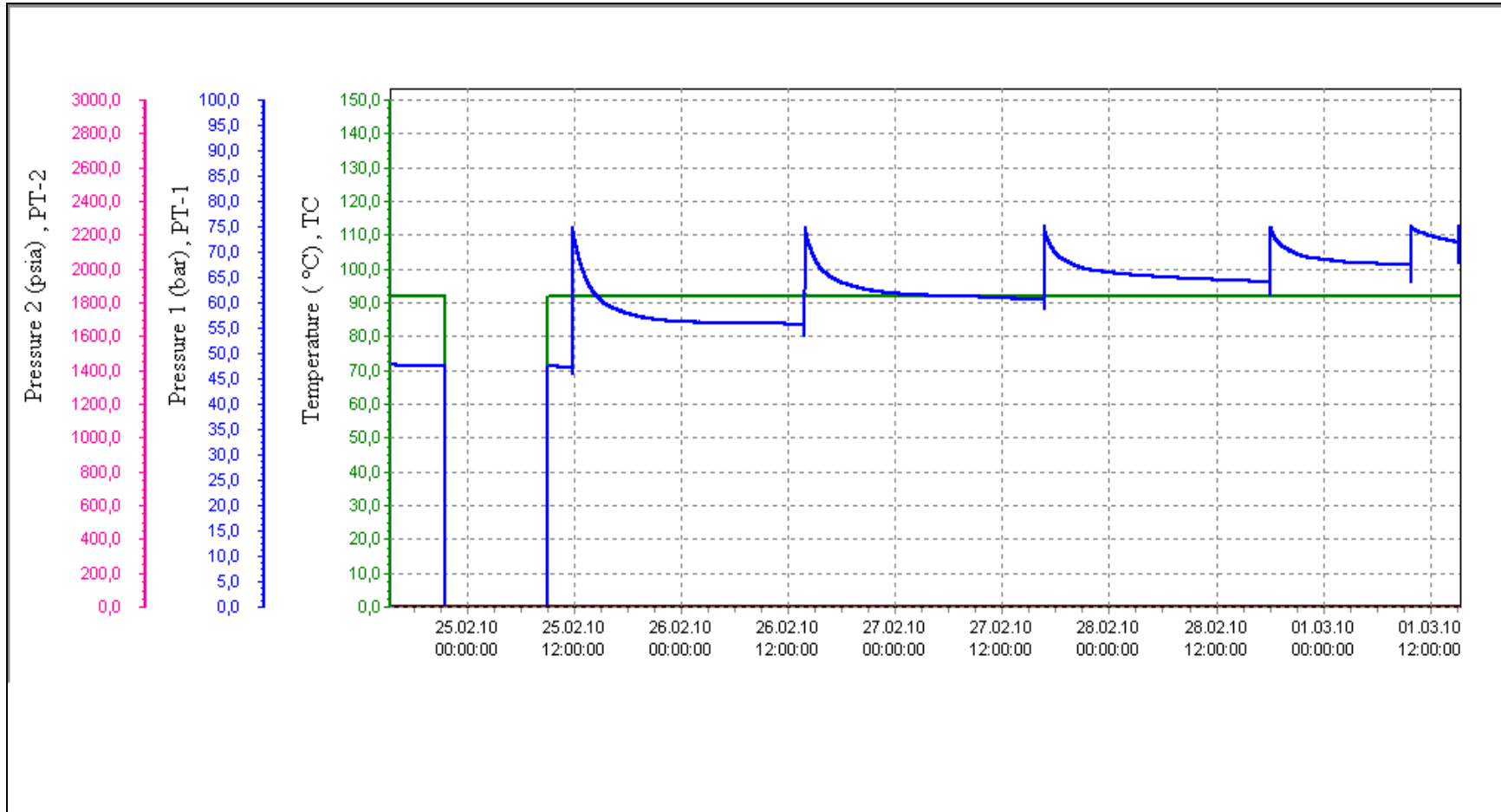


Figure 5. 6 Pressure stabilization during dissolution of CO₂ in the brine

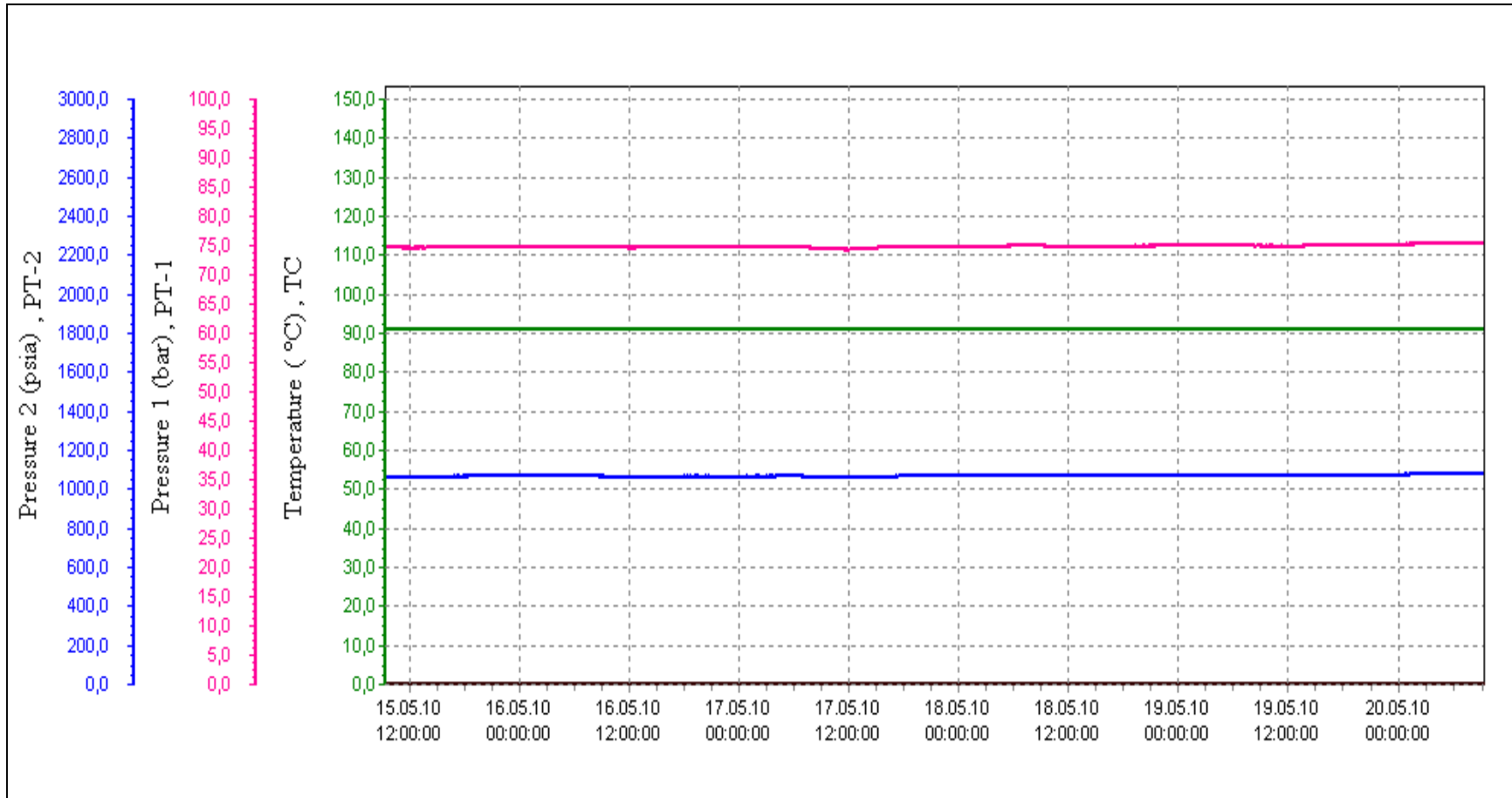


Figure 5. 7 Pressure and temperature recordings of the dynamic experiment (5 days)

5.2.6 Results and Discussion of the Dynamic Experiment

The ICP-OES analysis was carried out to detect the cations at the Central Laboratory of Middle East Technical University (METU). IC analysis was made to determine the anions at the Water Laboratory of Petroleum Research Center, METU. Table 5.17 gives the results of these fluid chemistry analyses.

Table 5. 17 Fluid Analysis of the Discharged Water

	ppm (prior to the exp.)	ppm (after 23 days)	ppm (after 75 days)	ppm (after 99 days)
Sodium	519.0 ± 2.1	602.6±11.2	509.4±9.2	568±6.6
Calcium	37.5 ± 0.6	219.9±3.1	87.95±1.73	35.29±0.01
Magnesium	45.0 ± 0.3	52.97±0.33	44.99±0.33	52.63±0.96
Iron	0.05 ± 0.002	0.081± 0.001	0.146±0.004	0.676±0.004
Sulfate	14.0806	477.3	26.79	25
Chloride	746.8860	723.25	840.58	979
Bicarbonate	658	74	866	732
Normal carbonate	-	444	-	
Silicon		21.72± 0.19	17.58±0.16	5.55±0.03
Aluminum		-	-	-
pH (24 °C)	7.789	8.360	6.678	5.928

As seen in Table 5.17, after 23, 75 and 99 days, fluid analyses were carried out to investigate the dissolved species in the water. Different from the initial dissolved ions, there is Si ion in the 23, 75 and 99 day- fluid analyses. This Si ion may come from the dissolution of Si- bearing primary minerals such as kaolinite and quartz. However, there is no Al ion detected in the fluid analyses. Thus, it is hard to say that kaolinite is dissolved as a result of the CO₂ saturated- cap rock interaction in the experiment.

Ca⁺² ion is increased in the after 23- day analysis from its initial concentration of 37.5 ppm up to around 220 ppm and then in the following two analyses (after 75 and 99 days) Ca⁺² ion concentration decreased to 87.95 and 35.29, respectively. As shown in Table 5.17, at the end of 99 days, Ca⁺² ion concentration is nearly same as that of the Ca⁺² of injected water. This is interpreted as calcite is dissolved in earlier time, like 23 days, of the experiment and the calcite available for reaction in the core is decreased due to injected water sweeping the dissolved elements to production end. At the end of 99 days, it is anticipated that Ca⁺² available for reaction is depleted and Ca⁺² produced is equal to injected Ca⁺².

CHAPTER 6

NUMERICAL MODELING OF CO₂-FLUID-ROCK INTERACTION

When assessing the impact of the long term CO₂ storage on geological formations, numerical modeling plays a crucial role geochemical reactions are very slow and laboratory work under the field conditions is limited in time and space. Once CO₂ is dissolved in water, it makes water acidic and it can change the physical and chemical properties of the well, the reservoir and cap rock and create the environmental and economic risk of CO₂ storage projects in geological formations (Gaus et al, 2008).

Today's numerical modeling for CO₂ storage applications can be divided into three categories:

- hydrodynamic modeling simulating structural, residual gas and dissolution trapping process
- geochemical modeling simulating batch geochemical reactivity (closed system without any fluid flow)
- reactive transport modeling combining the two previous types of simulation

Hydrodynamic modeling

Hydrodynamic simulation is efficiently performed by black oil reservoir simulators. Lindeberg and Bergmo (2003) have conducted simulation of the upward migration of the CO₂ bubble in the Utsira formation using the code ECLIPSE. In TUBITAK KAMAG (2009) project, the code ECLIPSE was also used for modeling CO₂ storage in the Caylarbasi field, which is an oil field located in southeastern Turkey.

Batch geochemical modeling

Batch geochemical modeling gives the simulation of geochemical fluid-rock interactions occurring within in the formation when formation water is saturated with CO₂. No flow is considered during batch geochemical simulation.

The first batch modeling works were carried out by Gunter et al. (2007), Gaus et al. (2005). They used the code PHREEQC developed by the United State Geological Survey (USGS) to perform a long-term batch geochemical simulation of two natural CO₂ analogues at Montmiral (France) and Messokampos (Greece). In this work, the code PHREEQC is also used to equilibrate the injected CO₂ with the synthetic formation water.

Reactive transport modeling

Reactive transport modeling is the most realistic modeling technique to quantify the long-term fate of CO₂. The code ToughReact is an extension of Tough2 V2, which has been upgraded by introducing reactive geochemistry into the Tough2 framework of multi-phase fluid and heat flow. Both dissolution and precipitation processes are integrated in this code with feedback on porosity and permeability changes.

Apart from the ToughReact code, there are several other codes, namely; SIMUSCOPP, STOMP, HYTEC, CHEMTOUGH, GEM-GHG, available in the market.

6.1 Reactive transport code TOUGHREACT

In this study, the reactive transport code, TOUGHREACT was used to assess the geochemical alterations in the Sayindere caprock.

The code TOUGHREACT has been developed as a comprehensive non-isothermal multi-component reactive fluid flow and geochemical transport simulator to investigate geologic systems and environmental problems. A number of subsurface thermo-

physical- chemical processes are considered under various thermo-hydrological and geochemical conditions of pressure, temperature, water saturation, and ionic strength.

This code can be used in 1-, 2- or 3- dimensional porous and fractured media with different physical and chemical properties. The code TOUGHREACT can accommodate any number of chemical species present in liquid, gas, and solid phases. A variety of equilibrium chemical reactions such as aqueous complexation, gas dissolution/exsolution and cation exchange are considered. Geochemical reactions can take place either subject to local equilibrium or kinetic conditions. Changes in porosity and permeability due to geochemical reactions can be considered.

TOUGHREACT provides the following different TOUGH2 fluid property or EOS (equation-of-state) modules:

- EOS1 for water or two waters with typical applications to hydrothermal problems
- EOS2 for multiphase mixtures of water and CO₂ also with typical applications to hydrothermal problems
- EOS3 for multiphase mixtures of water and air with typical applications to vadose zone and nuclear waste disposal problems
- EOS4 that has the same capabilities as EOS3 but with vapor pressure lowering effects due to capillary pressure
- EOS9 for single phase water (Richards. equation) with typical applications to ambient reactive geochemical transport problems
- ECO2 for multiphase mixtures of water, CO₂ and NaCl with typical applications to CO₂ disposal in deep brine aquifers.

TOUGHREACT uses a sequential iteration approach. The fluid velocities and phase saturations are used for chemical transport simulation, after solution of the flow equations. The chemical transport is solved on a component basis. The resulting concentrations obtained from the transport are substituted into the chemical reaction

model. The system of mixed equilibrium-kinetic chemical reaction equations is solved on a grid-block basis by Newton-Raphson iteration. The chemical transport and reactions are iteratively solved until convergence. (Xu et al, 2008).

6.2 PETRASIM

Petrasim is an interactive pre-processor and post-processor for the TOUGH family of codes. It helps users develop models faster and view results. PETRASIM helps users guide through the steps of a TOUGHREACT simulation as follows (Petrasim User's Guide, 2008):

- Specify the TOUGHREACT and the proper EOS
- Select the global properties to be used in the simulation
- Define the material properties
- Define the initial conditions
- Set the solver parameters in TOUGHREACT menu
- Set the output options in TOUGHREACT menu
- Specify the chemical components such as primary species, aqueous complexes, gaseous species and minerals
- Define geochemical zones
- Create the model boundary
- Create the grid
- Define the boundary condition
- Define solution and output controls
- Associate the geochemical zones with the grid
- Save the model and run the simulation
- View the results

CHAPTER 7

REACTIVE TRANSPORT MODELING OF THE DYNAMIC EXPERIMENT

Using the Petrasim/ToughReact, the reactive transport modeling of the dynamic experiment is also carried out. For the modeling study, the Sayindere cap rock formation water is taken to be same as the reservoir formation water of the Caylarbasi field. Caylarbasi reservoir formation water is modified by adding AlO_2^- , SiO_2 (aq), O_2 (aq) aqueous ions into the chemical species in a way that the cap rock minerals and cap rock fluid chemistry are consistent.

7.1 Geometric model and the cap rock properties

Simple 2-D radial model is used to simulate the CO_2 saturated fluid and Sayindere cap rock interaction in the dynamic experiment as explained in Chapter 6.2 of this thesis. The model boundary is 0.0127 m in radial direction (x-direction) and 0.055 m in depth, z-direction, which represents the packed core dimension in the dynamic experiment. The model is composed of 4 cells; 1 cells in x- direction and 4 cells z- direction since the model defined here is quite small. Figure 7.1 illustrates the schematic representation of the model used in this study.

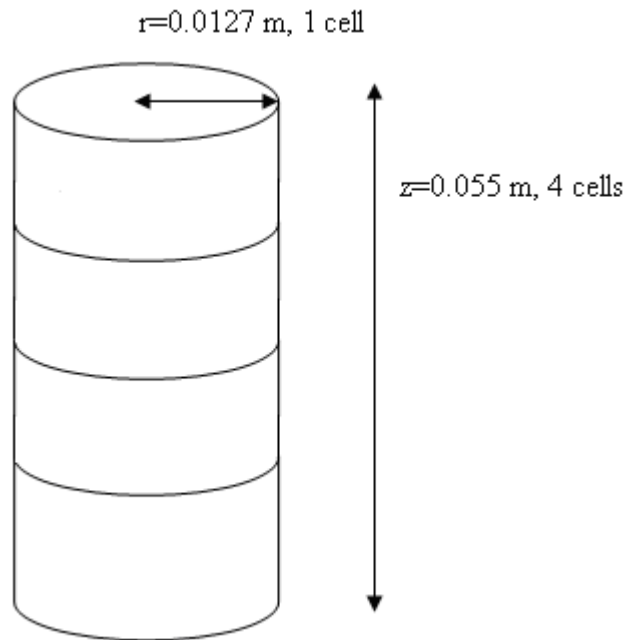


Figure 7. 1 Schematic representation of the model

The Sayindere core properties are given in Table 7.1. No capillary pressure effect is taken into account. The porosity and permeability were previously determined by running an experiment in which an unconsolidated pack was used. This unconsolidated pack was prepared by grinding a core into same mesh size as the Sayindere core was grinded in the dynamic experiment. The porosity and permeability calculations from this experiment are given in Appendix I. Formation heat conductivity and rock grain specific heat were taken to be equal to default values of the software.

Table 7. 1 Physical Properties of the Sayindere formation

Porosity (fraction)	0.28
Permeability (m ²)	1.8*10 ⁻¹⁴
Rock grain density (kg/m ³)	2695
Formation heat conductivity (W/m °C)	2.0
Rock grain specific heat (J/kg °C)	1000
Residual liquid saturation (fraction)	0.15
Liquid saturation (fraction)	1.0
Residual gas saturation (fraction)	0.0

The value 2695 kg/m³ of rock grain size density was calculated based on the weighted average of the mineral composition of the Sayindere formation, which is 0.76 for calcite, 0.227 for quartz and 0.013 for kaolinite. Calcite, quartz and kaolinite rock grain densities are taken as 2710, 2650 and 2600 kg/m³, respectively.

7.2 Formation mineralogy

Sayindere formation is known to be quite homogeneous. From the mineral investigation analyses, it revealed that Sayindere formation is composed of mainly calcite (76%) and quartz (22.7 %) and small amount of kaolinite (1.3 %).

Minerals allowed to precipitate as secondary phases during CO₂ injection are taken as magnesite (MgCO₃), siderite (FeCO₃), dolomite (CaMg(CO₃)₂) and hematite (Fe₂O₃). Magnesite, siderite and dolomite are the carbonates that can be precipitated due the CO₂ saturated water and the rock interaction. The reason of choosing hematite as a secondary phase that might be precipitated is that hematite was revealed in the thin section analysis (Figure B.6) although it was not revealed in the XRD analysis. Moreover, Fe³⁺ and O₂ (aq) aqueous ions are available in the formation water.

Mineral composition, as a required input in the TOUGHREACT software, is given in Table 7.2. The calcite, quartz and kaolinite mass fraction are from the XRD analysis. From Table 7.2, the secondary phase mineral mass compositions are taken to be equal to 0 since they are not the primary minerals of the Sayindere core but they might be precipitated due to the injection CO₂ saturated water into the core.

Table 7. 2 Mineral mass composition of Sayindere core used in this study.

Mineral Composition	(mass fraction)
Calcite	0.76
Quartz	0.227
Kaolinite	0.13
Magnesite	0.0
Siderite	0.0
Dolomite	0.0
Hematite	0.0

The mineral volume fraction composition (not the mass fraction) is required for the simulation analysis. Therefore, the mass fraction composition was converted into volume fraction, which is given in Table 7.3.

Table 7. 3 Mineral volume composition of Sayindere core used in this study

Mineral Composition	(mass fraction)	Density(g/cc)	Volume Fraction
Calcite	0.76	2.710	0.756
Quartz	0.227	2.650	0.231
Kaolinite	0.13	2.600	0.013
Magnesite	0.0	1.740	0.0
Siderite	0.0	3.740	0.0
Dolomite	0.0	2.830	0.0
Hematite	0.0	5.040	0.0

Table 7.4 shows the grain size and the surface area of each mineral. As seen in Table 7.4, grain sizes of all mineral are calculated to be 0.00025 m from the grinding the core into 250 micron. Surface areas are taken from PETRASIM TOUGHREACT example Manual (2008).

Table 7. 4 Mineral grain size and surface area

Mineral	Vol. Frac.	Grain size(m)	Surface area(g/cm ²)
calcite	0.756	0.00025	9.8
hematite	0.0	0.00025	12.87
kaolinite	0.013	0.00025	151.63
magnesite	0.0	0.00025	9.8
quartz	0.31	0.00025	9.8
siderite	0.0	0.00025	9.8
dolomite	0.0	0.00025	9.8

Table 7.5 gives the rate constant at room temperature and the activation energy of each mineral. These values are again taken from PETRASIM TOUGHREACT example Manual (2008). The temperature dependence of the reaction rate constant is expressed via an Arrhenius equation. The rate equation and the Arrhenius equation are given in Appendix J.

Table 7. 5 Kinetic parameters for mineral dissolution and precipitation

Mineral	$k_{25} (mol \cdot cm_{mineral}^{-2} \cdot sec^{-1})$	E_a
calcite	1.6e-09	41.87
hematite	2.514e-13	66.20
kaolinite	6.918e-14	22.20
magnesite	4.571e-10	23.50
quartz	1.023e-14	87.70
siderite	1.26e-09	62.76
dolomite	2.951e-08	52.20

7.3 Formation water of Sayindere cap rock

As mentioned above in the Chapter 7, for the Sayindere formation water, the Caylarbasi reservoir formation water is modified by adding AlO_2^- , $\text{SiO}_2(\text{aq})$, $\text{O}_2(\text{aq})$ aqueous ions into the chemical species already available in the Caylarbasi reservoir formation water in a way that the cap rock minerals and cap rock fluid chemistry are consistent.

In dynamic experiment, CO_2 saturated water was used. Therefore, it was assumed that all 0.642 mole of injected CO_2 was dissolved in the synthetic formation prior to the dynamic experiment. Using the code PHREEQC 2.18, the CO_2 was equilibrated with the initial formation water at the pressure of 75 bar and the temperature of 90 °C at the given fixed volume of 1340 cc. The results of the PHREEQC simulation are given in Appendix K. The resulting CO_2 saturated formation water composition is given Table 7.6. As seen from the Table, the first guess for the concentration, CGUESS for each species is taken to be equal to 10 % of actual concentration, CTOT.

Table 7. 6 Chemical composition of formation water (mol/kg)

	CGUESS	CTOT
AlO_2^-	1.89E-12	1.89E-11
Ca^{+2}	9.375E-5	9.375E-4
Cl^-	0.002111	0.02111
Fe^{+2}	8.98E-8	8.98E-7
H^+	7.26E-6	7.26E-6
H_2O	1.0	1.0
HCO_3^-	0.01694	0.1694
Mg^{+2}	0.0001855	0.001855
Na^+	0.002262	0.02262
$\text{O}_2(\text{aq})$	1.89E-12	1.89E-11
$\text{SiO}_2(\text{aq})$	1.89E-12	1.89E-11
SO_4^{-2}	1.469E-5	1.469E-4

7.4 CO₂ Injection into the Sayindere packed core

7.4.1 CO₂ Injection simulation scenario

CO₂ saturated formation water is injected into the bottom cell at the constant rate of $1.68 \cdot 10^{-3}$ cc/min ($2.8 \cdot 10^{-8}$ kg/s) and fluid was being produced from the top cell at the same rate. The rate of injection was determined from the fact that approximately total 240 cc of water was produced in 99 days, duration of the dynamic experiment.

In this simulation work, the CO₂ saturated water is injected into the bottom cells and produced from the top cells of the model at the same constant rate. However, in the dynamic experiment, the fluid was being injected at the constant pressure of 75 bar from the ISCO pump and the fluid was being discharged out of the packed core under 1 bar pressure difference.

Since CO₂ saturated water is being injected, the EOS1 module for a single phase is used. Maximum simulation time is 99 days, which is the dynamic experiment duration. The time step for the simulation is one second. Figure 7.2 shows the z-x cross section of the model. As shown in Figure 7.2, the grid consists of 4 cells; 1 in r- direction and 4 in z- direction. The bottom cells are the source; that is injection point. The top cells are the sink where the fluid is being produced.

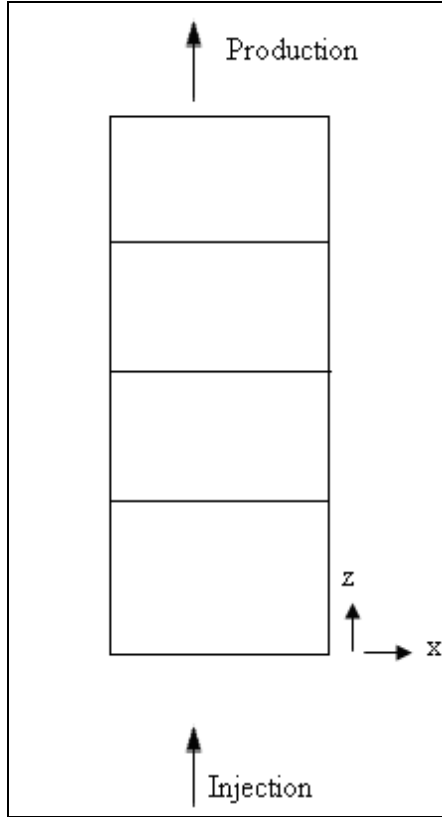


Figure 7. 2 Z-X cross section of the grid system

7.4.2 CO₂ Injection simulation results and discussion

The simulation was run. The results of the simulation work by TOUGHREACT are given in Appendix L.

When the time evolutions of chemical species in the formation water are examined, the most chemical species concentrations except for O₂(aq) are stabilized after around 2.0 E6 seconds (~ 23 days). From Figure L.3, the AlO₂⁻ ion concentration increased at the beginning of simulation and then stabilized. The increase of this species may come from the dissolution of the kaolinite mineral available in the Sayıdere core. The kaolinite mineral dissolution is observed throughout the simulation time (see Figure L.17). There is approximately 1.05 e-7 decrease in the volume fraction of the kaolinite.

As seen in Figure L.4, the Ca^{+2} ion concentration is increased up to $1.6 \text{ e-}4$ mol and then stabilized again like AlO_2^- ion. The Ca^{+2} ion increase at the beginning of the simulation may be explained in that way the initial dissolution process of the calcite mineral increased the Ca^{+2} ion concentration in the formation water. From Figure L.15, the calcite is firstly dissolved since the change in volume fraction is $-9.2\text{e-}6$. However, the change in volume fraction of the calcite increased up to $-4.0\text{e-}6$ from $-9.2\text{e-}6$, which shows that the calcite is re-precipitated.

Fe^{+2} ion concentration firstly increased and then decreased throughout the simulation (see Figure L.6). On the other hand, there are the hematite and siderite precipitation at the beginning of the CO_2 saturated water- the Sayindere cap rock minerals interaction simulation (see Figure L.16 and Figure L.20). Thus, Fe^{+2} ion may be firstly consumed by these precipitation reactions.

Mg^{+2} ion concentration is increased in a same way Fe^{+2} ion concentration (see Figure L.10). This increase may be due to the precipitated magnesite mineral dissolution (see Figure L.18).

As for the SiO_2 (aq) ion in the water, this ion concentration is firstly increased and then stabilized (see Figure L.13). This increase in the amount of the SiO_2 (aq) concentration may be related to the dissolution of the quartz, which is one of the primary minerals in the Sayindere cap rock. From Figure L.19, the quartz is continuously decreased during the simulation like the kaolinite.

From Figure L.21, dolomite is precipitated. This precipitation process consumes the Ca^{+2} , Mg^{+2} ions in the water. That may be why, even the calcite and precipitated magnesite continue to dissolve, and there are no increases in these ions during the simulation period.

The changes in the volume fractions of the minerals are very small indeed here. The simulation period is very short, 99 days, representing the dynamic experiment duration. The geologic mineral reactions normally take thousands and millions years to proceed. Moreover, the model is very small since it represents the core scale in the dynamic experiment as previously mentioned. If the model used in this study were in field scale and the simulation period were longer, the mineral evolution changes could be larger in amount.

Figure L. 22 and Figure L.23 show the time evolution of porosity and permeability of the Sayindere core in the simulation study. As the result of the CO₂ saturated- the cap rock interaction, the porosity and permeability are both decreased due to the new mineral precipitations such as siderite, magnesite and dolomite. The decreases are very small in amounts. The porosity is decreased by 0.01% and, on the other hand, the permeability is decreased by 0.03%. The porosity change is calculated as volume change as the results of the precipitation and dissolution in the code TOUGHREACT. The permeability change related with porosity change is calculated using simplified cubic law. The porosity and permeability change calculation formulas are given in Appendix M.

If, porosity and permeability decreases are observed in the simulation of injection of the CO₂ saturated water into the Sayindere core, this means that the Sayindere cap rock integrity will be enhanced and there will not be any possible leakage paths induced by the geochemical reactions due to the CO₂ saturated- rock interaction.

7.4.3 CO₂ Injection stop and investigating the CO₂-saturated water- cap rock mineral interaction in longer time period, 25 years

The CO₂ injection is stopped after 99 days of injection and the simulation is continued for further 25 years to monitor the cap rock mineralogical and the water chemistry evolutions and the long term effect on the porosity and permeability of the packed Sayindere core.

7.4.3.1 Results and discussion of the continuation run without CO₂ injection

The results of the continuation run are given in Appendix N. Simulation study of the investigation of the geochemical evolution of the model defined during 25 years after the CO₂ injection is stopped shows that all dissolved species are stabilized or in other words, reached to the equilibrium states after some time, 250 days (Figure N.2-N.14).

Calcite, hematite and kaolinite are firstly dissolved and then re-precipitated (Figure N.15-N.17). On the other hand, magnesite and quartz are continuously dissolved (Figure N. 18-N.19). In case magnesite, it is totally dissolved out. Actually it is one of the secondary minerals, which is expected to precipitate due to CO₂ saturated water injection into the packed core minerals of the Sayindere cap rock. It is precipitated indeed during the injection process (Figure L. 18), however but dissolved back as given in the simulation results of its long term evolution. In Figure N.20, there is no change in the siderite mineral volume fraction in 25 years of monitoring. For the dolomite mineral, it is continuously precipitated during this period (Figure N. 21).

From Figure N. 22- N.23, it is observed that the porosity and permeability are increased by 0.001% and 0.004 %, respectively as the result of the long term evolution of the rock minerals after the CO₂ injection is stopped. During the injection of the CO₂ saturated water, the porosity and permeability are decreased (Figure L.22-L.23), which were good

thing for the cap rock integrity. However, the increase observed in the continuation simulation after the injection is stopped is a unwanted thing in the monitoring and risk assessment of the CO₂ storage since the porosity and specially, the permeability increase in the cap rock can trigger possible already existing fractures in the rock and this may create leakage paths for the injected CO₂ into groundwater sources and even into the atmosphere back.

CHAPTER 8

RESULTS AND DISCUSSION

This thesis work is carried out to investigate the possible geochemical reactions induced by CO₂- water-rock interaction and these reactions' effect on the cap rock integrity. Both experimental and modeling and studies are performed. In modeling and simulation work, the reactive transport code, TOUGHREACT, is used.

The cores from the Sayindere formation are used in the experiments. Sayindere is the cap rock of the Caylarbasi field, one of the screened and selected fields in Turkey for the possible CO₂ injection in the future. The formation water analysis of Caylarbasi reservoir is available but not the Sayindere formation. Thus, the Sayindere formation water is assumed same as the Caylarbasi reservoir water and according to this water composition, the Sayindere cap rock water is synthetically prepared and used in the both static and dynamic experiments. Before carrying out the experiments, a thin section analysis of the Sayindere core is made to investigate what kinds of minerals are mainly available in the core. This analysis shows the core from the Sayindere cap rock is roughly composed of 85 % calcite, 1 % quartz, 0.5 % hematite and the remaining 13.5% percent clay. The clay type is later revealed as kaolinite in the XRD analysis. However, no hematite is discovered in the XRD analysis. Two different experiments are carried out: *static (batch)* and *dynamic (flow through)*. The static experiment is performed at the temperature of 90 °C and the pressure of approximately 100 bar, representing the field condition. In the static experiment, the original cores from the Sayindere cap rock are kept within the CO₂-synthetic formation water under the given reservoir pressure and temperature. The static experiment is composed of two experiments: *30-day experiment and 100-day experiment*. After 30 and 100 days of the static experiment, SEM analyses of the cores are made to see any mineralogical changes on the core surfaces. Moreover,

the fluid chemistry analyses of the mixtures in the core holders are made to investigate the possible geochemical reactions induced by CO₂-formation water. From the photos taken in SEM analysis of the 30 day experiment, it is seen that the near to surface are more loose than the inner part of the core, which shows the CO₂ diffusion into the core. Also there is a very tiny thin deposition layer, which is whiter colored. This deposition layer is even thicker in SEM photos of the 100 day experiment. Since there was no flow in the static experiment, there was no transport of the reactant and reaction products. Thus, the formation of deposition layer is explained as the dissolved particles, specifically the dissolved calcite from the core minerals were deposited back on the core surfaces. The fluid chemistry analyses of the 30- and 100- day experiments show that the calcite is dissolved. Moreover, it is observed in the mineral investigation by SEM analysis of 100-day experiment that there are wormholes on the core used in the experiment, possibly created due to the heterogeneous pattern of calcite dissolution induced by the CO₂-formation water. In both 30- and 100-day experiments, it is observed that the inner parts of the original cores are not influenced by CO₂-formation water.

In dynamic experiment, the cores from Sayindere cap rock are grinded and packed into a core holder and CO₂ saturated- synthetically prepared water is injected through the packed core for 99 days. Since the cores were very impermeable, they were ground so that a flow could be maintained throughout the experiment. Before the dynamic experiment, the carbonate removal from the grinded powder of the cores with acid treatment and XRD analysis are performed. From these analyses, the core from the Sayindere cap rock is composed of 76% calcite, 22.7 % quartz and 1.3 % kaolinite.

The experimental condition was at a temperature of 90 °C and an injection pressure of 75 bar. The outlet pressure is set at the pressure of 74 bar. The fluid is discharging out of the core holder under 1 bar pressure difference. The discharged fluid is collected and water analyses are carried out from collected water samples at 3 different times (23, 75 and 99 days) throughout the experiment to see changes in the amount of the dissolved

species in the synthetic formation water. Mineral analysis after the dynamic experiment is not performed since it is difficult to quantify the mineralogical changes by the available techniques. Only water chemistry analyses of the dynamic experiment are made. Based on the water chemistry analysis, this is interpreted as calcite is dissolved in earlier time, like 23 days, of the experiment and the calcite available for reaction in the core is decreased due to injected water sweeping the dissolved elements to production end. At the end of 99 days, it is anticipated that Ca^{+2} available for reaction is depleted and Ca^{+2} produced is equal to injected Ca^{+2} .

Moreover, the modeling and simulation study of the dynamic experiment is carried out by using the code TOUGHREACT. Simple 2-D radial model composed of 4 cells is used to simulate the CO_2 saturated fluid and Sayindere core minerals interaction in the dynamic experiment. The water composition is slightly different than that of the dynamic experiment. In the dynamic experiment, the Caylarbasi reservoir water composition is directly adopted as the cap rock formation water. However, in the simulation work, for the Sayindere cap rock formation water, the Caylarbasi reservoir formation water is modified in a way that the cap rock minerals and cap rock fluid chemistry are consistent. The results of the simulation work show that calcite is firstly dissolved and started to re-precipitated (Figure L.15). Moreover, continuous dissolutions of quartz and kaolinite are observed (Figure L.19 and Figure L.17). Formation of new, secondary minerals (hematite, magnesite and siderite) are observed but dissolved back in the simulation period. Dolomite, which is also considered to be a secondary mineral in the simulation, is continuously precipitated throughout the simulation time (Figure L.21). Most importantly, the decreases in the porosity and permeability of the packed core minerals of the Sayindere cap rock are observed during the simulation (Figure L.22- L.23). In fact, the decreases are very small in amounts. The porosity is decreased by 0.01% and, on the other hand, the permeability is decreased by 0.03%. This decrease could be larger if the simulation period was longer. In this case, the simulation time is 99 days, representing injecting time of CO_2 saturated water in the dynamic experiment of this study. In field case, it is obviously longer such as couple of decades or more. The

decreases in the porosity and permeability shows that due to the geochemical reactions induced by CO₂-saturated water and the cap rock minerals will result in the decrease in the porosity and permeability and this means that the Sayındere cap rock integrity will be enhanced and there will not be any possible leakage paths caused by the dissolution and precipitation reactions between the CO₂ saturated water- the cap rock minerals.

In addition to the simulation of the injection, the CO₂ saturated water injection into the packed core minerals of the Sayındere formation is stopped after 99 days of the injection and the simulation is continued for further 25 years to monitor the cap rock mineralogical and the water chemistry evolutions and particularly, the long term effect on the porosity and permeability of the packed Sayındere core. Different from the injection period, the porosity and permeability of the packed core are increased in long term after the injection process (Figure N.22-N.23). The porosity and permeability are increased by 0.001% and 0.004%, respectively. From the point of view of the monitoring CO₂ storage after the injection and risk assessment associated with the CO₂ storage, the porosity and permeability increases as results of the geochemical reactions induced of CO₂ storage are not desirable since these increases can result in possible leakage paths for the CO₂ to escape into groundwater sources and finally into the atmosphere back. The increases in porosity and permeability show that the Sayındere cap rock integrity must be monitored in the field if application is planned.

CHAPTER 9

CONCLUSION

- The mineral investigation of the Sayindere cap rock is made. It is composed of the 76% calcite, 22.7% quartz and the remaining, 1.3% is kaolinite.
- From the photographs taken in SEM analysis of the 30 day experiment, it is interpreted that the near to surface appears looser than the inner part of the core, which may be due to CO₂ diffusion into the core.
- The fluid chemistry analyses of the both 30- and 100- day static experiments show that the calcite is dissolved in the water as a result of the CO₂- water-rock interaction.
- A deposition layer is observed in SEM photos of the 100 day experiment. The formation of deposition layer is explained as the dissolved particles, specifically the dissolved calcite from the core minerals were deposited back on the core surfaces.
- It is observed in the mineral investigation by SEM analysis of 100-day experiment that there are wormholes on the core used in the experiment, possibly created due to the heterogeneous pattern of calcite dissolution induced by the CO₂-formation water.
- In both 30- and 100-day experiments, it is observed that the inner parts of the original cores are not influenced by CO₂-formation water.

- Only water chemistry analyses of the dynamic experiment are made. Based on the water chemistry analysis, it is interpreted that calcite is dissolved, which is also observed in the static experiments.
- The modeling and simulation study of the dynamic experiment is carried out by using the code TOUGHREACT. The results of the simulation work show that calcite is firstly dissolved and started to re-precipitated.
- Formation of new, secondary minerals (hematite, magnesite and siderite) are observed but dissolved back during the simulation period. Dolomite, which is also considered to be a secondary mineral in the simulation, is continuously precipitated throughout the simulation time.
- The decreases in the porosity (0.01%) and permeability (0.03%) of the packed core minerals of the Sayindere cap rock are observed during the simulation
- This shows that due to the geochemical reactions induced by CO₂-saturated water and the cap rock minerals will result in the decrease in the porosity and permeability and this means that the Sayindere cap rock integrity will be enhanced by the geochemical reactions between the CO₂ saturated water- the cap rock minerals.
- The simulation is continued for further 25 years, without CO₂ saturated water injection to monitor the cap rock mineralogical and the water chemistry evolutions and particularly, the long term effect on the porosity and permeability of the packed Sayindere core.
- At the end of 25 years, the porosity and permeability increase of 0.001% and 0.0039% respectively were simulated after stopping the injection process.

- This is a unwanted result in the monitoring and risk assessment of the CO₂ storage. The increases in porosity and permeability show that the Sayindere cap rock integrity must be monitored in the field if application is planned.

REFERENCE

Andre, L., Audigane, P., Azaroual, M., Menjot, A., 2007. Numerical modeling of fluid-rock interactions at the supercritical CO₂-liquid interface during CO₂ injection into carbonate reservoir, the Dogger aquifer (Paris Basin, France). *Energy Conversion and Management* 48 (2007) 1782-1797.

Bachu, S., 2002. Sequestration of CO₂ in geological media in response to climate change: road map for site selection using the transform of the geological space into the CO₂ phase space, *Energy Conversion and Management*, 35, 269-279.

Baklid, A., Korbol, K., Owren, G., 1996. Sleipner vest CO₂ disposal, CO₂ injection into swallow underground aquifer, SPE 00036600.

Bateman, K., Turner, G., Pearce, J.M., Noy, D.J., Birchall, D., Rochelle, C.A., 2005. Large-Scale Column Experiment: Study of CO₂, Porewater, Rock Reactions and Model Test Case Oil & Gas Science and Technology – Rev. IFP, Vol. 60 No. 1, pp. 161-175

Calabrese, M., Masserano, F., 2006. Simulation of physical-chemical processes during CO₂ sequestration in Geological Structures, paper SPE 95820

Duan and Sun (2002). An Improved model calculating CO₂ solubility in pure water and aqueous NaCl solutions from 273 to 533 K and from 0 to 2000 bar. *Chemical Geology*, 193, 257-271

Department of Energy: <http://www.energy.gov> (last visited on 01.07.2010)

Dodds, W.S., Stutzman, L.F., Sollami, B.J., 1956. CO₂ solubility in Water, Industrial and engineering chemistry, vol.1 no.1, 92-95.

Egermann, P., Bazin, B., and Vizika, O., 2005. An Experimental Investigation of Reaction-Transport Phenomena During CO₂ Injection.

Frank, R.T., Edward, F., 1943, laboratory manual for chemical and bacterial analysis of water and sewage.

Gaus, I., Azaroual, M., Czernichowski-Lauriol, I., 2005. Reactive transport modelling of the impact of CO₂ injection on the clayey cap rock at Sleipner (North Sea). Chem. Geol. 217, 319–337

Gaus, I., Audigane, P., Andre,L., Lions, J., Jacquemet, N., Durst, P., Czernichowski-Lauriol, I., Azaroual, M., 2008, Geochemical and solute transport modelling for CO₂ storage, What to expect from it? International Journal of Greenhouse Gas Control 2, 60 5 – 62 5

Gherardi, F., Xu, T., Pruess, K., 2007. Numerical modeling of self-limiting and self-enhancing caprock alteration induced by CO₂ storage in a depleted gas reservoir. Chem. Geol. 244, 103-129

Göncüoğlu, C., 2010. Department of Geological Engineering, METU- personal communication

International Energy Agency Greenhouse Gas Technology: <http://www.ieaghg.org/> (last visited on 01.07.2010)

IPCC Special Report, 2005

Gunter, W.D., Wiwchar, B., Perkins, E.H., 1997. Aquifer disposal of CO₂-rich greenhouse gases: extension of the time scale of experiment for CO₂-sequestering reactions by geochemical modelling. *Mineral. Petrol.* 59, 121–140

Kaszuba, J.P., Janecky, D.R., Snow, M.G., 2005. Experimental evaluation of mixed fluid reactions between supercritical carbon dioxide and NaCl brine: relevance to the integrity of a geologic carbon repository. *Chem. Geol.* 217, 277–293

Lagneau, V., Pipart, A., Catalette, H., 2005. Reactive Transport Modelling of CO₂ Sequestration in Deep Saline Aquifers. *Oil & Gas Science and Technology* 60, 231-247

Lin, H., Fujii, T., Takisawa, R., Takahashi, T., Hashida, T., 2007, Experimental evaluation of interactions in supercritical CO₂/water/rock minerals system under geologic CO₂ sequestration conditions, *Journal of Materials Science* Volume 43, Number 7, DOI:10.1007/s10853-007-2029-4

Lindeberg, E., Bergmo, P., 2003. The long-term fate of CO₂ injected into an aquifer. *Greenhouse Gas Technologies* 1, 489-494.

Nergescu, M., 2008. Economic Modeling of an Oil and Gas Project Involving Carbon Capture and Storage: Snohvit LNG Field (Barents Sea, Norway), SPE 107430-PA.

Phreeqc (Version 2) User's Guide.

Petrsim User's Guide, 2008.

PetraSim Toughreact Example Manual, Thunderhead engineering, 2008.

Sengul, M., 2006. CO₂ Sequestration - A Safe Transition Technology, SPE 98617-MS

TUBITAK KAMAG REPORT, “Evaluation of CO₂ Emission From Industrial Sectors in Turkey and Determination of Possible CO₂ Storage Sites in Turkey and Modeling & Simulation of CO₂ Sequestration in an Oil Field in Turkey”- funded by the Scientific & Technological Research Council of Turkey (2007- 2009)

Türkmenoğlu, A.G., 2010. Department of Geological Engineering, METU- personal communication

Wright, I.W., Lee, A., Middleton, P., Lowe, C., and Miracca, Ivano., 2004. CO₂ Capture Project: Initial Results, SPE 00086602.

Wright, I.W., 2007. The In Salah Gas CO₂ Storage Project, IPTC 11326.

Xu, T., Apps, J.A., Pruess, K., 2005. Mineral sequestration of carbon dioxide in a sandstone–shale system. Chem. Geol. 217, 295-318

Xu, T., Sonnenthal, E., Spucher, N., Pruess, K., 2008. TOUGHREACT User’s guide: A Simulation Program for Nonisothermal Multiphase Reactive Geochemical Transport in Variably Saturated Geologic Media, V1.2.1

APPENDIX A

ALKALINITY MEASUREMENT

There are 3 kinds of alkalinity, hydroxide (OH), normal carbonate (CO₃), bicarbonate (HCO₃). In order to distinguish between the kinds of alkalinity present in a sample and determine the quantities of each, a titration is made with a standard acid using two indicators successively. The standard solution is 0.02 N H₂SO₄ and the indicators are phenolphthalein and methyl orange test solutions.

The HCO₃ ion composition available in the synthetically prepared water was measured by titration technique. The procedure of titration process to determine the alkalinity is given as following:

- a) Pipette 100 ml of the sample into one Erlenmeyer flask and same quantity of distilled water into another.
- b) Add 3 drops of phenolphthalein to each
- c) If the sample becomes pink, add 0.02 N H₂SO₄ acids from a burette until the pink color just disappears and record the number of ml of acid used (P).
- d) Add 3 drops of methyl orange to each flask.
- e) If the sample becomes yellow, add 0.02 N H₂SO₄ acid until the first difference in color is noted when compared with the distilled water. The end point is a slight orange tinge. Record the ml of acid used (T).

There are 5 possible conditions:

$$P = T, \text{ Hydroxide}(ppm) = (2P - T) * 10$$

$$P > \frac{1}{2}T, \text{ Hydroxide}(ppm) = (2P - T) * 10$$

$$\text{NormalCarbonate}(ppm) = 2(T - P) * 10$$

$$P = \frac{1}{2}T, \text{ NormalCarbonate}(ppm) = T * 10$$

$$P < \frac{1}{2}T, \text{ NormalCarbonate}(ppm) = 2P * 10$$

$$\text{Bicarbonate}(ppm) = (T - 2P) * 10$$

$$P = 0, \text{ Bicarbonate}(ppm) = T * 10$$

For the titration measurement, 0.02N H₂SO₄, Methyl Orange Test Solution and Pheolphthalein Test Solution are needed. Their preparations are done in the following ways (Frank and Edward, 1943).

How to prepare 0,02N H₂SO₄ from highly concentrated H₂SO₄ solution

Concentrated H₂SO₄ is 98% with a density of 1.84gms/mL. That means that in 1 liter of H₂SO₄, there are 1840 grams of which 98% is H₂SO₄ =1803.2 gram of H₂SO₄ in one liter.

The normality of an acid is defined as the number of equivalents per liter. An equivalent is equal to the amount of acid that generates one mole of protons. H₂SO₄ is a diprotic acid so one molar H₂SO₄ contains two moles of protons. So the equivalent weight to generate one mole of protons is the formula weight divided by 2.

The number of equivalent of H₂SO₄ of concentrated acid is $1803.2/98/2 = 36.8$
36.8 equivalents per liter of acid = 36.8 N . Using the following formula,

$$Vol_1 * N_1 = Vol_2 * N_2$$

to prepare 1000 mL 0.02 N H₂SO₄ from concentrated acid,

$1000(0.02) = (x \text{ mL}) (36.8) = \text{add } 0.54 \text{ mL of concentrated H}_2\text{SO}_4 \text{ slowly and}$
carefully to ~ 800 mL of water and dilute to 1000 mL of 0.02 N H₂SO₄

How to prepare Methyl Orange Test Solution

Dissolve 100 mg of methyl orange in 100 ml of water and filter if necessary.

How to prepare Phenolphthalein Test Solution

Prepare 100 ml of solution by dissolving 0,5 g phenolphthalein in 50 ml ethyl alcohol and dilute to 100 ml with water.

After prepared the necessary solutions, the titration process was carried out. As given in the procedure, firstly 3 drops of phenolphthalein were added and the sample did not go to pink, so there was only bicarbonate ion in the sample, which was expected. The formation water does not contain any normal carbonate and hydroxide as alkalinity. The bicarbonate composition was found as 613 ppm, whose expected value is 984.96 ppm.

APPENDIX B

THIN SECTION ANALYSIS PHOTOS

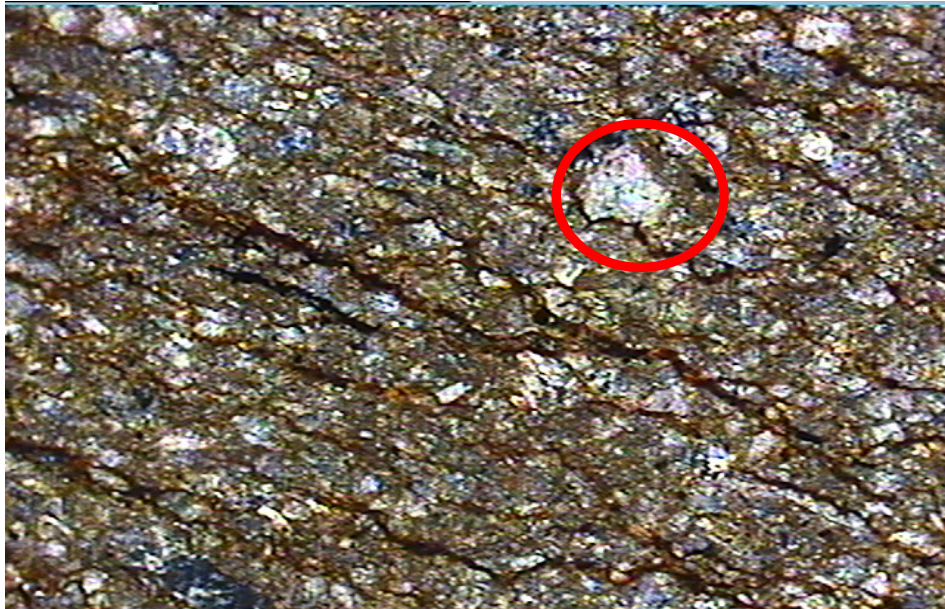


Figure B. 1 Calcite grains



Figure B. 2 Calcite veins



Figure B. 3 Fossils



Figure B. 4 Glauconite

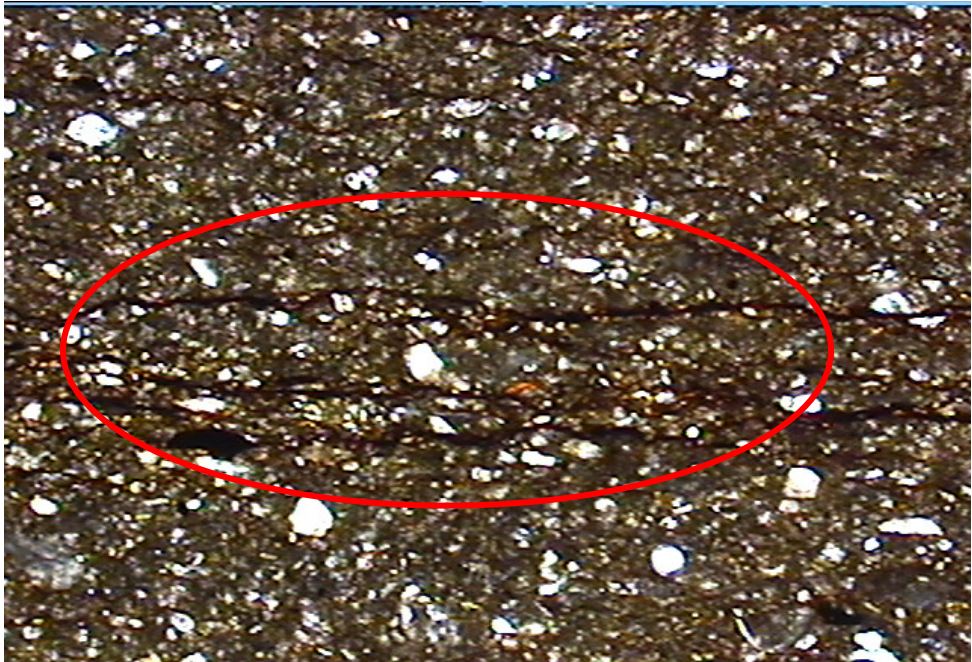


Figure B. 5 Laminations.



Figure B. 6 Hematite.



Figure B. 7 Quartz

APPENDIX C

PHOTOS OF THE STATIC EXPERIMENT



Figure C. 1 Mixing cylinder and core holders inside the oven



Figure C. 2 Side view of experimental set-up



Figure C. 3 Whole part of the experimental set-up

APPENDIX D

SEM/EDX ANALYSIS RESULTS OF THE 30 DAY-STATIC EXPERIMENT

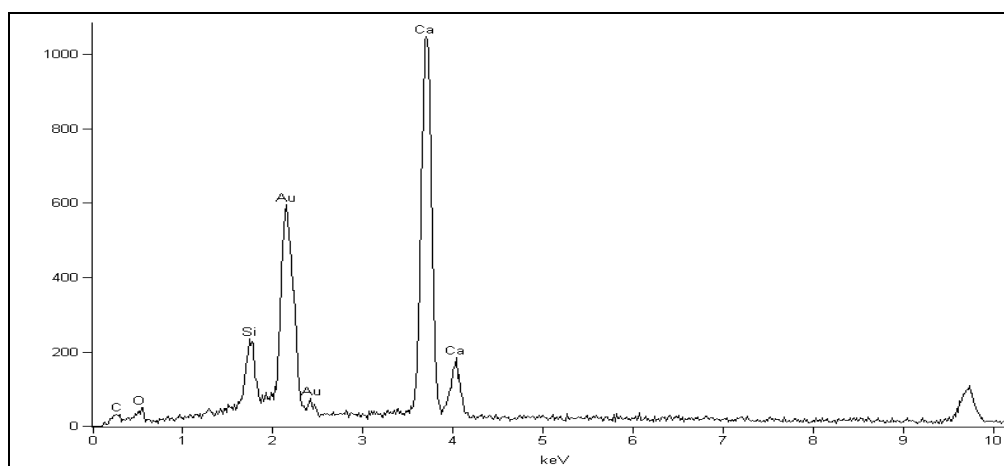


Figure D. 1In-Depth SEM/EDX Micrograph (inner part)-after the 30 day-experiment

Table D. 1In-Depth SEM element analysis (inner part) -after the 30 day-experiment

<i>Element</i>	<i>Weight Conc %</i>	<i>Atom Conc %</i>	<i>Compnd Conc %</i>	<i>Formula</i>
<i>O</i>	31.54	52.71	0.00	
<i>Si</i>	5.69	5.42	12.17	SiO ₂
<i>Ca</i>	62.77	41.88	87.83	CaO

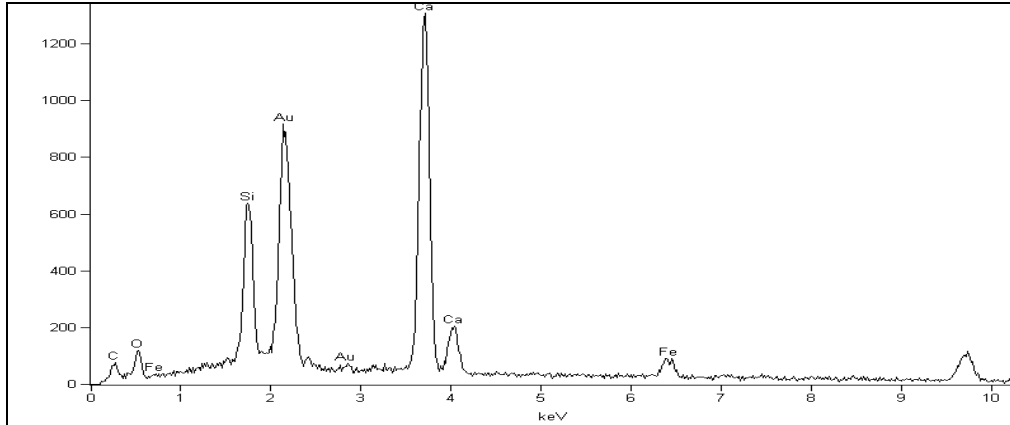


Figure D. 2 In-Depth SEM/EDX Micrograph (near to surface_1) -after the 30 day-experiment

Table D. 2 In-Depth SEM element analysis (near to surface_1) -after the 30 day-experiment

<i>Element</i>	<i>Weight Conc %</i>	<i>Atom Conc %</i>	<i>Compnd Conc %</i>	<i>Formula</i>
O	35.14	56.34	0.00	
Si	12.23	11.17	26.17	SiO2
Ca	46.07	29.48	64.45	CaO
Fe	6.55	3.01	9.37	Fe2O3

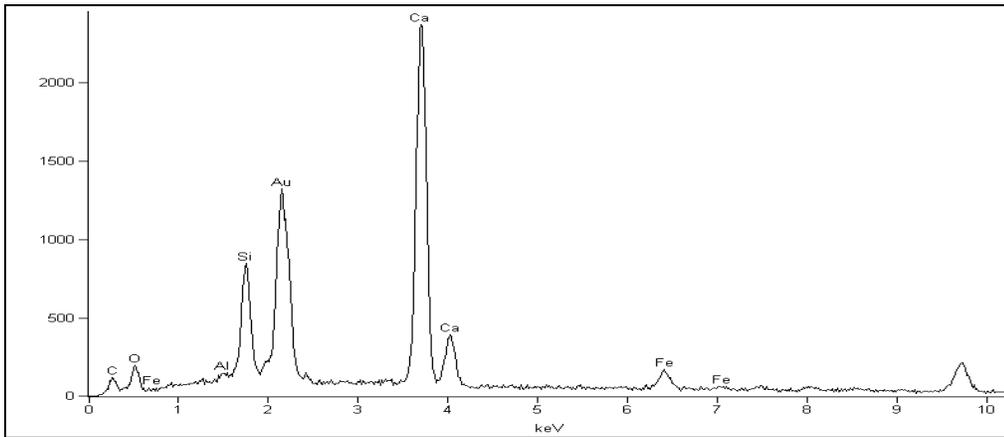


Figure D. 3 In-Depth SEM/EDX Micrograph (near to surface_2) -after the 30 day-experiment

Table D. 3 In-Depth SEM element analysis (near to surface_2) -after the 30 day-experiment

<i>Element</i>	<i>Weight Conc %</i>	<i>Atom Conc %</i>	<i>Compnd Conc %</i>	<i>Formula</i>
O	33.67	55.14	0.00	
Al	0.51	0.50	0.96	Al2O3
Si	9.11	8.50	19.50	SiO2
Ca	50.19	32.81	70.22	CaO
Fe	6.51	3.06	9.31	Fe2O3

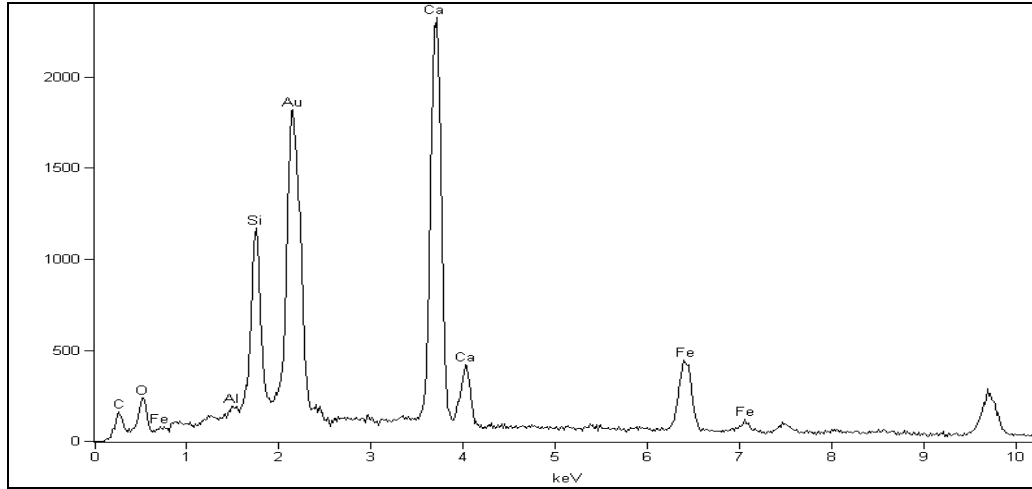


Figure D. 4 In-Depth SEM/EDX Micrograph (near to surface_3) -after the 30 day-experiment

Table D. 4 In-Depth SEM element analysis (near to surface_3) -after the 30 day-experiment

<i>Element</i>	<i>Weight Conc %</i>	<i>Atom Conc %</i>	<i>Compnd Conc %</i>	<i>Formula</i>
O	34.41	56.87	0.00	
Al	0.31	0.30	0.58	Al ₂ O ₃
Si	10.23	9.63	21.89	SiO ₂
Ca	38.36	25.30	53.68	CaO
Fe	16.68	7.90	23.85	Fe ₂ O ₃

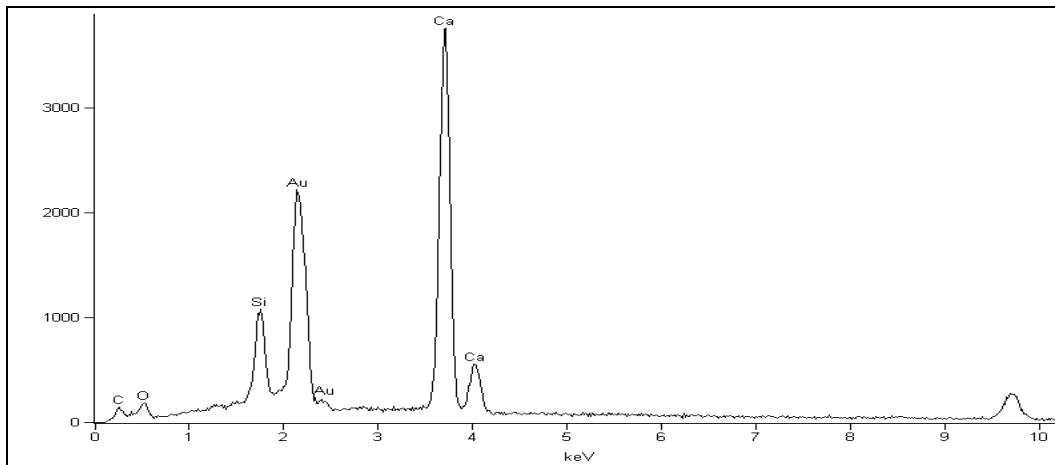


Figure D. 5 In-Depth SEM/EDX Micrograph (near to surface_1) -prior to the 30 day-experiment

Table D. 5 In-Depth SEM element analysis (near to surface_1) -prior to the 30 day-experiment

<i>Element</i>	<i>Weight Conc %</i>	<i>Atom Conc %</i>	<i>Compnd Conc %</i>	<i>Formula</i>
O	32.91	53.86	0.00	
Si	8.29	7.72	17.73	SiO ₂
Ca	58.80	38.41	82.27	CaO

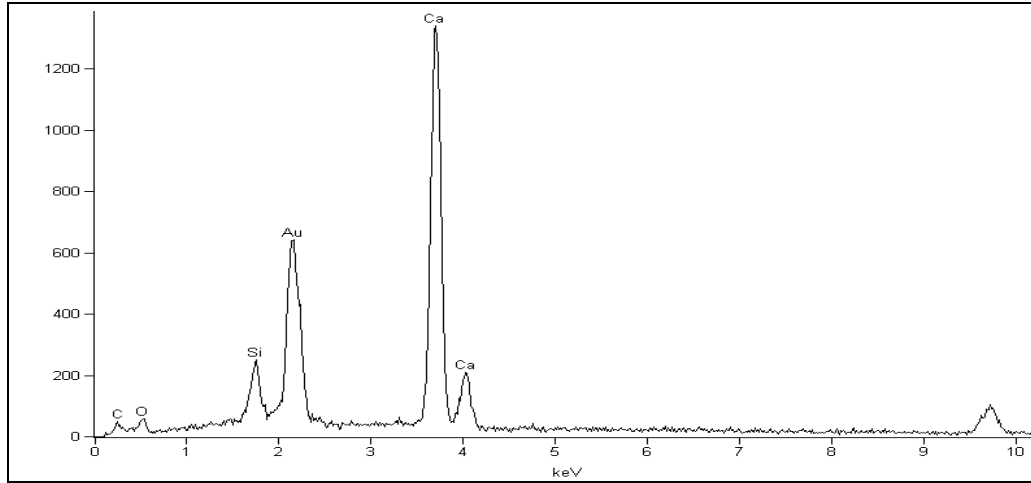


Figure D. 6 In-Depth SEM/EDX Micrograph (inner part)-prior to the 30 day-experiment

Table D. 6 In-Depth SEM element analysis (inner part) -prior to the 30 day-experiment

<i>Element</i>	<i>Weight Conc %</i>	<i>Atom Conc %</i>	<i>Compnd Conc %</i>	<i>Formula</i>
<i>O</i>	31.13	52.36	0.00	
<i>Si</i>	4.92	4.72	10.53	SiO ₂
<i>Ca</i>	63.94	42.93	89.47	CaO

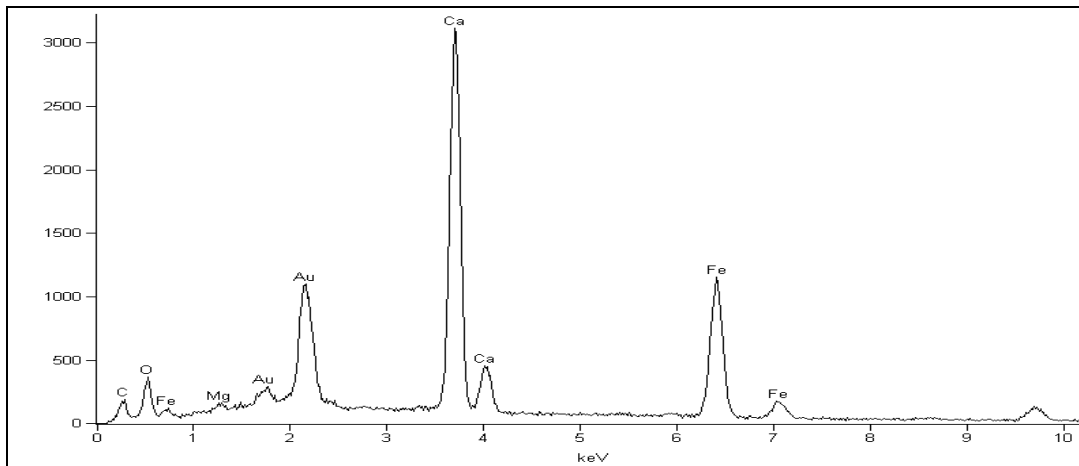


Figure D. 7 Top Surface SEM/EDX Micrograph_1-after the 30 day-experiment

Table D. 7 Top Surface SEM element analysis_1-after the 30 day-experiment

<i>Element</i>	<i>Weight Conc %</i>	<i>Atom Conc %</i>	<i>Compnd Conc %</i>	<i>Formula</i>
<i>O</i>	29.40	54.39	0.00	
<i>Mg</i>	0.80	0.98	1.33	MgO
<i>Ca</i>	36.65	27.07	51.28	CaO
<i>Fe</i>	33.14	17.57	47.39	Fe ₂ O ₃

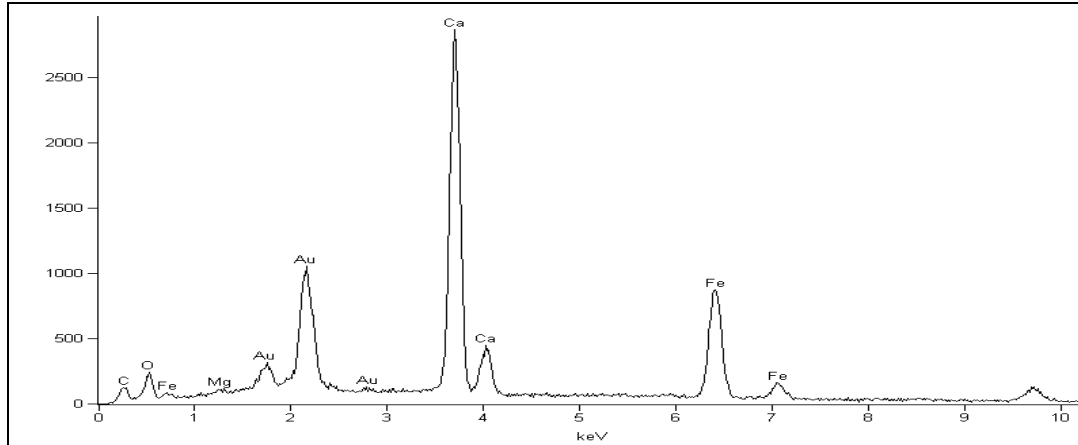


Figure D. 8 Top Surface SEM/EDX Micrograph_2-after the 30 day-experiment

Table D. 8 Top Surface SEM element analysis_2-after the 30 day-experiment

<i>Element</i>	<i>Weight Conc %</i>	<i>Atom Conc %</i>	<i>Compnd Conc %</i>	<i>Formula</i>
O	29.32	54.14	0.00	
Mg	0.58	0.71	0.96	MgO
Ca	38.83	28.62	54.33	CaO
Fe	31.27	16.54	44.71	Fe ₂ O ₃

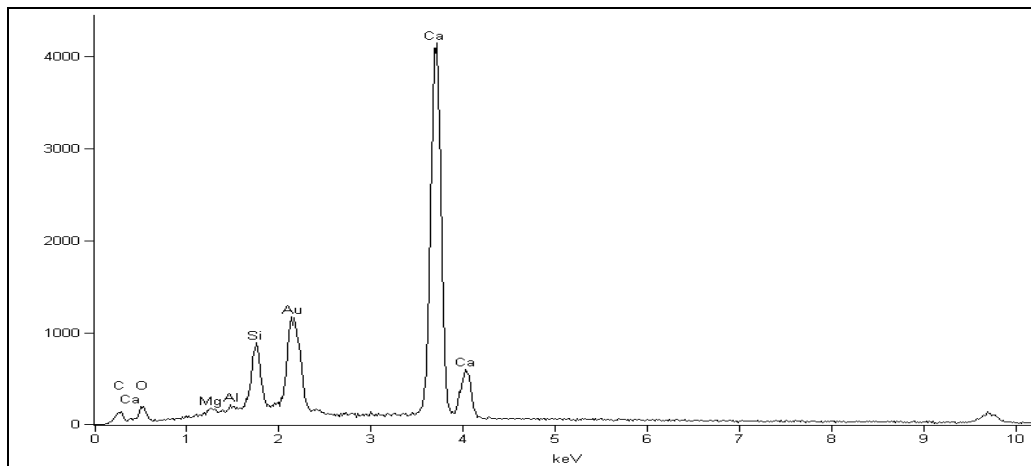


Figure D. 9 Top Surface SEM/EDX Micrograph_1-prior to the 30 day-experiment

Table D. 9 Top Surface SEM element analysis_1-prior to the 30 day-experiment

<i>Element</i>	<i>Weight Conc %</i>	<i>Atom Conc %</i>	<i>Compnd Conc %</i>	<i>Formula</i>
O	32.25	53.13	0.00	
Mg	0.84	0.91	1.40	MgO
Al	0.48	0.47	0.90	Al ₂ O ₃
Si	6.43	6.03	13.76	SiO ₂
Ca	60.00	39.45	83.95	CaO

APPENDIX E

SEM PHOTOS OF THE 30 DAY-STATIC EXPERIMENT

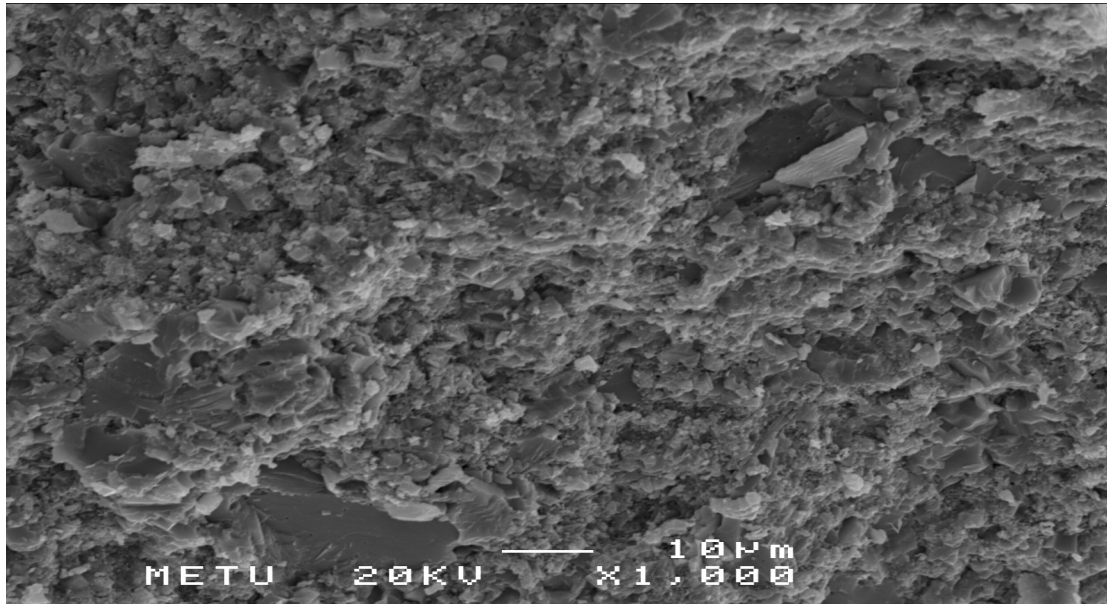


Figure E. 1 Near to surface view of in depth SEM Analysis -prior to the 30 day-experiment

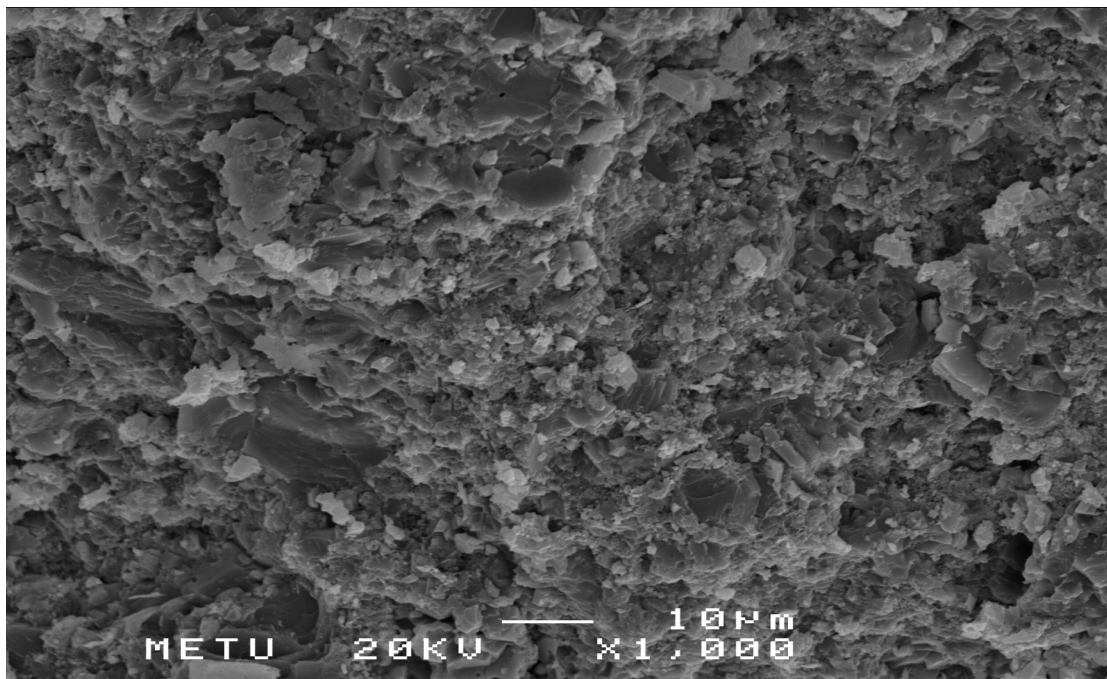


Figure E. 2 Inner view of in depth SEM Analysis -prior to the 30 day-experiment

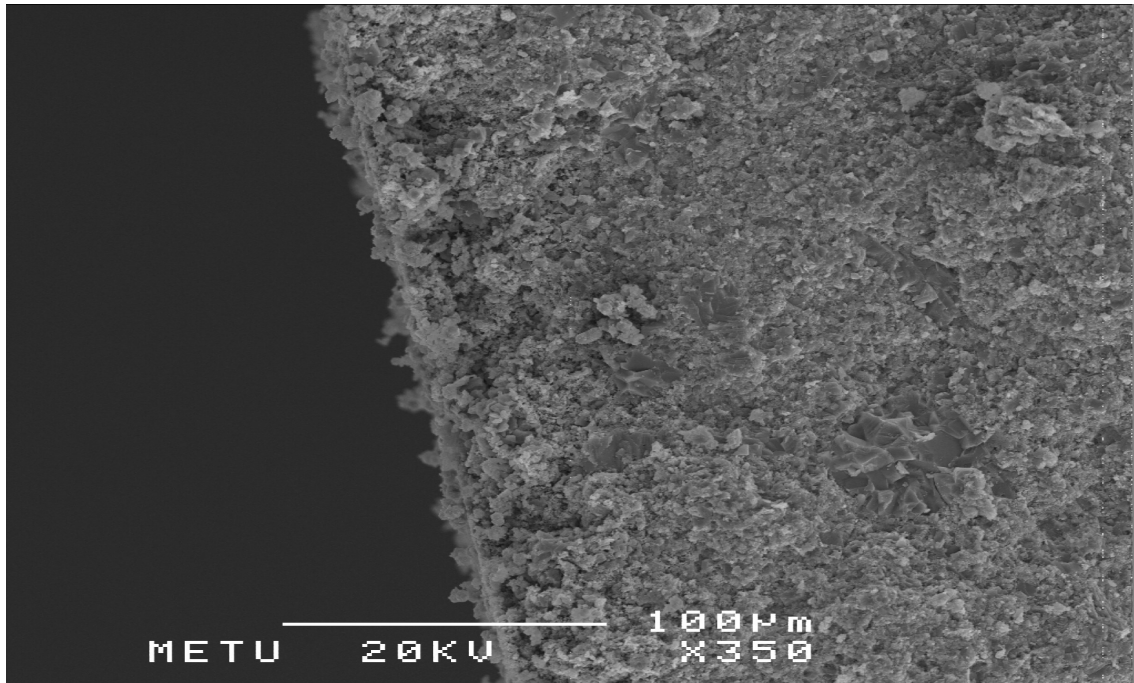


Figure E. 3 Near to surface view of in depth SEM Analysis_1- after the 30 day-experiment

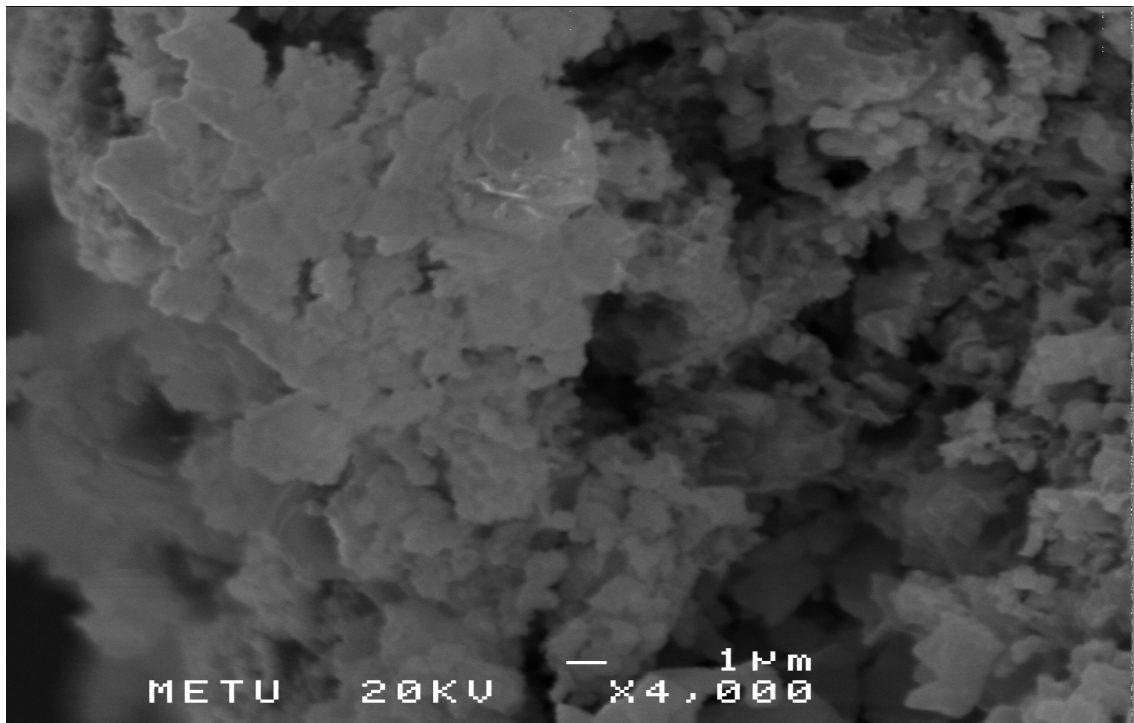


Figure E. 4 Near to surface view of in depth SEM Analysis_2- after the 30 day-experiment

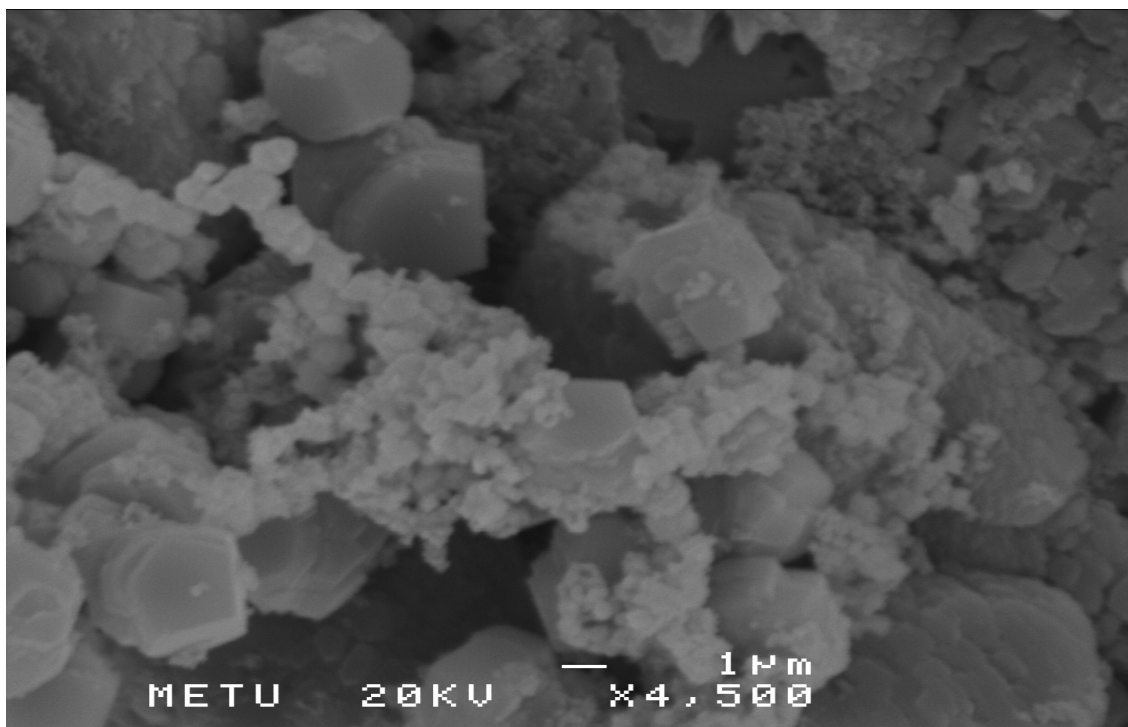


Figure E. 5 Top surface SEM Analysis_1- after the 30 day-experiment

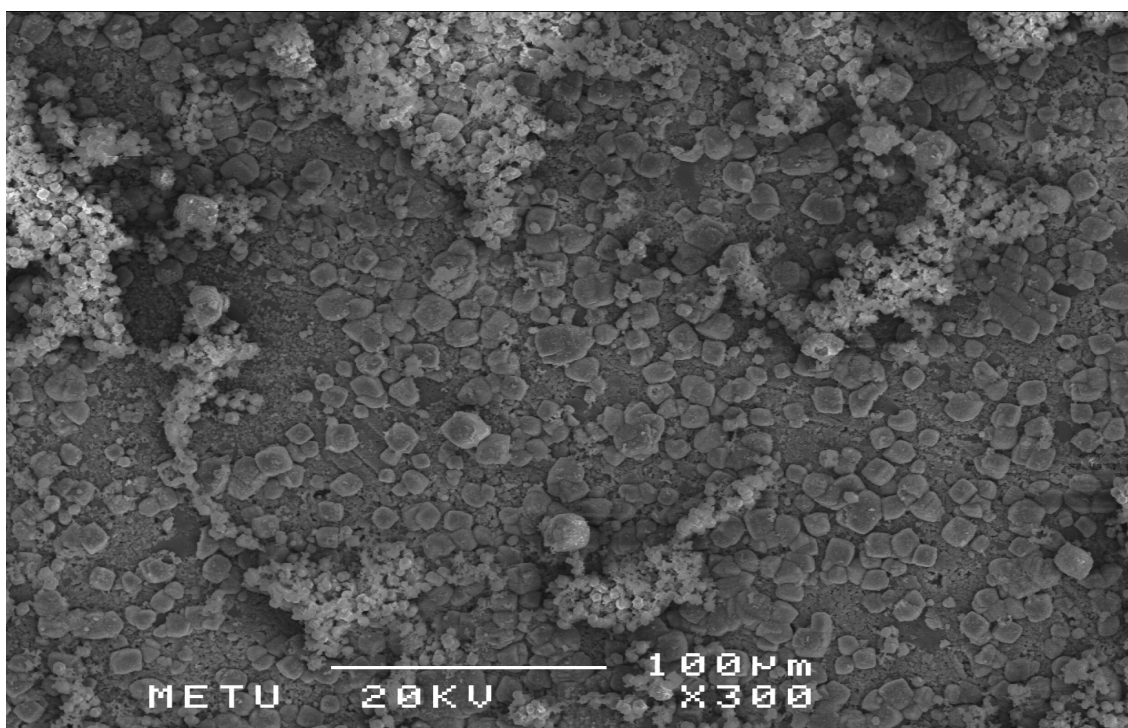


Figure E. 6 Top surface SEM Analysis_2- after the 30 day-experiment

APPENDIX F

SEM/EDX ANALYSIS RESULTS OF THE 100 DAY-STATIC EXPERIMENT

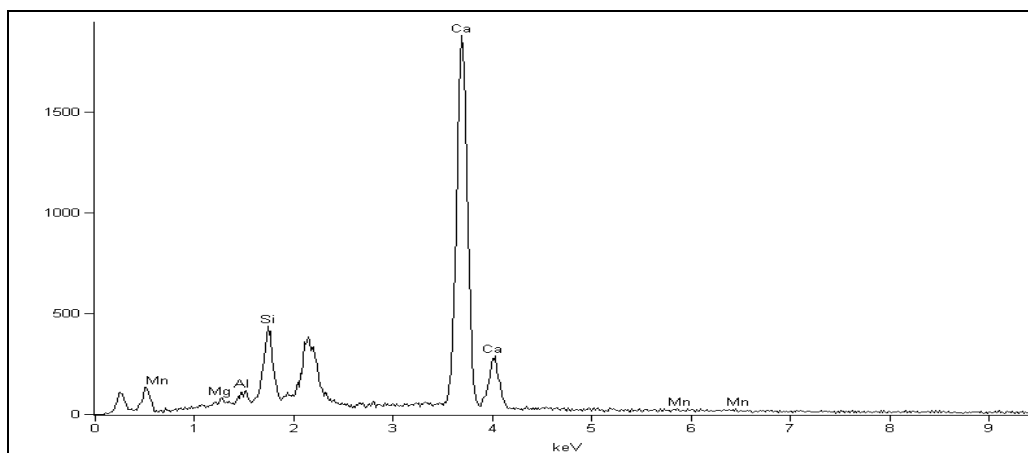


Figure F. 1In -Depth SEM/EDX Micrograph (inner part)-prior to the 100 day-experiment

Table F. 1In-Depth SEM element analysis (inner part) –prior to the 100 day-experiment

<i>Element</i>	<i>Weight Conc %</i>	<i>Atom Conc %</i>
<i>Mg</i>	1.16	1.79
<i>Al</i>	1.78	2.48
<i>Si</i>	11.22	15.05
<i>Ca</i>	85.85	80.68
<i>Mn</i>	0.00	0.00

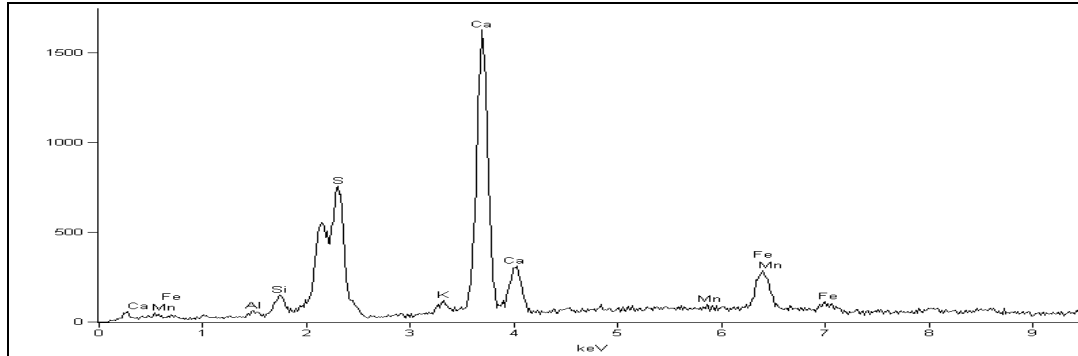


Figure F. 2 In-Depth SEM/EDX Micrograph (near to surface_1) –prior to the 100 day-experiment

Table F. 2 In-Depth SEM element analysis (near to surface_1) - prior to the 100 day-experiment

<i>Element</i>	<i>Weight Conc %</i>	<i>Atom Conc %</i>
<i>Al</i>	0.97	1.45
<i>Si</i>	4.01	5.76
<i>S</i>	12.19	15.35
<i>K</i>	1.90	1.96
<i>Ca</i>	59.71	60.14
<i>Mn</i>	0.80	0.59
<i>Fe</i>	20.42	14.76

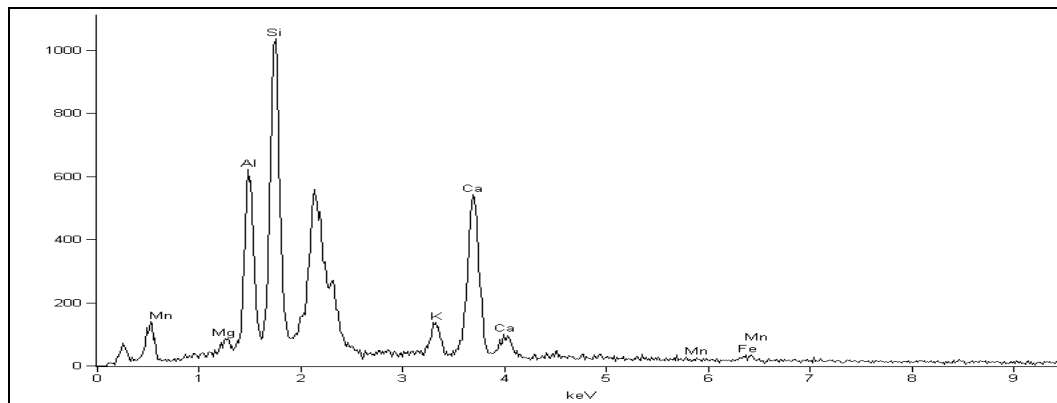


Figure F. 3 In-Depth SEM/EDX Micrograph (near to surface_2) –prior to the 100 day-experiment

Table F. 3 In-Depth SEM element analysis (near to surface_2) - prior to the 100 day-experiment

<i>Element</i>	<i>Weight Conc %</i>	<i>Atom Conc %</i>
<i>Mg</i>	1.22	1.58
<i>Al</i>	18.98	22.12
<i>Si</i>	42.19	47.23
<i>K</i>	3.74	3.01
<i>Ca</i>	31.57	24.77
<i>Mn</i>	0.00	0.00
<i>Fe</i>	2.29	1.29

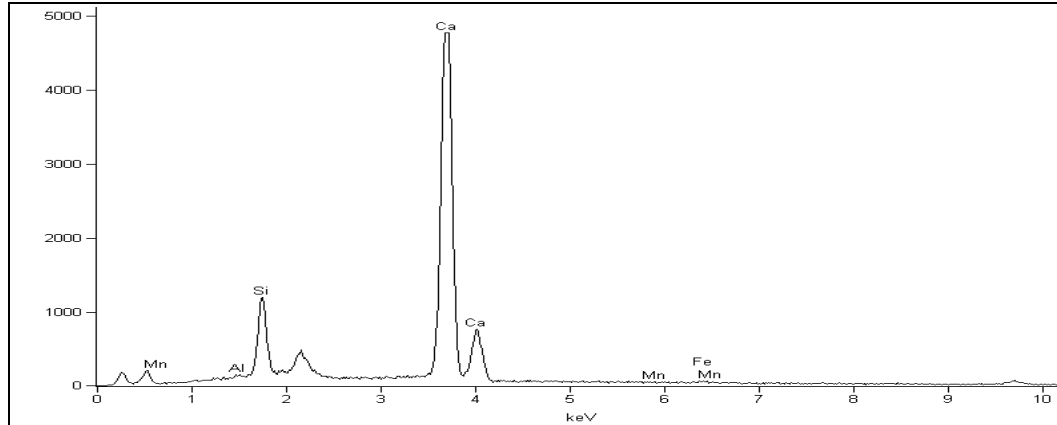


Figure F. 4 Top Surface SEM/EDX Micrograph_1-prior to the 100 day-experiment

Table F. 4 Top Surface SEM element analysis_1-prior to the 100 day-experiment

<i>Element</i>	<i>Weight Conc %</i>	<i>Atom Conc %</i>
<i>Al</i>	0.24	0.35
<i>Si</i>	10.56	14.44
<i>Ca</i>	88.40	84.67
<i>Mn</i>	0.01	0.01
<i>Fe</i>	0.78	0.54

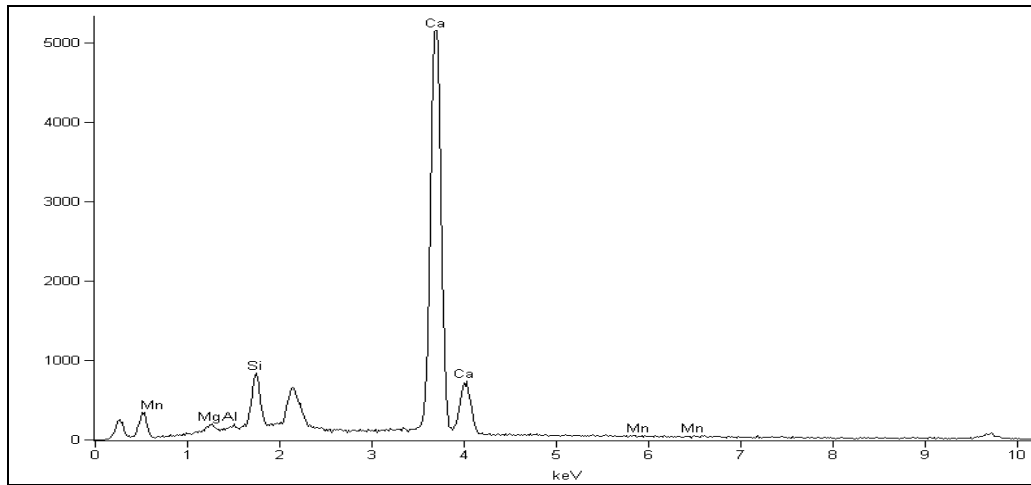


Figure F. 5 Top Surface SEM/EDX Micrograph_2-prior to the 100 day-experiment

Table F. 5 Top Surface SEM element analysis_2-prior to the 100 day-experiment

<i>Element</i>	<i>Weight Conc %</i>	<i>Atom Conc %</i>
<i>Mg</i>	1.48	2.34
<i>Al</i>	0.49	0.70
<i>Si</i>	7.81	10.66
<i>Ca</i>	90.12	86.23
<i>Mn</i>	0.10	0.07

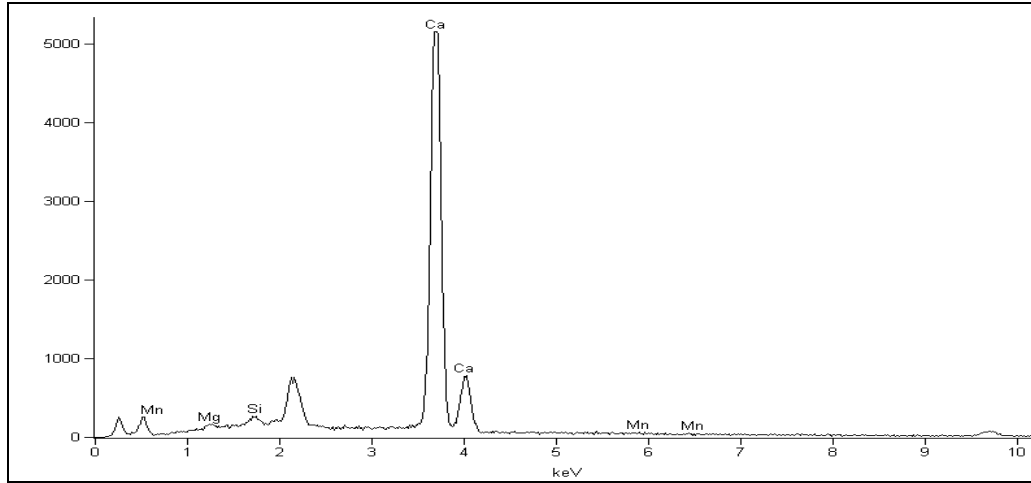


Figure F. 6 Top Surface SEM/EDX Micrograph_3-prior to the 100 day-experiment

Table F. 6 Top Surface SEM element analysis_3-prior to the 100 day-experiment

<i>Element</i>	<i>Weight Conc %</i>	<i>Atom Conc %</i>
Mg	1.00	1.63
Si	1.93	2.72
Ca	96.98	95.60
Mn	0.08	0.06

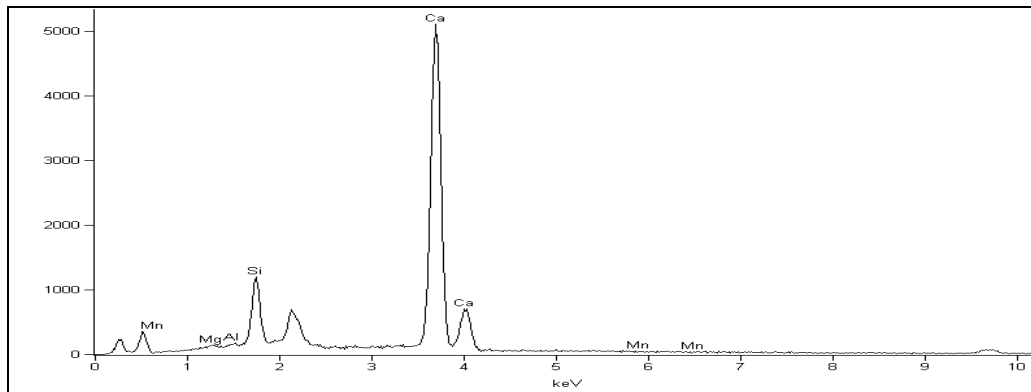


Figure F. 7 Top Surface SEM/EDX Micrograph_4-prior to the 100 day-experiment

Table F. 7 Top Surface SEM element analysis_4-prior to the 100 day-experiment

<i>Element</i>	<i>Weight Conc %</i>	<i>Atom Conc %</i>
Mg	0.64	0.99
Al	0.33	0.47
Si	11.30	15.29
Ca	87.74	83.24
Mn	0.00	0.00

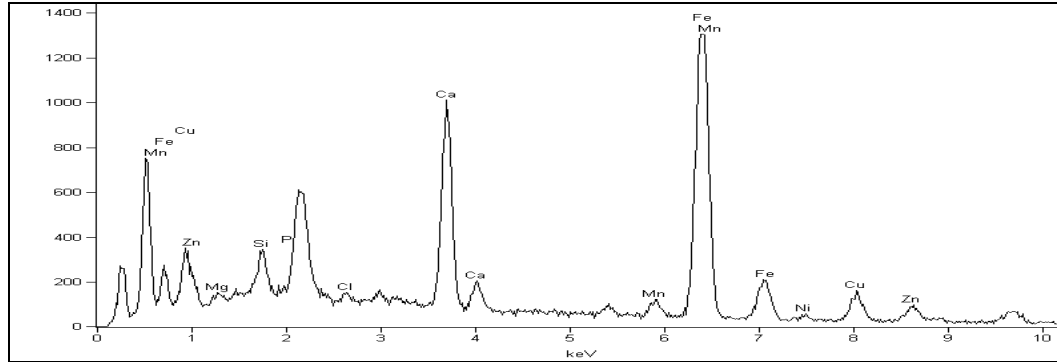


Figure F. 8 In-Depth SEM/EDX Micrograph (near to surface_1) –after the 100 day-experiment

Table F. 8 In-Depth SEM element analysis (near to surface_1) - after the 100 day-experiment

<i>Element</i>	<i>Weight Conc %</i>	<i>Atom Conc %</i>
<i>Mg</i>	1.48	3.06
<i>Si</i>	4.44	7.94
<i>P</i>	0.00	0.00
<i>Cl</i>	0.75	1.07
<i>Ca</i>	16.50	20.69
<i>Mn</i>	2.11	1.93
<i>Fe</i>	57.62	51.84
<i>Ni</i>	1.27	1.09
<i>Cu</i>	9.54	7.55
<i>Zn</i>	6.28	4.83

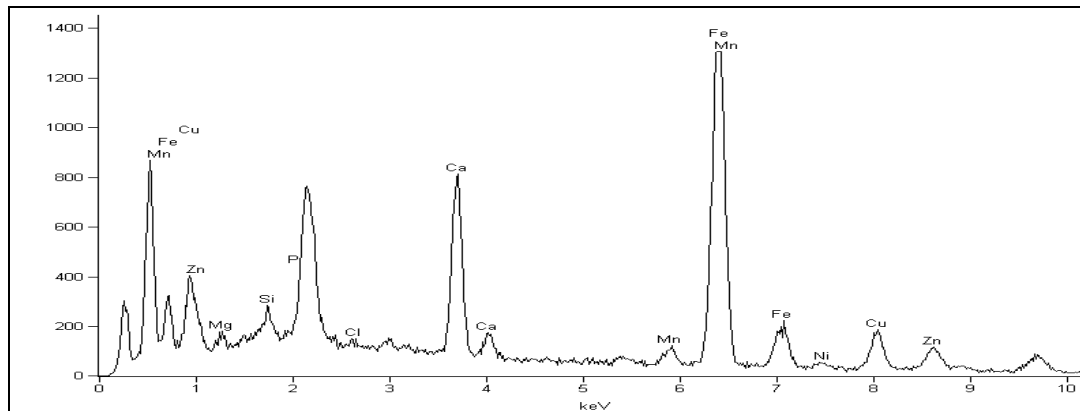


Figure F. 9 In-Depth SEM/EDX Micrograph (near to surface_2) –after the 100 day- experiment

Table F. 9 In-Depth SEM element analysis (near to surface_2) - after the 100 day-experiment

<i>Element</i>	<i>Weight Conc %</i>	<i>Atom Conc %</i>
Mg	2.18	4.66
Si	2.19	4.05
P	0.00	0.00
Cl	0.56	0.82
Ca	13.11	16.97
Mn	2.69	2.54
Fe	56.82	52.78
Ni	1.13	1.00
Cu	11.88	9.70
Zn	9.43	7.49

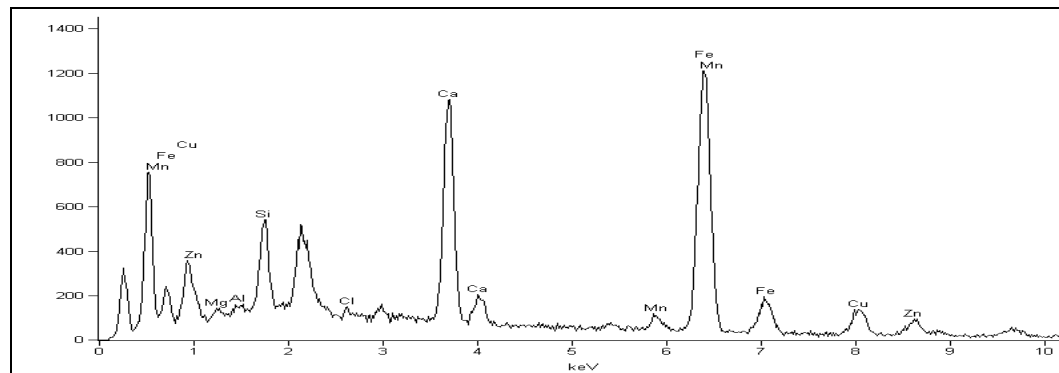


Figure F. 10 In-Depth SEM/EDX Micrograph (near to surface_3) –after the 100 day-experiment

Table F. 10 In-Depth SEM element analysis (near to surface_3) - after the 100 day-experiment

<i>Element</i>	<i>Weight Conc %</i>	<i>Atom Conc %</i>
Mg	1.11	2.20
Al	0.91	1.64
Si	7.76	13.33
Cl	0.56	0.76
Ca	18.96	22.83
Mn	1.90	1.67
Fe	52.27	45.16
Cu	10.58	8.03
Zn	5.93	4.38

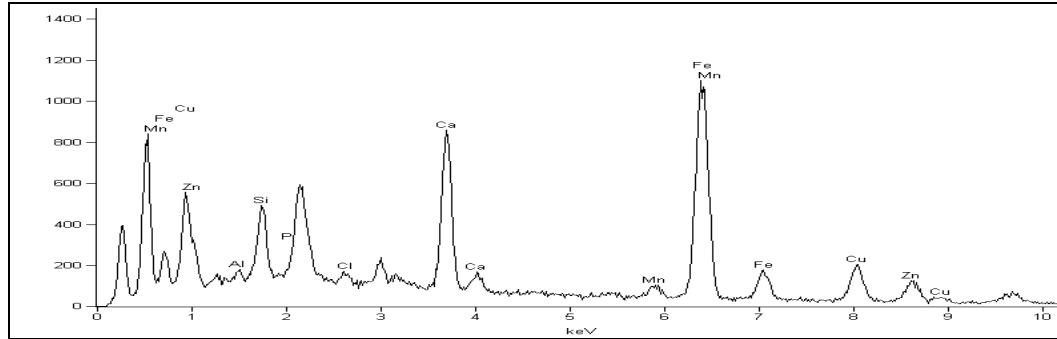


Figure F. 11 In-Depth SEM/EDX Micrograph (near to surface_4) –after the 100 day-experiment

Table F. 11 In-Depth SEM element analysis (near to surface_4) - after the 100 day-experiment

<i>Element</i>	<i>Weight Conc %</i>	<i>Atom Conc %</i>
<i>Al</i>	0.85	1.58
<i>Si</i>	7.60	13.50
<i>P</i>	0.00	0.00
<i>Cl</i>	1.64	2.31
<i>Ca</i>	14.84	18.47
<i>Mn</i>	1.98	1.80
<i>Fe</i>	47.82	42.73
<i>Cu</i>	14.56	11.43
<i>Zn</i>	10.71	8.18

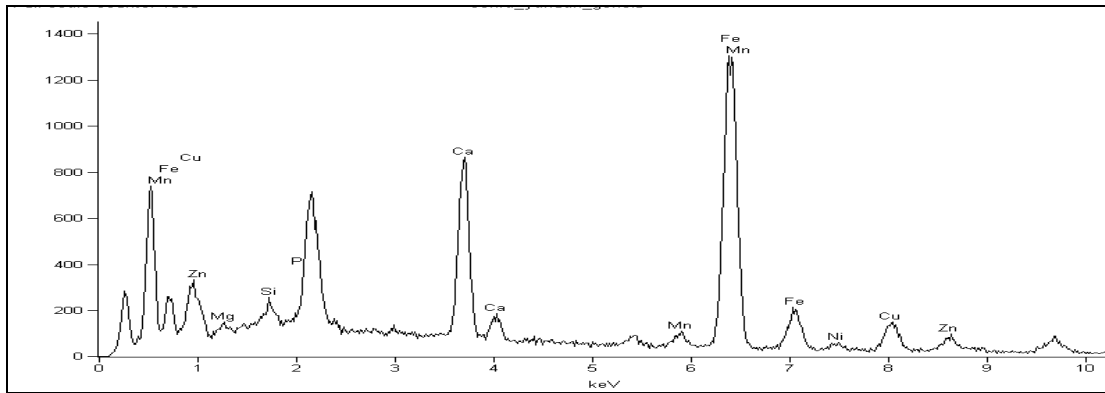


Figure F. 12 In-Depth SEM/EDX Micrograph (near to surface_5) –after the 100 day-experiment

Table F. 12 In-Depth SEM element analysis (near to surface_5) - after the 100 day-experiment

<i>Element</i>	<i>Weight Conc %</i>	<i>Atom Conc %</i>
<i>Mg</i>	1.66	3.53
<i>Si</i>	1.91	3.52
<i>P</i>	0.00	0.00
<i>Ca</i>	15.22	19.70
<i>Mn</i>	2.24	2.12
<i>Fe</i>	59.59	55.33
<i>Ni</i>	1.85	1.63
<i>Cu</i>	11.40	9.30
<i>Zn</i>	6.14	4.87

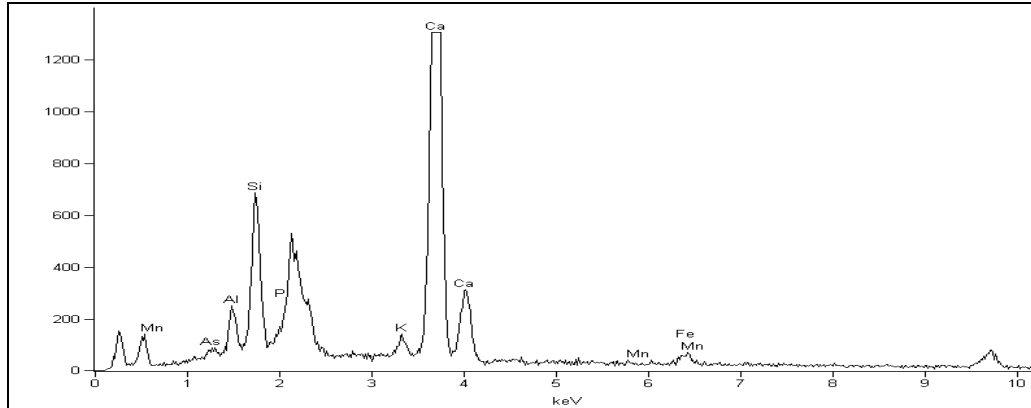


Figure F. 13 In -Depth SEM/EDX Micrograph (inner part)-after to the 100 day-experiment

Table F. 13 In -Depth SEM element analysis (inner part)-after to the 100 day-experiment

<i>Element</i>	<i>Weight Conc %</i>	<i>Atom Conc %</i>
<i>Al</i>	4.91	6.79
<i>Si</i>	14.13	18.76
<i>P</i>	0.00	0.00
<i>K</i>	2.00	1.91
<i>Ca</i>	75.34	70.12
<i>Mn</i>	0.00	0.00
<i>Fe</i>	3.62	2.42

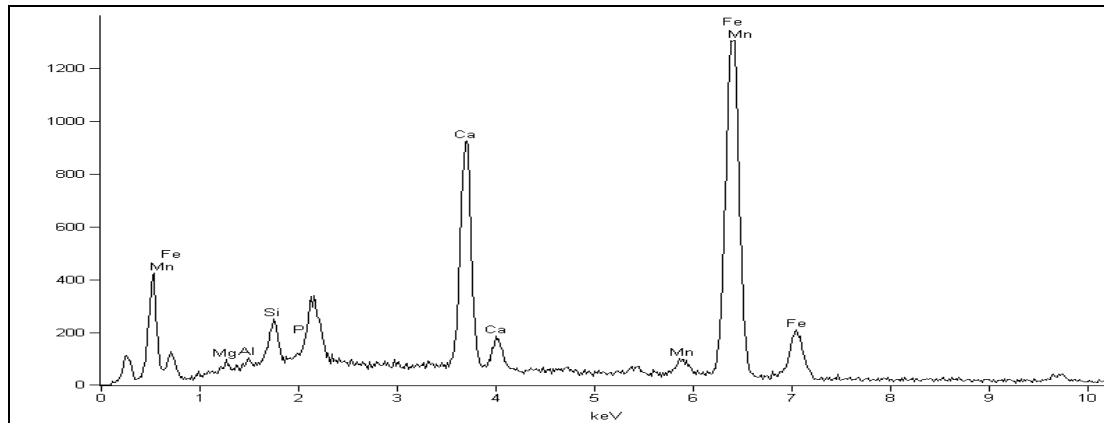


Figure F. 14 Top Surface SEM/EDX Micrograph_1-after the 100 day-experiment

Table F. 14 Top Surface SEM element analysis _1-after the 100 day-experiment

<i>Element</i>	<i>Weight Conc %</i>	<i>Atom Conc %</i>
<i>Mg</i>	1.04	2.10
<i>Al</i>	0.56	1.03
<i>Si</i>	3.94	6.90
<i>Ca</i>	19.18	23.56
<i>Mn</i>	2.85	2.56
<i>Fe</i>	72.43	63.85

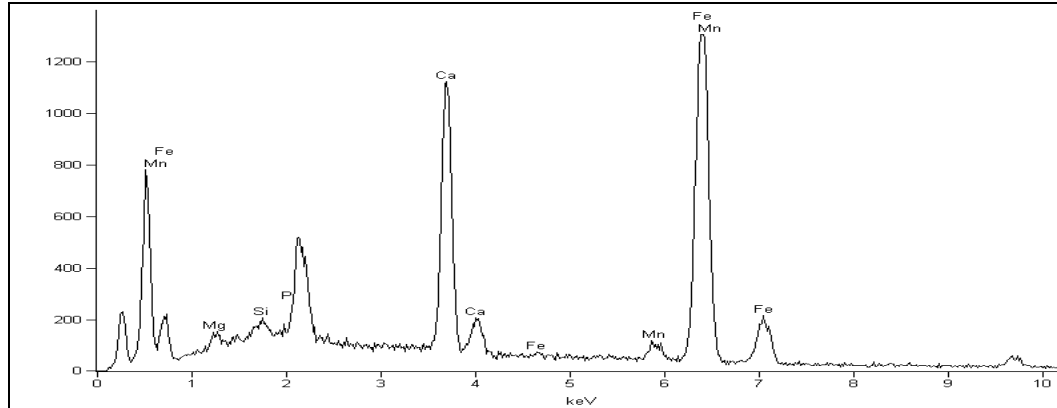


Figure F. 15 Top Surface SEM/EDX Micrograph_2-after the e100 day-xperiment

Table F. 15 Top Surface SEM element analysis_2-after the 100 day-experiment

<i>Element</i>	<i>Weight Conc %</i>	<i>Atom Conc %</i>
<i>Mg</i>	1.91	3.91
<i>Si</i>	1.39	2.45
<i>P</i>	0.00	0.00
<i>Ca</i>	21.93	27.15
<i>Mn</i>	3.30	2.98
<i>Fe</i>	71.47	63.51

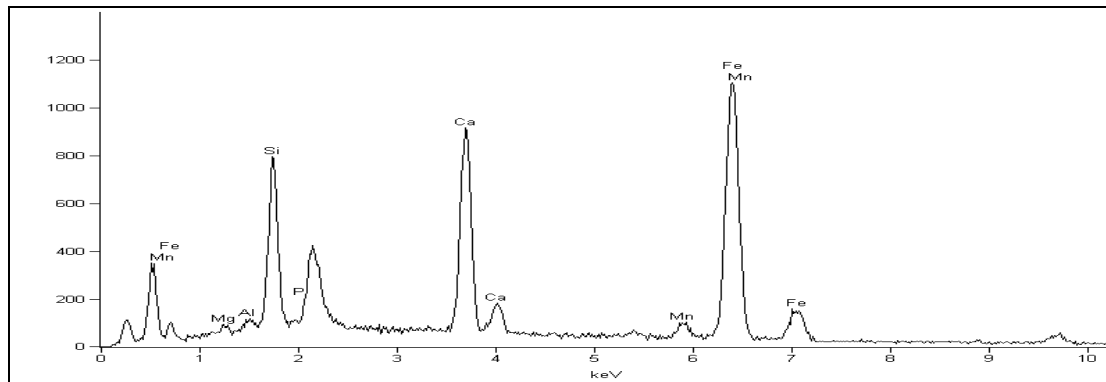


Figure F. 16 Top Surface SEM/EDX Micrograph_3-after the 100 day-experiment

Table F. 16 Top Surface SEM element analysis_3-after the 100 day-experiment

<i>Element</i>	<i>Weight Conc %</i>	<i>Atom Conc %</i>
<i>Mg</i>	1.05	1.94
<i>Al</i>	1.08	1.79
<i>Si</i>	14.30	22.81
<i>P</i>	0.00	0.00
<i>Ca</i>	20.31	22.69
<i>Mn</i>	2.30	1.88
<i>Fe</i>	60.96	48.90

APPENDIX G

SEM PHOTOS OF THE 100 DAY-STATIC EXPERIMENT

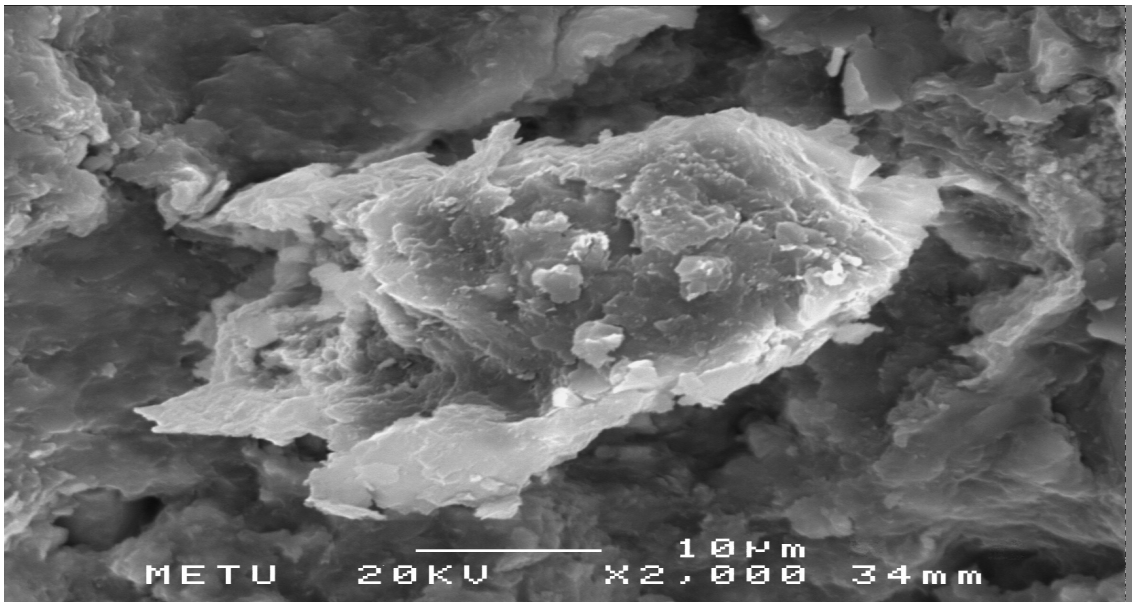


Figure G. 1 Near to surface view of in depth SEM Analysis -prior to the 100 day-experiment

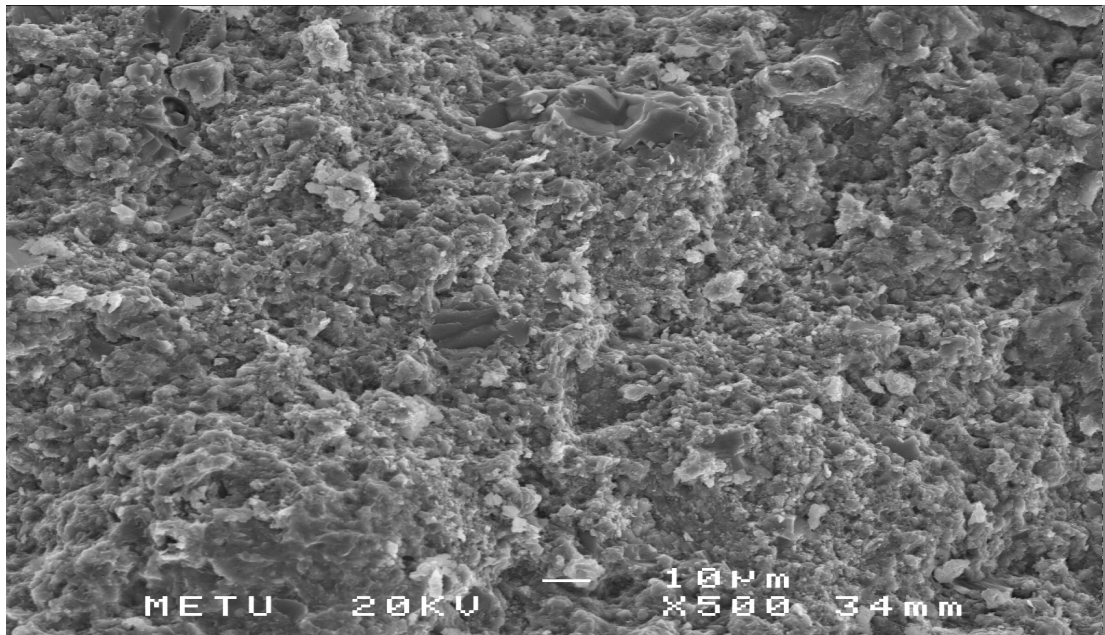


Figure G. 2 Inner view of in depth SEM Analysis -prior to the 100 day-experiment

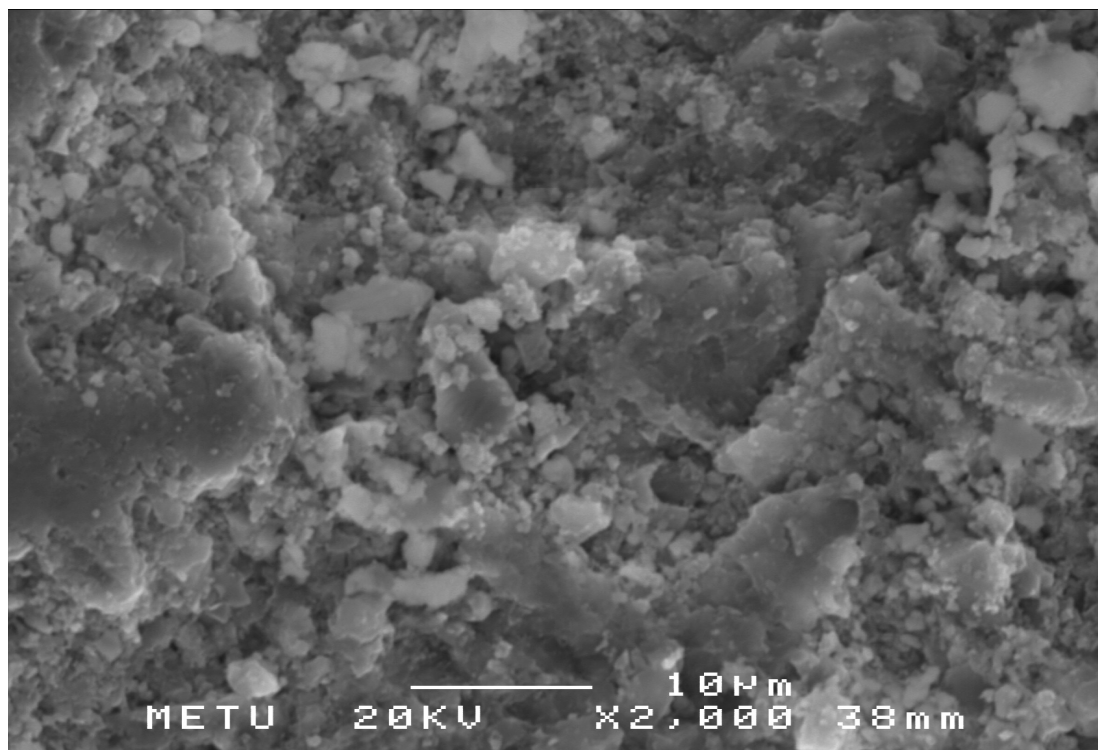


Figure G. 3 Top surface SEM Analysis -prior the 100 day-experiment

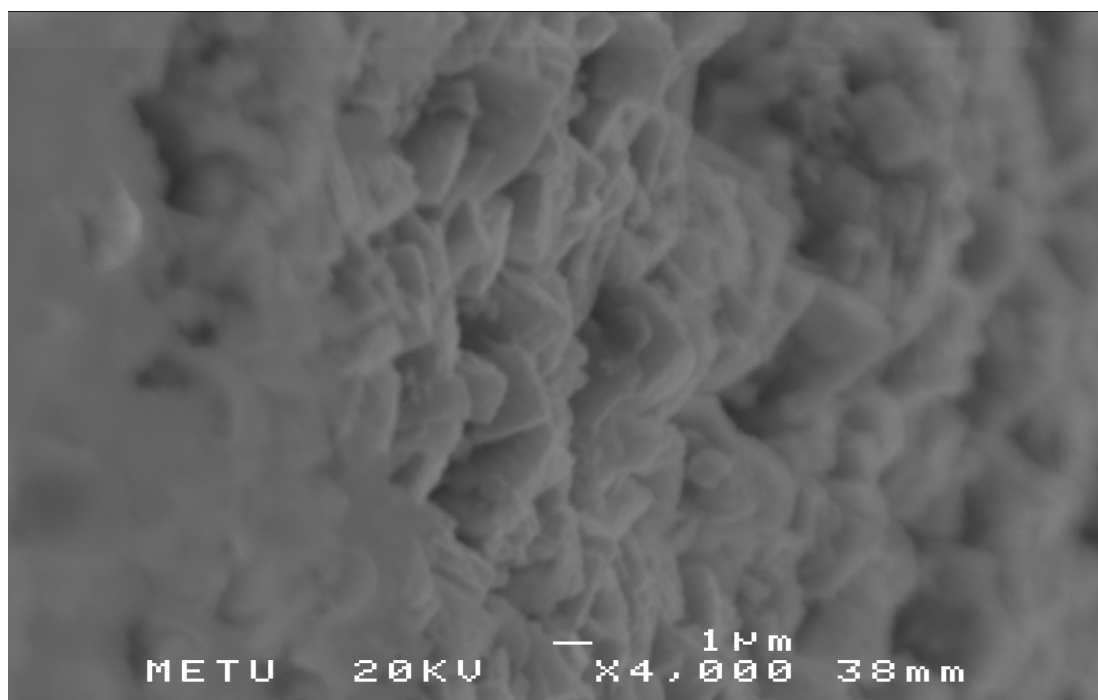


Figure G. 4 Near to surface view of in depth SEM Analysis _1-after the 100 day-experiment

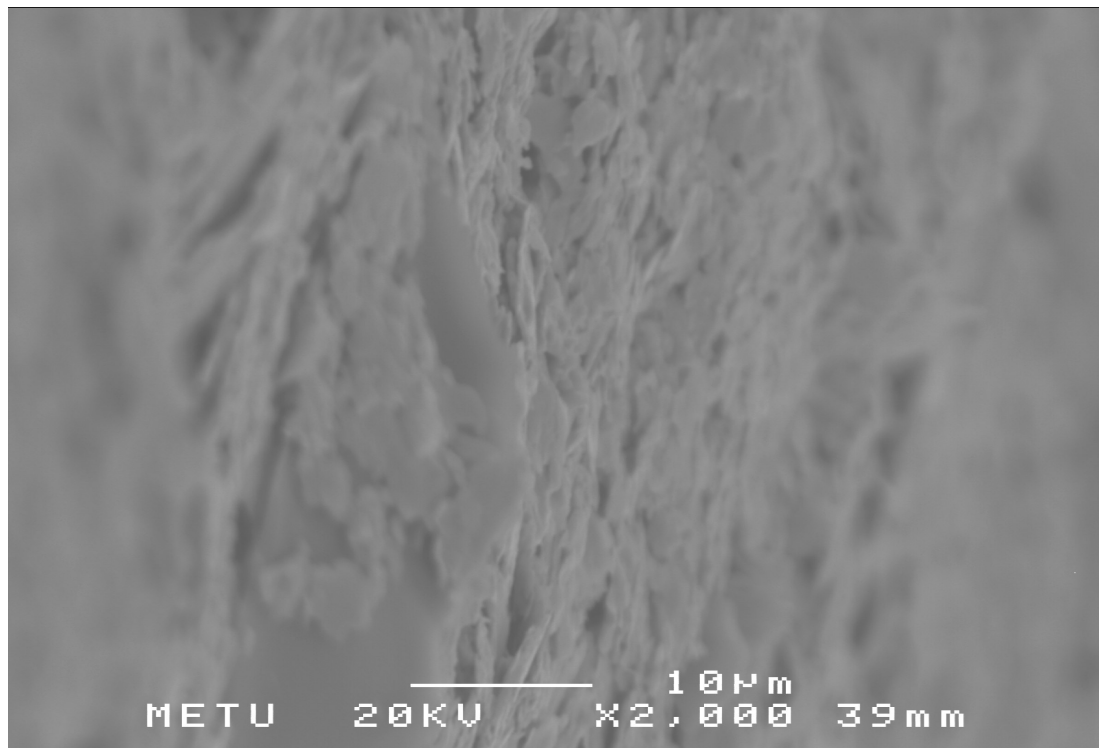


Figure G. 5 Near to surface view of in depth SEM Analysis_2-1 after the 100 day-experiment

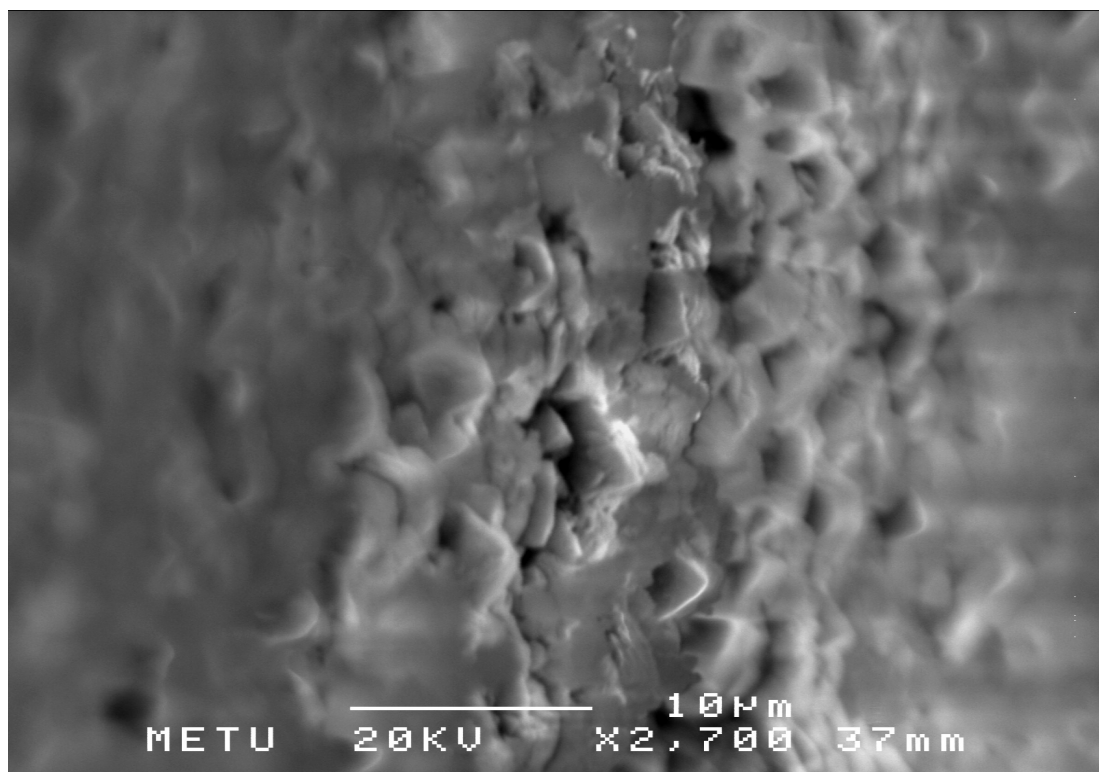


Figure G. 6 Near to surface view of in depth SEM Analysis_3- after the 100 day-experiment

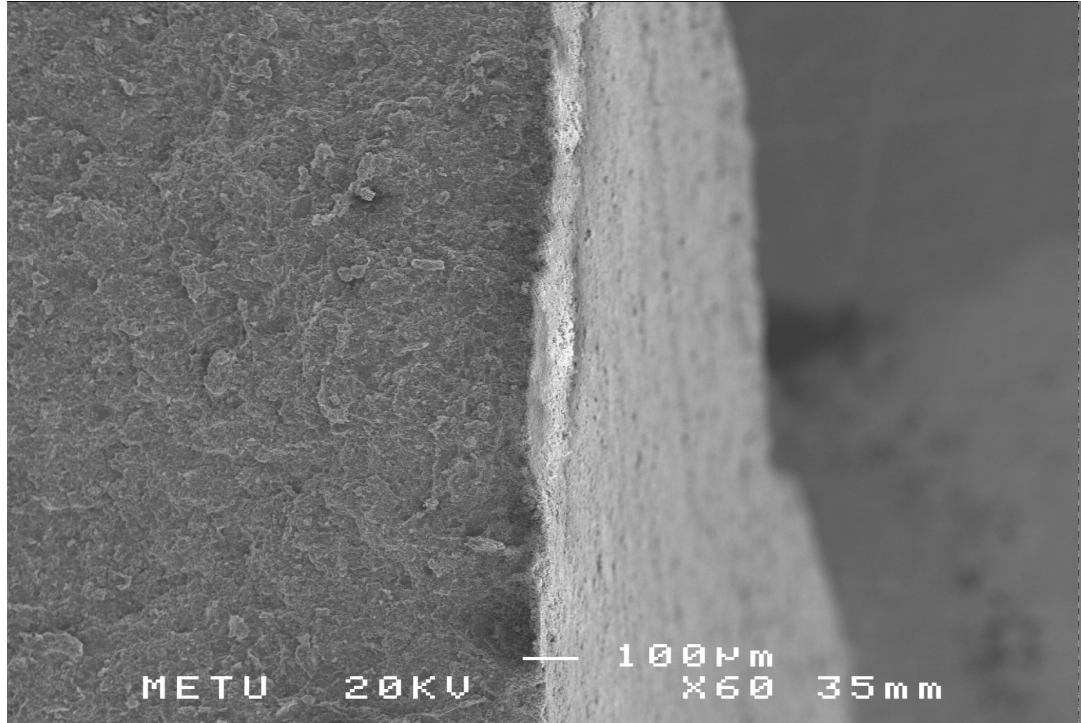


Figure G. 7 Near to surface view of in depth SEM Analysis-4-after the 100 day-experiment

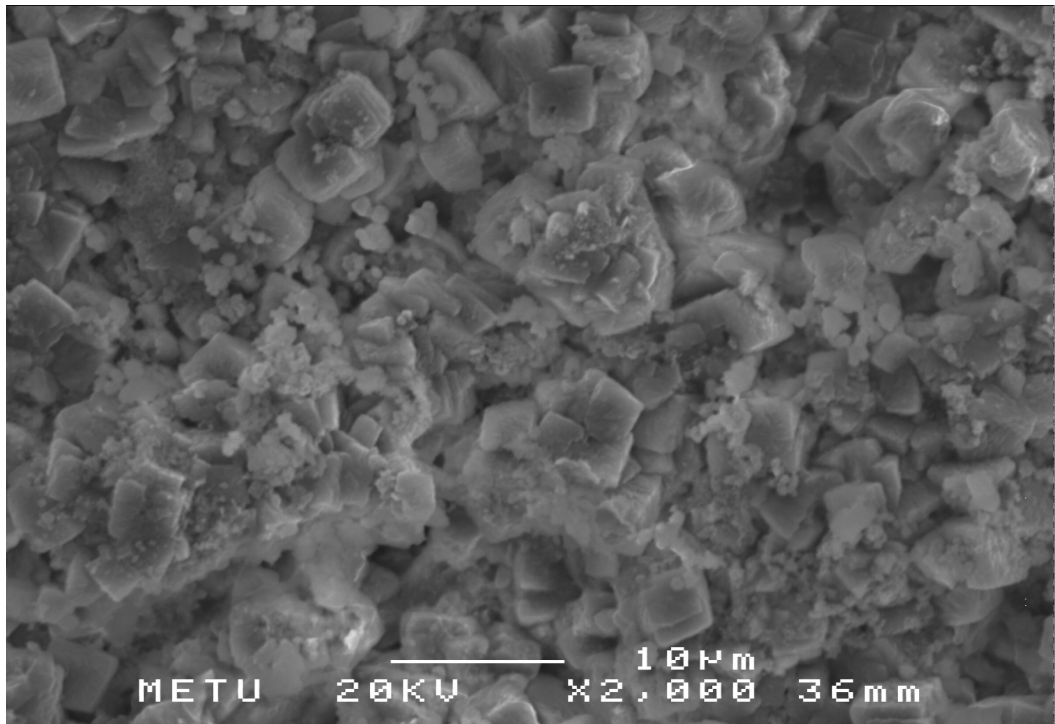


Figure G. 8 Top Surface SEM Analysis_1- after the 100 day-experiment

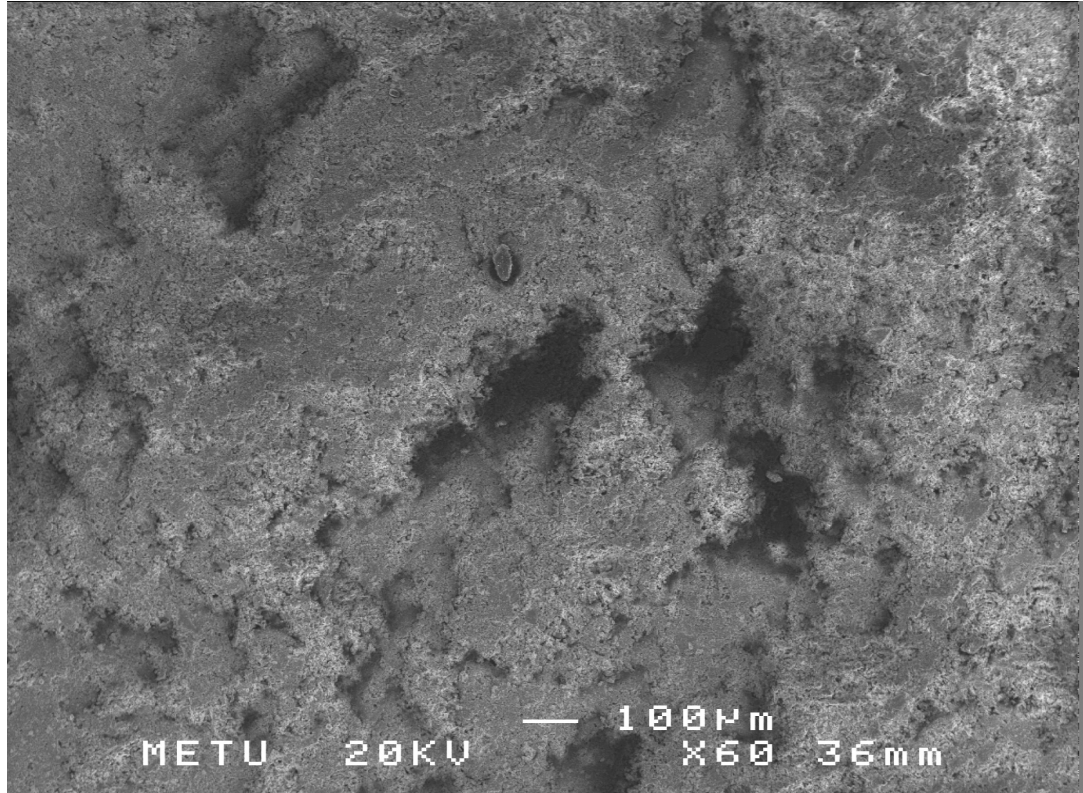


Figure G. 9 Top Surface SEM Analysis_2- after the 100 day-experiment (wormholes)

APPENDIX H

XRD ANALYSIS RESULTS (DYNAMIC EXPERIMENT)

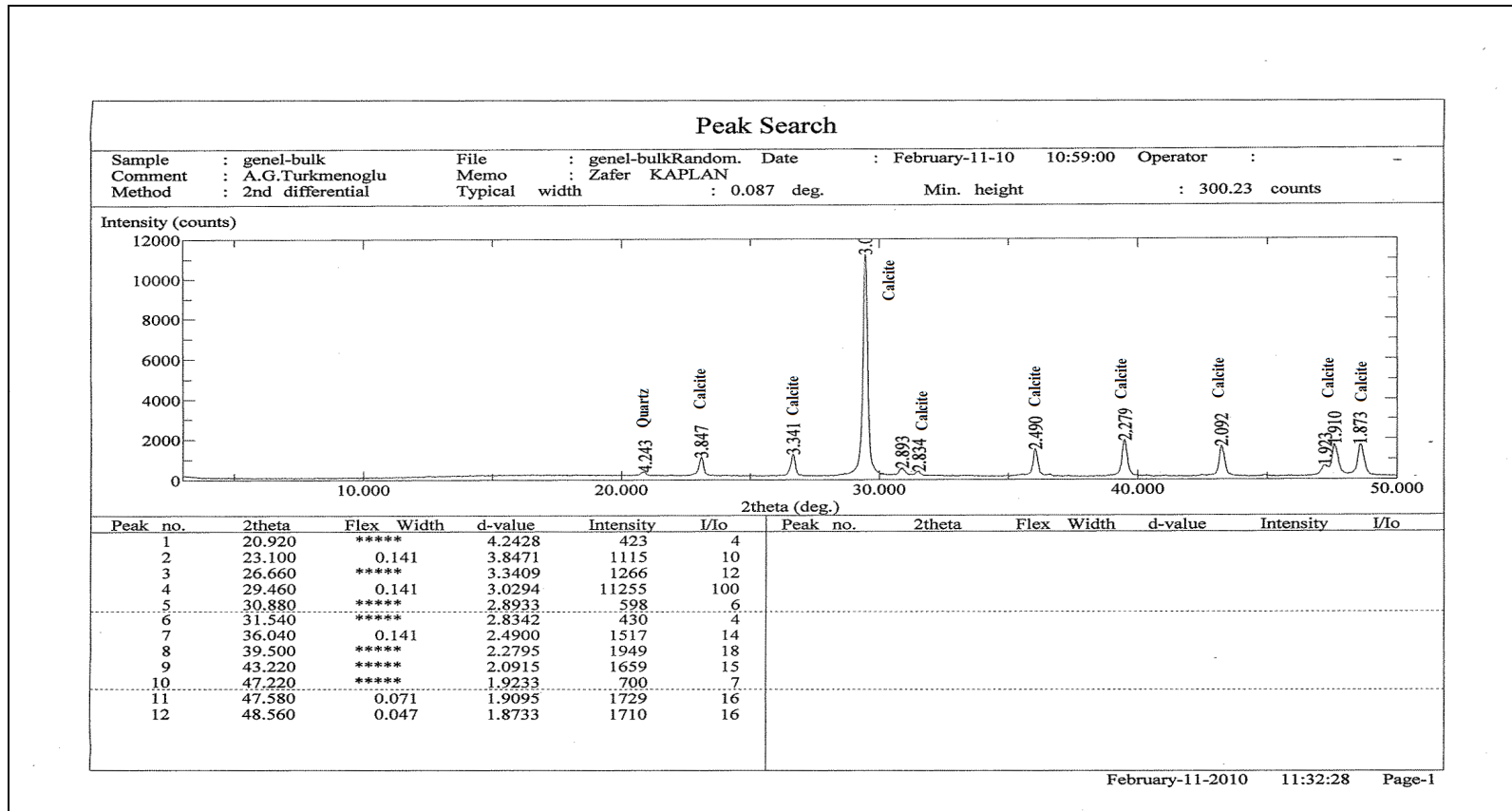


Figure H. 1XRD Analysis of the original grinded core

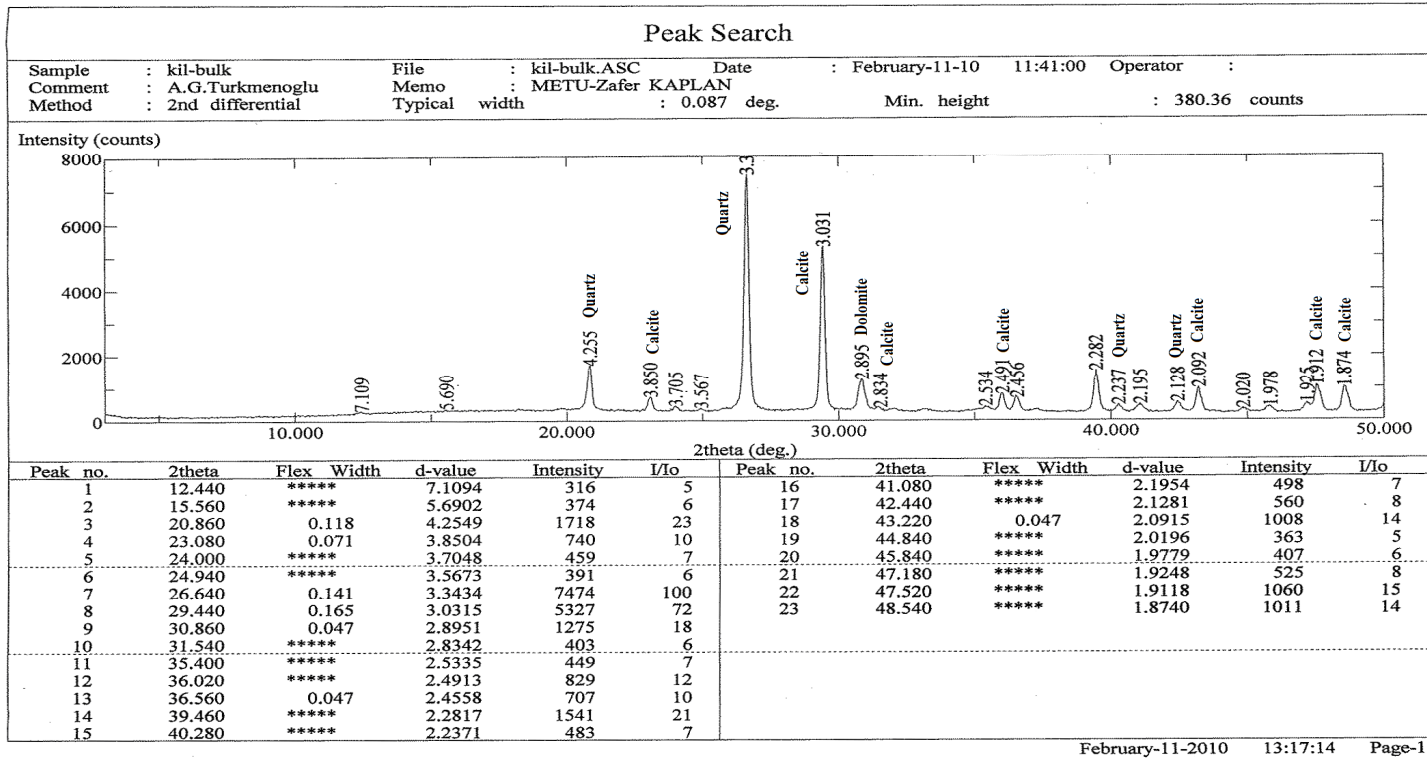


Figure H. 2 XRD Analysis after the acid treatment

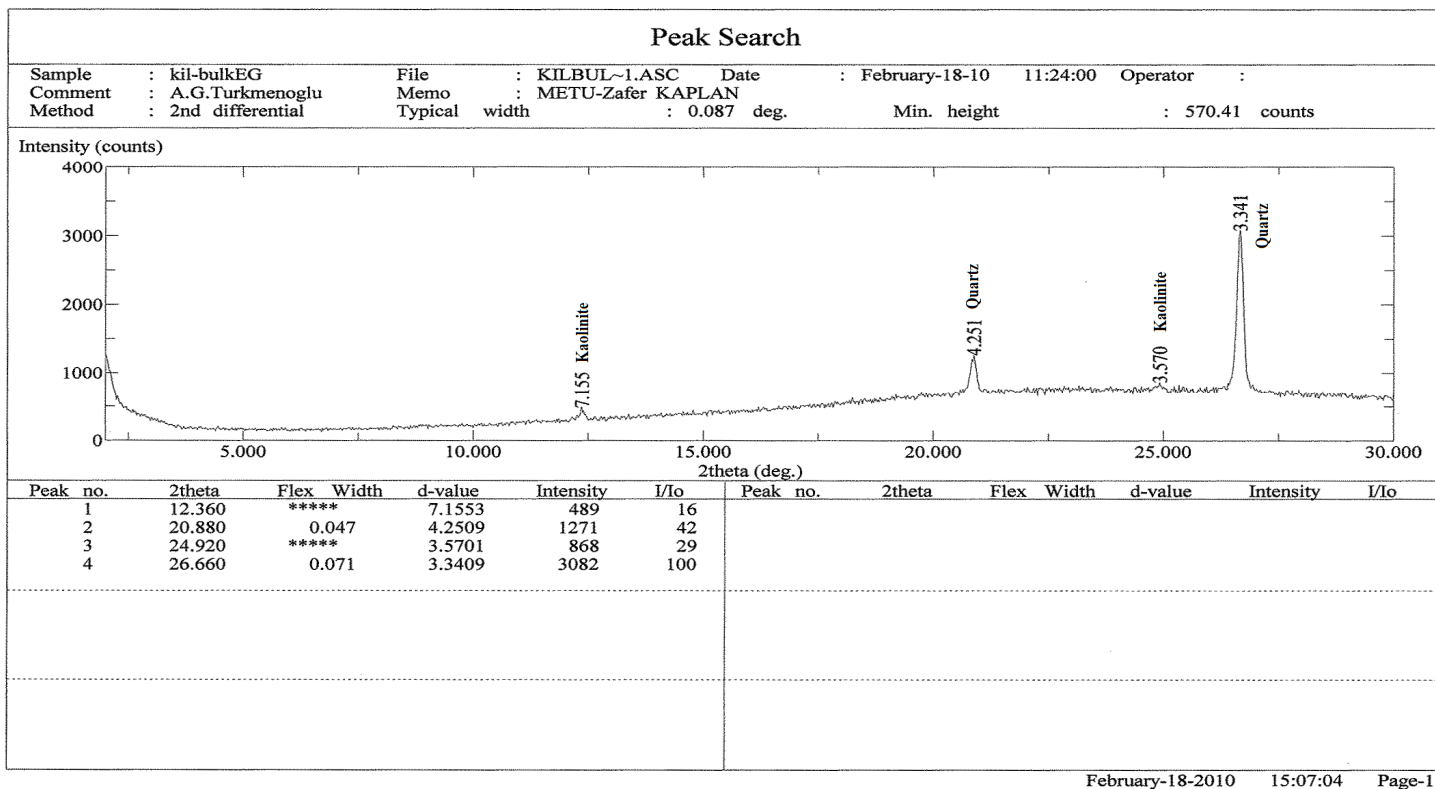


Figure H. 3 Analysis of the sample waited in ethylene glycol

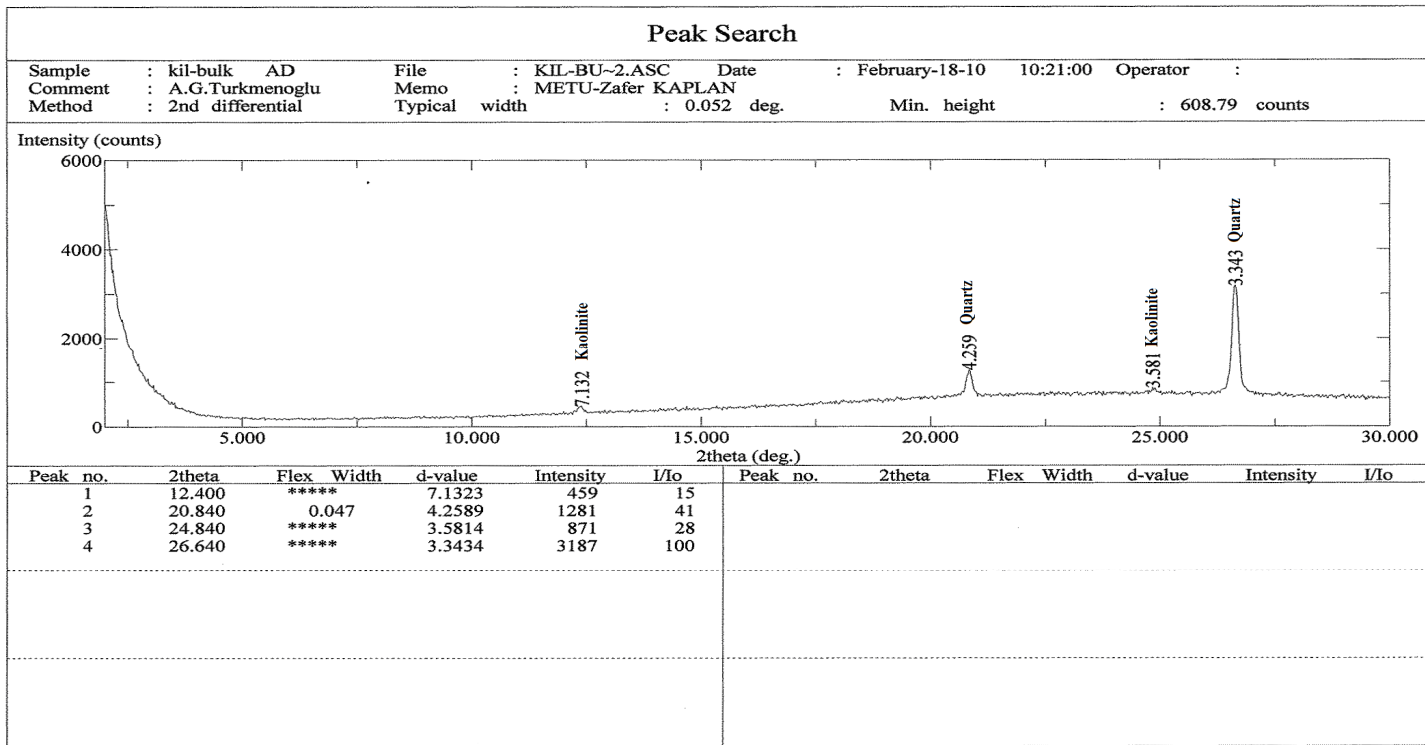
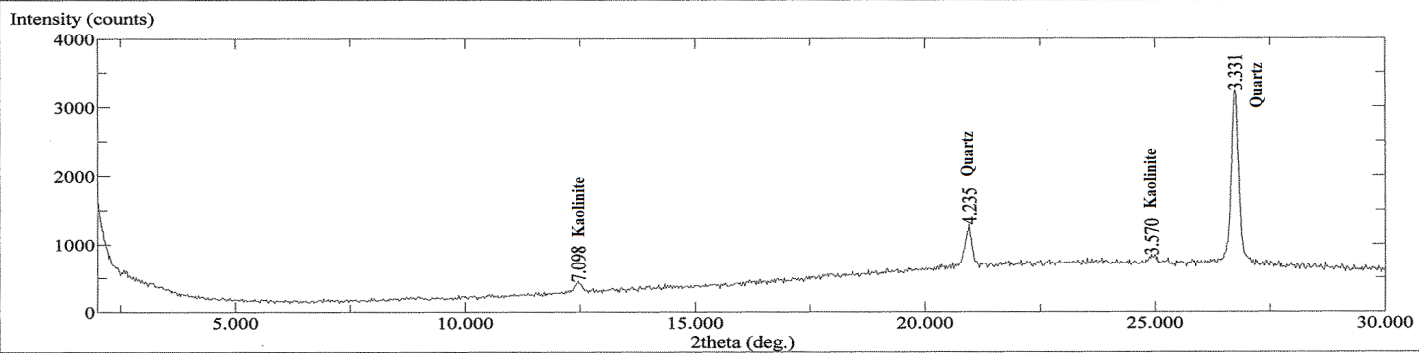


Figure H. 4 Analysis of the air dried sample

Peak Search

Sample : kil-b ulk 300 File : KIL-BU~2Peak.ASC Date : February-18-10 10:46:00 Operator :
 Comment : A.G.Turkmenoglu Memo : METU-Zafer KAPLAN
 Method : 2nd differential Typical width : 0.087 deg. Min. height : 555.91 counts



Peak no.	2theta	Flex	Width	d-value	Intensity	I/Io	Peak no.	2theta	Flex	Width	d-value	Intensity	I/Io
1	12.460	*****		7.0981	455	15							
2	20.960	*****		4.2348	1301	41							
3	24.920	*****		3.5701	846	27							
4	26.740	0.094		3.3311	3237	100							

Figure H. 5 Analysis of the sample dried at 300 °C

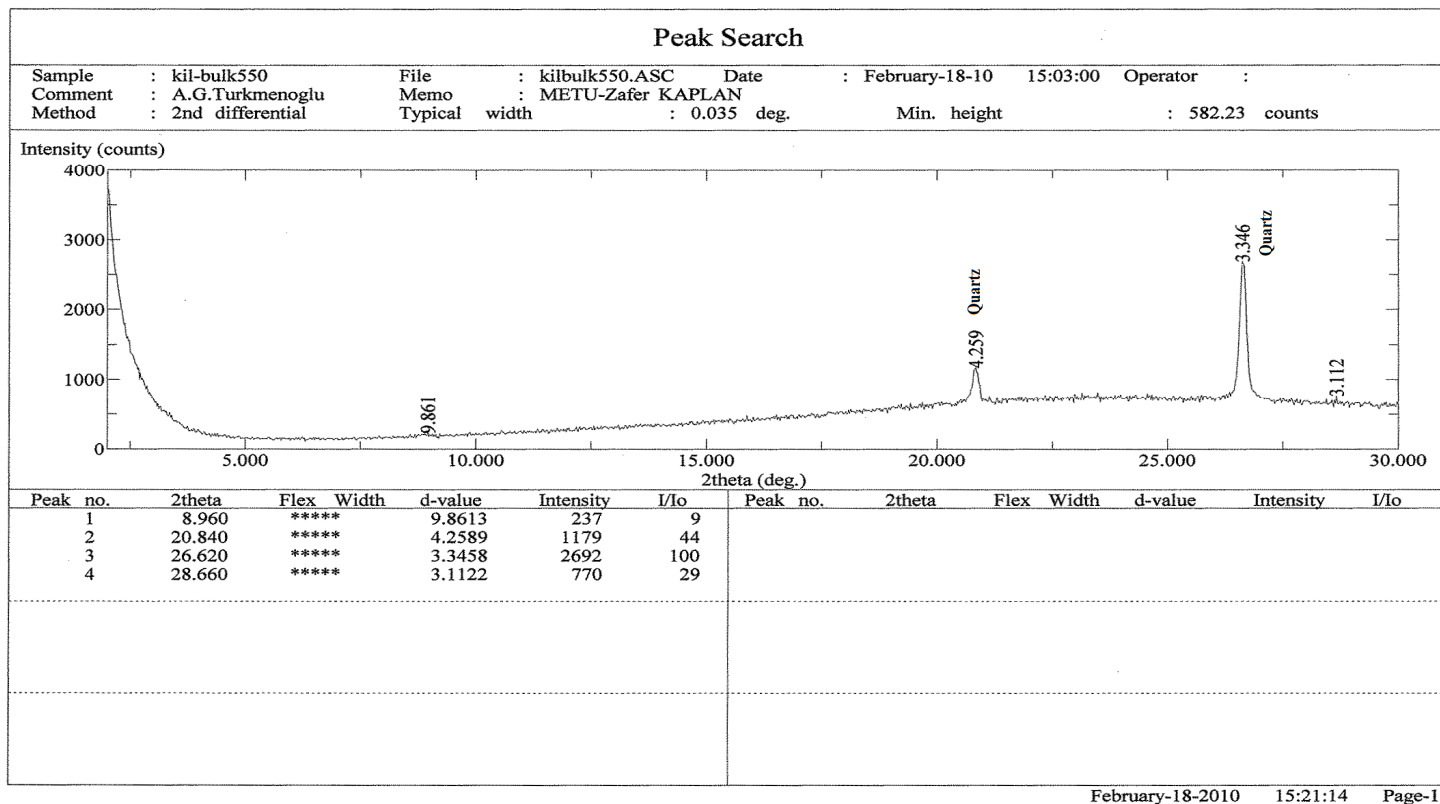


Figure H. 6 XRD Analysis of the sample dried at 550 °C

APPENDIX I

DETERMINATION OF THE POROSITY AND PERMEABILITY

Before carrying out the dynamic experiment, an experiment is conducted to determine the porosity and permeability, in which same grain sized packed limestone (60 mesh size) is used.

Determination of porosity

Porosity is determined by weight difference method. It is calculated as 0.28 as given in Table I.1.

Table I. 1 Porosity calculation

Packed dry core (g)	50
Water saturated packed core (g)	57.8761
Water amount in the packed core(g)	7.8761
Pore volume (cc)	7.8761
Packed pore volume(cc)	27.869
Porosity (fraction)	0.28

Determination of permeability

Water is injected through the packed core at different flow rates at room conditions. The viscosity of the injected fluid at this condition is 1.124 cp.

Table I.2 shows the recordings of the experiment. Table I.3 gives the dimensions of the packed core used in this experiment.

Table I. 2 Recordings of the experiment with the packed core of L=5.5 cm, D=2.54

Qpump (cm3/min)	Qpump (cm3/sec)	P1(bar)	P2(bar)	ΔP (bar)	ΔP (atm)	Qpump/A	$\Delta P/L$
						0,0000	0,0000
0,5	0,008	0	10,10	10,10	10,23	0,0016	1,8364
1	0,017	0	11,40	11,40	11,55	0,0033	2,0727
1,5	0,025	0	21,20	21,20	21,48	0,0049	3,8545
2	0,033	0	26,80	26,80	27,16	0,0066	4,8727

Using the Darcy equation following, permeability was calculated as 0.0018 darcy or $1.8 \cdot 10^{-14} \text{ m}^2$.

$$Q/A = -\kappa/\mu * \nabla P/L$$

The obtained values of porosity and permeability from this experiment are used in the simulation study.

APPENDIX J

KINETICS OF MINERAL DISSOLUTION AND PRECIPITATION

Rate equation:

$$rate = r_m = \pm k_m * A_m * \left\{ 1 - \left(\frac{Q}{K} \right)^\mu \right\}^\eta$$

A positive value for r_m corresponds to dissolution of the mineral m , negative value for precipitation.

A_m – reactive surface area, m_{mineral}^2

k_m – kinetic rate constant at fixed at T and pH, $mol \cdot m_{\text{mineral}}^{-2} \cdot \text{sec}^{-1}$

Q – ion activity

K – the equilibrium constant for specific mineral-water reaction,

$mol \cdot m_{\text{mineral}}^{-2} \cdot \text{sec}^{-1}$

μ and η – two constants which depend on experimental data: they are usually but not always taken equal to 1.

In this study, these values are taken as 1.

The temperature dependence of the reaction rate constant is expressed via an Arrhenius equation.

Arrhenius Equation:

$$k_m = k_{25} \cdot \exp\left[\frac{-E_a}{R} \cdot \left(\frac{1}{T} - \frac{1}{298.15}\right)\right]$$

k_{25} – the rate constant at 25°C, $\text{mol} \cdot \text{m}_{\text{ineral}}^{-2} \cdot \text{sec}^{-1}$

R – the universal gas constant, $8.314472 \cdot 10^{-3} \frac{\text{kJ}}{\text{K mol}}$

E_a – the activation energy, $\frac{\text{kJ}}{\text{mol}}$

T – absolute temperature, K

APPENDIX K

RESULTS OF THE CO₂ EQUILIBRATION WITH THE FORMATION WATER

Input file for the PHREEQC simulation:

Input file: C:\Documents and Settings\Owner\Desktop\try_2.pqi
Output file: C:\Documents and Settings\Owner\Desktop\try_2.pgo
Database file: C:\Program Files\USGS\Phreeqc Interactive 2.15.0\phreeqc.dat

Reading data base.

SOLUTION_MASTER_SPECIES
SOLUTION_SPECIES
PHASES
EXCHANGE_MASTER_SPECIES
EXCHANGE_SPECIES
SURFACE_MASTER_SPECIES
SURFACE_SPECIES
RATES
END

Reading input data for simulation 1.

DATABASE C:\Program Files\USGS\Phreeqc Interactive 2.15.0\phreeqc.dat
SOLUTION 1
temp 90
pH 7.789
pe 4
redox pe
units ppm
density 1
Na 519
Ca 37.5
Mg 45
Fe(3) 0.05
S(6) 14.08
Cl 746.88
Alkalinity 658
water 1 # kg

SAVE solution 1
 GAS_PHASE 1
 fixed_pressure
 pressure 13.8
 volume 1.36
 temperature 90
 CO2(g) 13.8

 Beginning of initial solution calculations.

Initial solution 1.

-----Solution composition-----

Elements	Molality	Moles
Alkalinity	1.317e-002	1.317e-002
Ca	9.375e-004	9.375e-004
Cl	2.111e-002	2.111e-002
Fe(3)	8.971e-007	8.971e-007
Mg	1.855e-003	1.855e-003
Na	2.262e-002	2.262e-002
S(6)	1.469e-004	1.469e-004

-----Description of solution-----

pH = 7.789
 pe = 4.000
 Activity of water = 0.999
 Ionic strength = 3.257e-002
 Mass of water (kg) = 1.000e+000
 Total carbon (mol/kg) = 1.289e-002
 Total CO2 (mol/kg) = 1.289e-002
 Temperature (deg C) = 90.000
 Electrical balance (eq) = -6.372e-003
 Percent error, 100*(Cat-|Anl|)/(Cat+|Anl|) = -10.56
 Iterations = 8
 Total H = 1.110244e+002
 Total O = 5.554516e+001

-----Distribution of species-----

Species	Molality	Log Activity	Log Molality	Log Activity	Gamma
OH-	2.788e-005	2.281e-005	-4.555	-4.642	-0.087
H+	1.901e-008	1.626e-008	-7.721	-7.789	-0.068
H2O	5.551e+001	9.990e-001	1.744	-0.000	0.000

C(4)	1.289e-002					
HCO3-	1.155e-002	9.621e-003	-1.937	-2.017	-0.079	
CO2	3.711e-004	3.739e-004	-3.431	-3.427	0.003	
NaCO3-	2.660e-004	2.193e-004	-3.575	-3.659	-0.084	
MgHCO3+	1.894e-004	1.562e-004	-3.723	-3.806	-0.084	
CaCO3	1.618e-004	1.631e-004	-3.791	-3.788	0.003	
NaHCO3	9.882e-005	9.956e-005	-4.005	-4.002	0.003	
CO3-2	9.012e-005	4.337e-005	-4.045	-4.363	-0.318	
MgCO3	8.328e-005	8.390e-005	-4.079	-4.076	0.003	
CaHCO3+	7.833e-005	6.524e-005	-4.106	-4.185	-0.079	
Ca	9.375e-004					
Ca+2	6.922e-004	3.327e-004	-3.160	-3.478	-0.318	
CaCO3	1.618e-004	1.631e-004	-3.791	-3.788	0.003	
CaHCO3+	7.833e-005	6.524e-005	-4.106	-4.185	-0.079	
CaSO4	5.196e-006	5.235e-006	-5.284	-5.281	0.003	
CaOH+	4.115e-009	3.393e-009	-8.386	-8.469	-0.084	
CaHSO4+	2.012e-012	1.658e-012	-11.696	-11.780	-0.084	
Cl	2.111e-002					
Cl-	2.111e-002	1.730e-002	-1.676	-1.762	-0.087	
FeCl+2	3.024e-020	1.397e-020	-19.519	-19.855	-0.335	
FeCl2+	2.412e-022	1.988e-022	-21.618	-21.702	-0.084	
FeCl3	3.413e-025	3.439e-025	-24.467	-24.464	0.003	
Fe(3)	8.971e-007					
Fe(OH)3	5.607e-007	5.649e-007	-6.251	-6.248	0.003	
Fe(OH)4-	3.280e-007	2.704e-007	-6.484	-6.568	-0.084	
Fe(OH)2+	8.453e-009	6.969e-009	-8.073	-8.157	-0.084	
FeOH+2	9.795e-014	4.525e-014	-13.009	-13.344	-0.335	
FeCl+2	3.024e-020	1.397e-020	-19.519	-19.855	-0.335	
Fe+3	2.020e-020	4.927e-021	-19.695	-20.307	-0.613	
FeSO4+	1.023e-020	8.433e-021	-19.990	-20.074	-0.084	
FeCl2+	2.412e-022	1.988e-022	-21.618	-21.702	-0.084	
Fe(SO4)2-	1.321e-023	1.089e-023	-22.879	-22.963	-0.084	
FeCl3	3.413e-025	3.439e-025	-24.467	-24.464	0.003	
Fe2(OH)2+4	1.334e-025	6.074e-027	-24.875	-26.217	-1.342	
FeHSO4+2	1.336e-027	6.170e-028	-26.874	-27.210	-0.335	
Fe3(OH)4+5	8.023e-033	6.429e-035	-32.096	-34.192	-2.096	
H(0)	2.183e-027					
H2	1.091e-027	1.100e-027	-26.962	-26.959	0.003	
Mg	1.855e-003					
Mg+2	1.524e-003	7.471e-004	-2.817	-3.127	-0.310	
MgHCO3+	1.894e-004	1.562e-004	-3.723	-3.806	-0.084	
MgCO3	8.328e-005	8.390e-005	-4.079	-4.076	0.003	
MgSO4	3.292e-005	3.317e-005	-4.483	-4.479	0.003	
MgOH+	2.504e-005	2.064e-005	-4.601	-4.685	-0.084	
Na	2.262e-002					
Na+	2.225e-002	1.840e-002	-1.653	-1.735	-0.082	
NaCO3-	2.660e-004	2.193e-004	-3.575	-3.659	-0.084	
NaHCO3	9.882e-005	9.956e-005	-4.005	-4.002	0.003	
NaSO4-	7.518e-006	6.198e-006	-5.124	-5.208	-0.084	

NaOH	7.416e-009	7.472e-009	-8.130	-8.127	0.003
O(0)	1.140e-021				
O2	5.700e-022	5.742e-022	-21.244	-21.241	0.003
S(6)	1.469e-004				
SO4-2	1.012e-004	4.791e-005	-3.995	-4.320	-0.325
MgSO4	3.292e-005	3.317e-005	-4.483	-4.479	0.003
NaSO4-	7.518e-006	6.198e-006	-5.124	-5.208	-0.084
CaSO4	5.196e-006	5.235e-006	-5.284	-5.281	0.003
HSO4-	5.030e-010	4.147e-010	-9.298	-9.382	-0.084
CaHSO4+	2.012e-012	1.658e-012	-11.696	-11.780	-0.084
FeSO4+	1.023e-020	8.433e-021	-19.990	-20.074	-0.084
Fe(SO4)2-	1.321e-023	1.089e-023	-22.879	-22.963	-0.084
FeHSO4+2	1.336e-027	6.170e-028	-26.874	-27.210	-0.335

-----Saturation indices-----

Phase	SI	log IAP	log KT	
Anhydrite	-2.66	-7.80	-5.14	CaSO4
Aragonite	1.18	-7.84	-9.02	CaCO3
Calcite	1.28	-7.84	-9.12	CaCO3
CO2(g)	-1.48	-3.43	-1.94	CO2
Dolomite	3.00	-15.33	-18.33	CaMg(CO3)2
Fe(OH)3(a)	-1.83	3.06	4.89	Fe(OH)3
Goethite	5.96	3.06	-2.90	FeOOH
Gypsum	-3.00	-7.80	-4.79	CaSO4:2H2O
H2(g)	-23.58	-26.96	-3.38	H2
H2O(g)	-0.13	-0.00	0.13	H2O
Halite	-5.20	-3.50	1.70	NaCl
Hematite	14.17	6.12	-8.05	Fe2O3
O2(g)	-18.13	-21.24	-3.11	O2

Beginning of batch-reaction calculations.

Reaction step 1.

Using solution 1.

Using gas phase 1.

-----Gas phase-----

Total pressure: 13.8000 atmospheres

Gas volume: 1.02e+000 liters

Moles in gas

Component	log P	P	Initial	Final	Delta
CO2(g)	1.14	1.380e+001	6.298e-001	4.732e-001	-1.566e-001

-----Solution composition-----

Elements	Molality	Moles
C	1.694e-001	1.694e-001
Ca	9.375e-004	9.375e-004
Cl	2.111e-002	2.111e-002
Fe	8.971e-007	8.971e-007
Mg	1.855e-003	1.855e-003
Na	2.262e-002	2.262e-002
S	1.469e-004	1.469e-004

-----Description of solution-----

pH = 5.208 Charge balance
 pe = 9.212 Adjusted to redox equilibrium
 Activity of water = 0.996
 Ionic strength = 3.341e-002
 Mass of water (kg) = 1.000e+000
 Total alkalinity (eq/kg) = 1.317e-002
 Total CO2 (mol/kg) = 1.694e-001
 Temperature (deg C) = 90.000
 Electrical balance (eq) = -6.372e-003
 Percent error, 100*(Cat-IAn)/(Cat+IAn) = -10.32
 Iterations = 21
 Total H = 1.110244e+002
 Total O = 5.585827e+001

-----Distribution of species-----

Species	Molality	Log Activity	Log Molality	Log Activity	Gamma
H+	7.260e-006	6.199e-006	-5.139	-5.208	-0.069
OH-	7.306e-008	5.967e-008	-7.136	-7.224	-0.088
H2O	5.551e+001	9.963e-001	1.744	-0.002	0.000
C(-4)	0.000e+000				
CH4	0.000e+000	0.000e+000	-99.614	-99.611	0.003
C(4)	1.694e-001				
CO2	1.563e-001	1.575e-001	-0.806	-0.803	0.003
HCO3-	1.275e-002	1.060e-002	-1.895	-1.975	-0.080
MgHCO3+	2.184e-004	1.797e-004	-3.661	-3.745	-0.085
NaHCO3	1.099e-004	1.107e-004	-3.959	-3.956	0.003
CaHCO3+	1.027e-004	8.540e-005	-3.988	-4.069	-0.080
NaCO3-	7.772e-007	6.396e-007	-6.109	-6.194	-0.085

CaCO3	5.554e-007	5.597e-007	-6.255	-6.252	0.003
CO3-2	2.622e-007	1.253e-007	-6.581	-6.902	-0.321
MgCO3	2.512e-007	2.532e-007	-6.600	-6.597	0.003
FeHCO3+	2.877e-011	2.367e-011	-10.541	-10.626	-0.085
FeCO3	6.662e-014	6.713e-014	-13.176	-13.173	0.003
Ca	9.375e-004				
Ca+2	8.282e-004	3.953e-004	-3.082	-3.403	-0.321
CaHCO3+	1.027e-004	8.540e-005	-3.988	-4.069	-0.080
CaSO4	6.031e-006	6.077e-006	-5.220	-5.216	0.003
CaCO3	5.554e-007	5.597e-007	-6.255	-6.252	0.003
CaHSO4+	8.922e-010	7.341e-010	-9.050	-9.134	-0.085
CaOH+	1.281e-011	1.054e-011	-10.892	-10.977	-0.085
Cl	2.111e-002				
Cl-	2.111e-002	1.726e-002	-1.676	-1.763	-0.087
FeCl+	6.467e-013	5.322e-013	-12.189	-12.274	-0.085
FeCl+2	3.998e-013	1.833e-013	-12.398	-12.737	-0.339
FeCl2+	3.163e-015	2.603e-015	-14.500	-14.585	-0.085
FeCl3	4.458e-018	4.493e-018	-17.351	-17.347	0.003
Fe(2)	7.586e-011				
Fe+2	4.581e-011	2.234e-011	-10.339	-10.651	-0.312
FeHCO3+	2.877e-011	2.367e-011	-10.541	-10.626	-0.085
FeCl+	6.467e-013	5.322e-013	-12.189	-12.274	-0.085
FeSO4	4.895e-013	4.933e-013	-12.310	-12.307	0.003
FeOH+	7.440e-014	6.122e-014	-13.128	-13.213	-0.085
FeCO3	6.662e-014	6.713e-014	-13.176	-13.173	0.003
FeHSO4+	5.041e-017	4.148e-017	-16.297	-16.382	-0.085
Fe(HS)2	0.000e+000	0.000e+000	-199.968	-199.965	0.003
Fe(HS)3-	0.000e+000	0.000e+000	-296.975	-297.060	-0.085
Fe(3)	8.970e-007				
Fe(OH)2+	7.616e-007	6.267e-007	-6.118	-6.203	-0.085
Fe(OH)3	1.318e-007	1.329e-007	-6.880	-6.877	0.003
FeOH+2	3.393e-009	1.556e-009	-8.469	-8.808	-0.339
Fe(OH)4-	2.021e-010	1.663e-010	-9.694	-9.779	-0.085
FeCl+2	3.998e-013	1.833e-013	-12.398	-12.737	-0.339
Fe+3	2.687e-013	6.477e-014	-12.571	-13.189	-0.618
FeSO4+	1.316e-013	1.083e-013	-12.881	-12.965	-0.085
FeCl2+	3.163e-015	2.603e-015	-14.500	-14.585	-0.085
Fe(SO4)2-	1.660e-016	1.366e-016	-15.780	-15.864	-0.085
Fe2(OH)2+4	1.625e-016	7.180e-018	-15.789	-17.144	-1.355
FeHSO4+2	6.591e-018	3.022e-018	-17.181	-17.520	-0.339
FeCl3	4.458e-018	4.493e-018	-17.351	-17.347	0.003
Fe3(OH)4+5	8.944e-022	6.835e-024	-21.048	-23.165	-2.117
H(0)	1.193e-032				
H2	5.966e-033	6.012e-033	-32.224	-32.221	0.003
Mg	1.855e-003				
Mg+2	1.602e-003	7.803e-004	-2.795	-3.108	-0.312
MgHCO3+	2.184e-004	1.797e-004	-3.661	-3.745	-0.085
MgSO4	3.359e-005	3.385e-005	-4.474	-4.470	0.003
MgCO3	2.512e-007	2.532e-007	-6.600	-6.597	0.003

MgOH+	6.853e-008	5.639e-008	-7.164	-7.249	-0.085
Na	2.262e-002				
Na+	2.250e-002	1.858e-002	-1.648	-1.731	-0.083
NaHCO3	1.099e-004	1.107e-004	-3.959	-3.956	0.003
NaSO4-	7.429e-006	6.113e-006	-5.129	-5.214	-0.085
NaCO3-	7.772e-007	6.396e-007	-6.109	-6.194	-0.085
NaOH	1.958e-011	1.973e-011	-10.708	-10.705	0.003
O(0)	3.792e-011				
O2	1.896e-011	1.911e-011	-10.722	-10.719	0.003
S(-2)	0.000e+000				
H2S	0.000e+000	0.000e+000	-97.819	-97.816	0.003
HS-	0.000e+000	0.000e+000	-99.044	-99.132	-0.088
S-2	0.000e+000	0.000e+000	-104.928	-105.255	-0.327
Fe(HS)2	0.000e+000	0.000e+000	-199.968	-199.965	0.003
Fe(HS)3-	0.000e+000	0.000e+000	-296.975	-297.060	-0.085
S(6)	1.469e-004				
SO4-2	9.963e-005	4.681e-005	-4.002	-4.330	-0.328
MgSO4	3.359e-005	3.385e-005	-4.474	-4.470	0.003
NaSO4-	7.429e-006	6.113e-006	-5.129	-5.214	-0.085
CaSO4	6.031e-006	6.077e-006	-5.220	-5.216	0.003
HSO4-	1.877e-007	1.545e-007	-6.726	-6.811	-0.085
CaHSO4+	8.922e-010	7.341e-010	-9.050	-9.134	-0.085
FeSO4	4.895e-013	4.933e-013	-12.310	-12.307	0.003
FeSO4+	1.316e-013	1.083e-013	-12.881	-12.965	-0.085
Fe(SO4)2-	1.660e-016	1.366e-016	-15.780	-15.864	-0.085
FeHSO4+	5.041e-017	4.148e-017	-16.297	-16.382	-0.085
FeHSO4+2	6.591e-018	3.022e-018	-17.181	-17.520	-0.339

-----Saturation indices-----

Phase	SI	log IAP	log KT	
Anhydrite	-2.60	-7.73	-5.14	CaSO4
Aragonite	-1.29	-10.31	-9.02	CaCO3
Calcite	-1.18	-10.31	-9.12	CaCO3
CH4(g)	-96.31	-99.61	-3.30	CH4
CO2(g)	1.14	-0.80	-1.94	CO2
Dolomite	-1.99	-20.31	-18.33	CaMg(CO3)2
Fe(OH)3(a)	-2.46	2.43	4.89	Fe(OH)3
FeS(ppt)	-100.66	-104.58	-3.92	FeS
Goethite	5.33	2.43	-2.90	FeOOH
Gypsum	-2.94	-7.74	-4.79	CaSO4:2H2O
H2(g)	-28.84	-32.22	-3.38	H2
H2O(g)	-0.13	-0.00	0.13	H2O
H2S(g)	-96.22	-97.82	-1.60	H2S
Halite	-5.20	-3.49	1.70	NaCl
Hematite	12.92	4.86	-8.05	Fe2O3
Mackinawite	-99.93	-104.58	-4.65	FeS
Melanterite	-13.30	-14.99	-1.69	FeSO4:7H2O

O2(g)	-7.61	-10.72	-3.11	O2
Pyrite	-163.08	-180.07	-17.00	FeS2
Siderite	-6.34	-17.55	-11.22	FeCO3
Sulfur	-72.61	-68.98	3.64	S

End of simulation.

APPENDIX L

RESULTS OF THE SIMULATION OF THE DYNAMIC EXPERIMENT

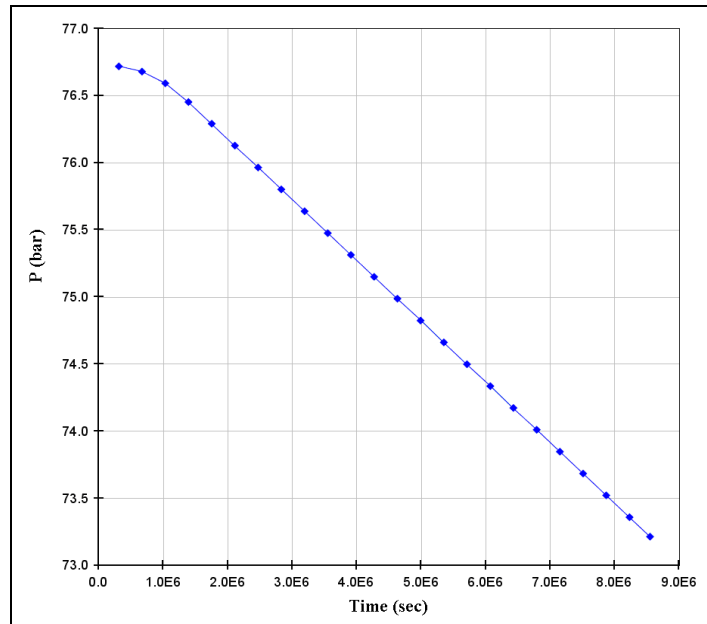


Figure L. 1 Time evolution of pressure during the 99 day-simulation

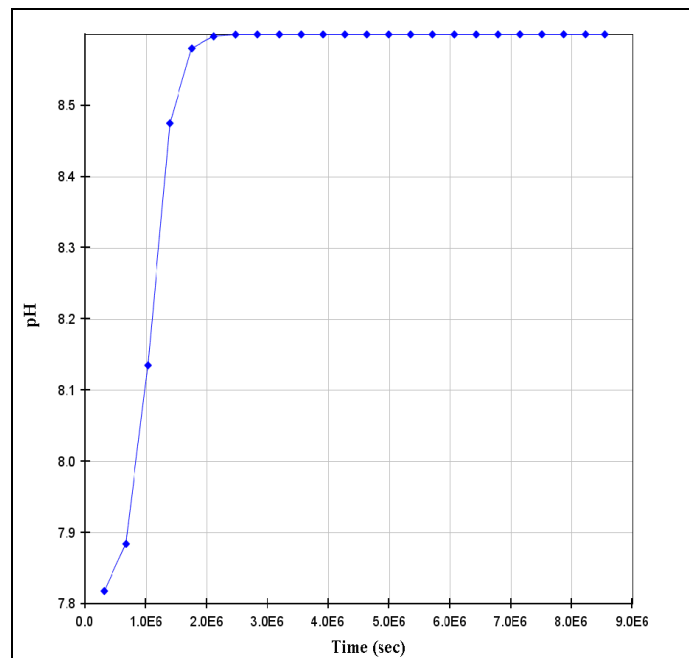


Figure L. 2 Time evolution of pH during the 99 day-simulation

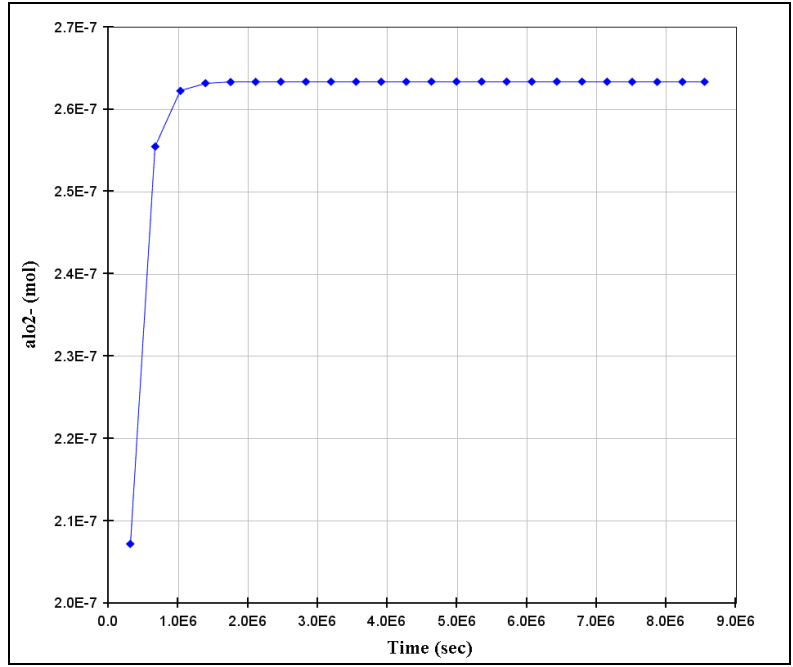


Figure L. 3 Time evolution of AlO_2^- during the 99 day-simulation

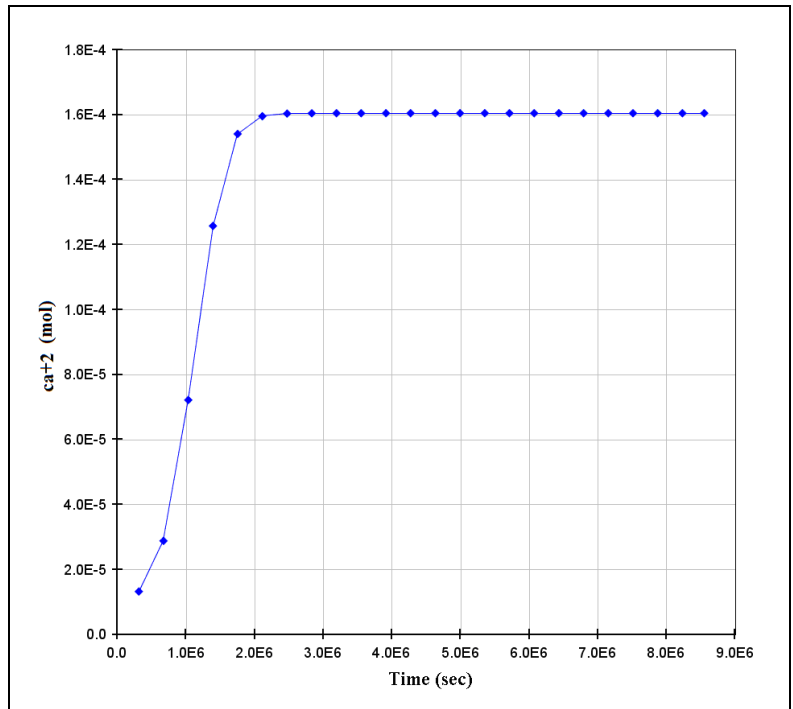


Figure L. 4 Time evolution of Ca^{+2} during the 99 day-simulation

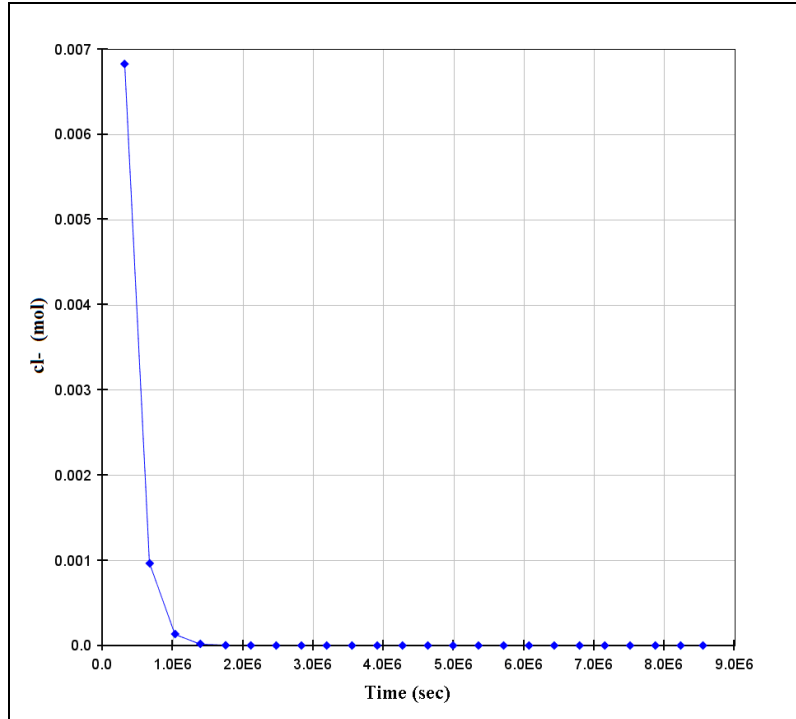


Figure L. 5 Time evolution of Cl⁻ during the 99 day-simulation

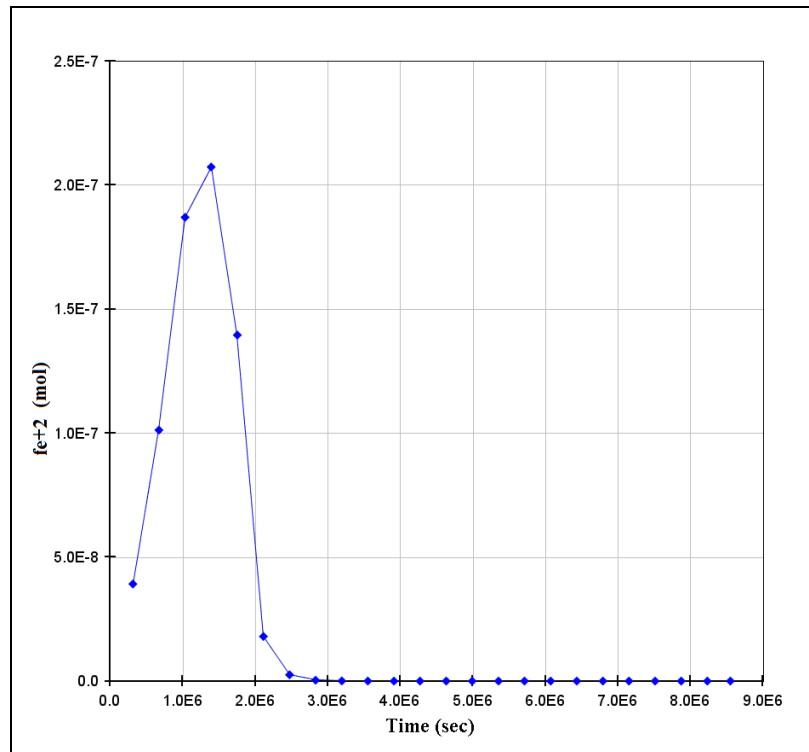


Figure L. 6 Time evolution of Fe⁺² during the 99 day-simulation

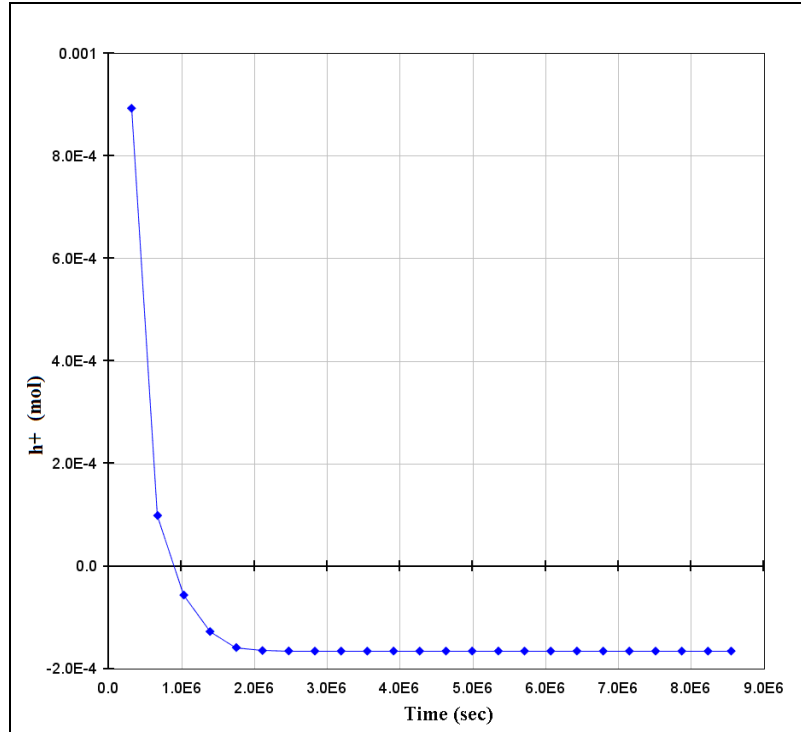


Figure L. 7 Time evolution of H⁺ during the 99 day-simulation

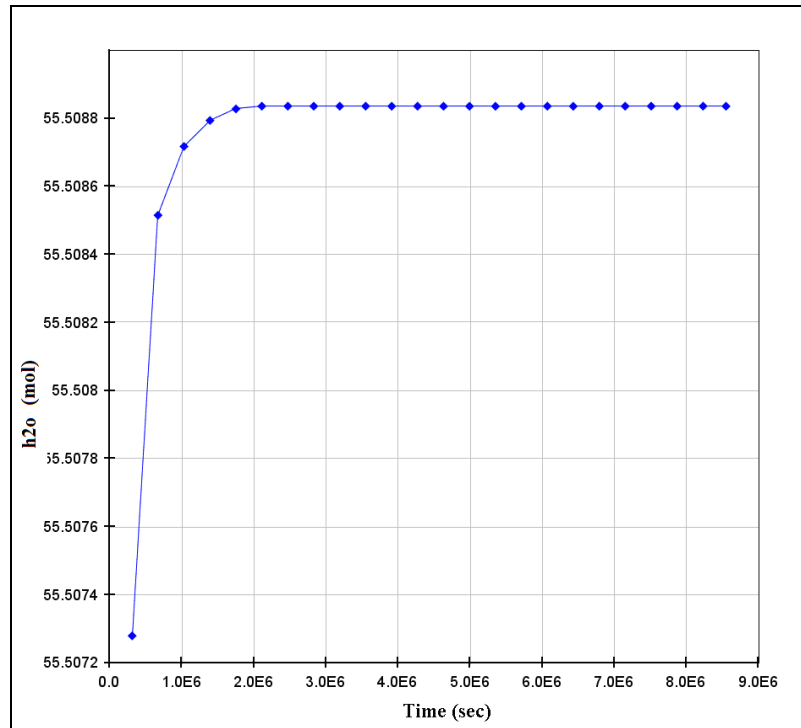


Figure L. 8 Time evolution of H₂O during the 99 day-simulation

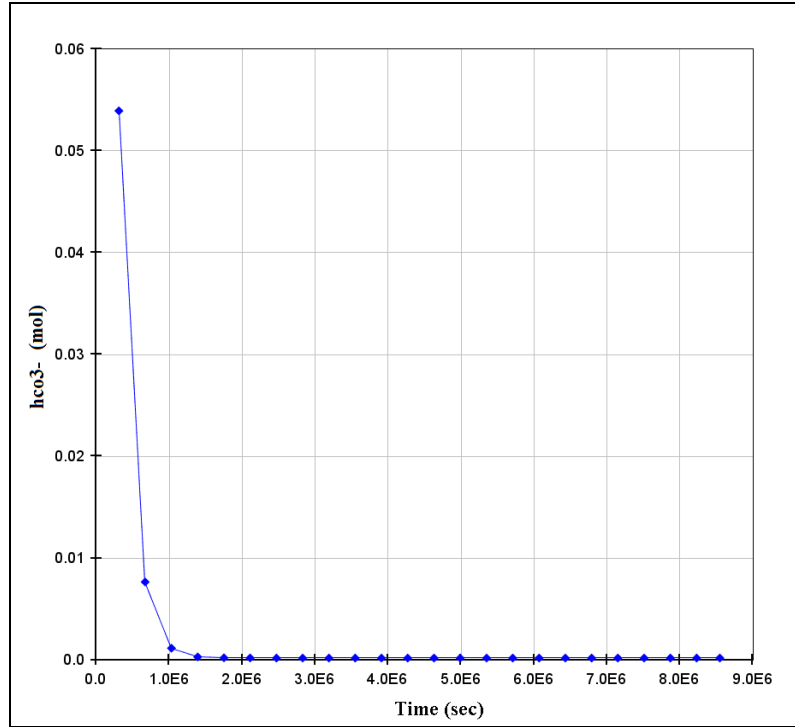


Figure L. 9 Time evolution of HCO_3^- during the 99 day-simulation

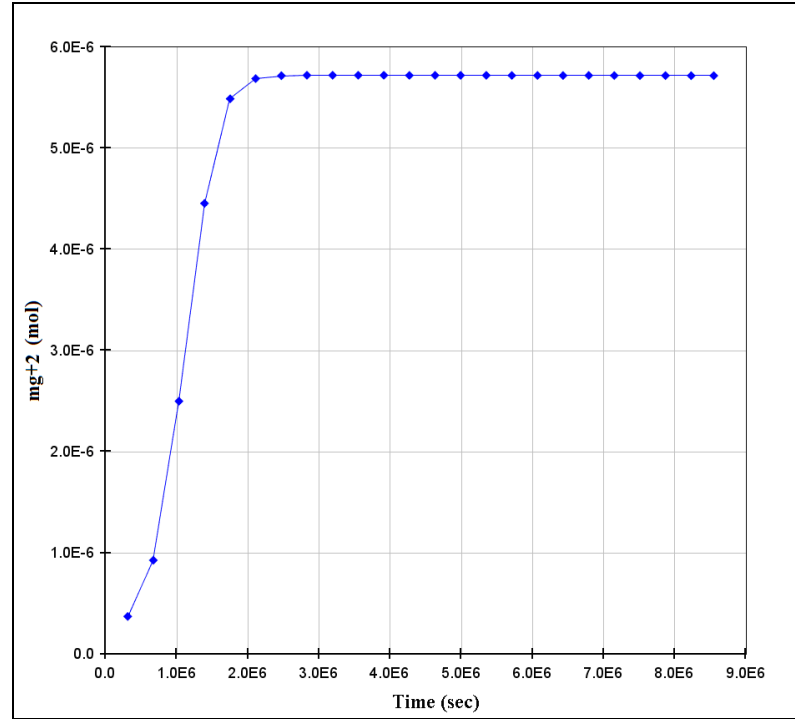


Figure L. 10 Time evolution of Mg^{+2} during the 99 day-simulation

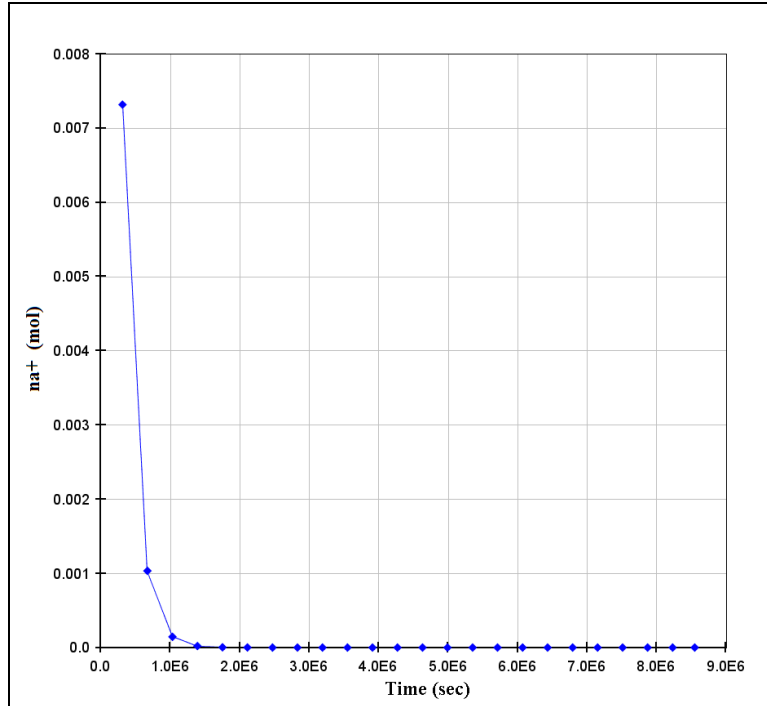


Figure L. 11 Time evolution of Na⁺ during the 99 day-simulation

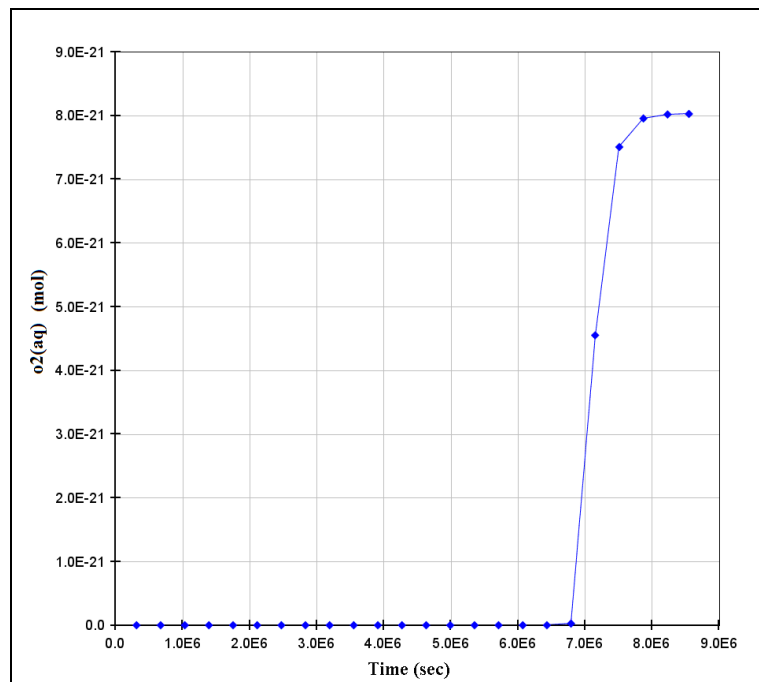


Figure L. 12 Time evolution of O₂(aq) during the 99 day-simulation

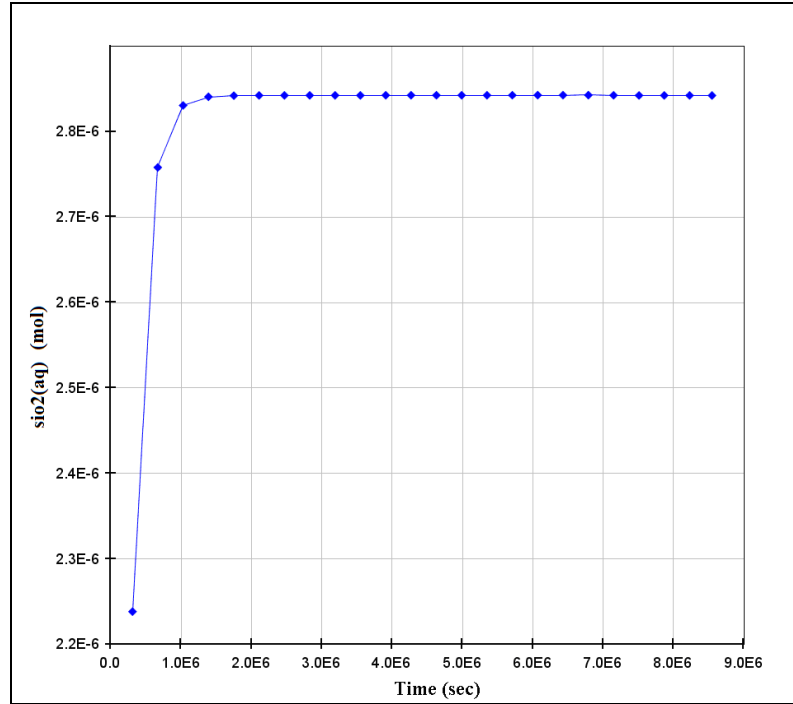


Figure L. 13 Time evolution of SiO₂(aq) during the 99 day-simulation

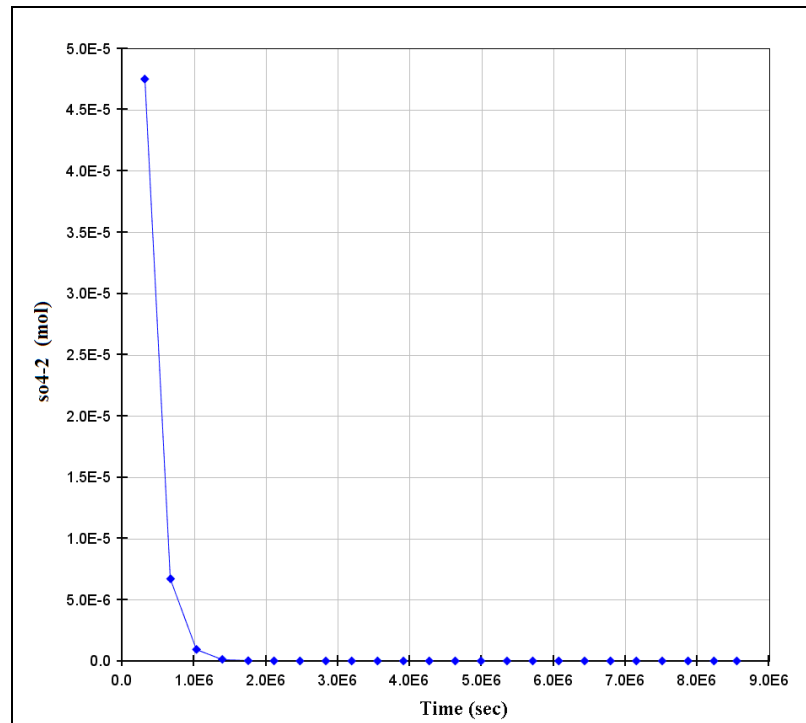


Figure L. 14 Time evolution of SO₄⁻² during the 99 day-simulation

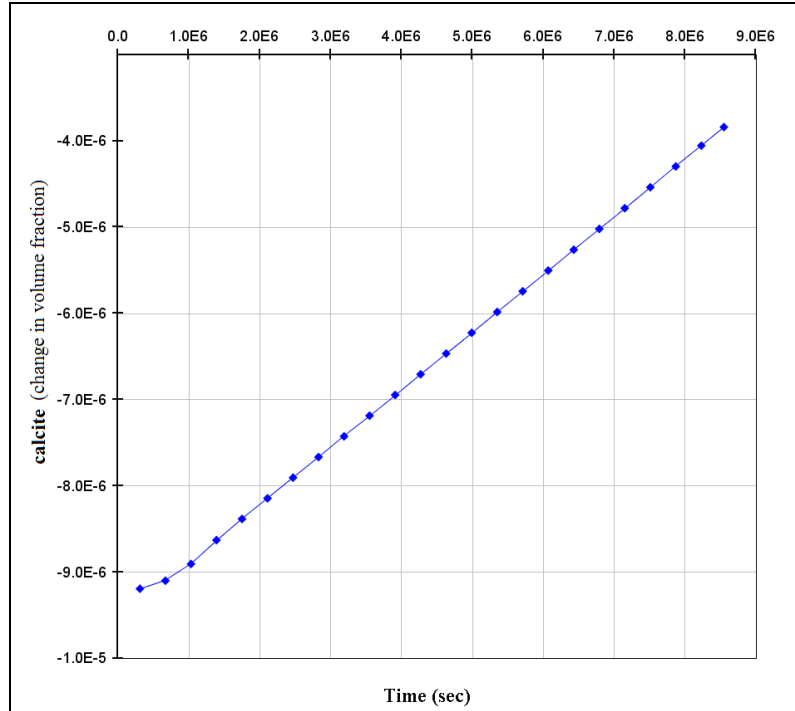


Figure L. 15 Variation in volume fraction of calcite during the 99 day-simulation

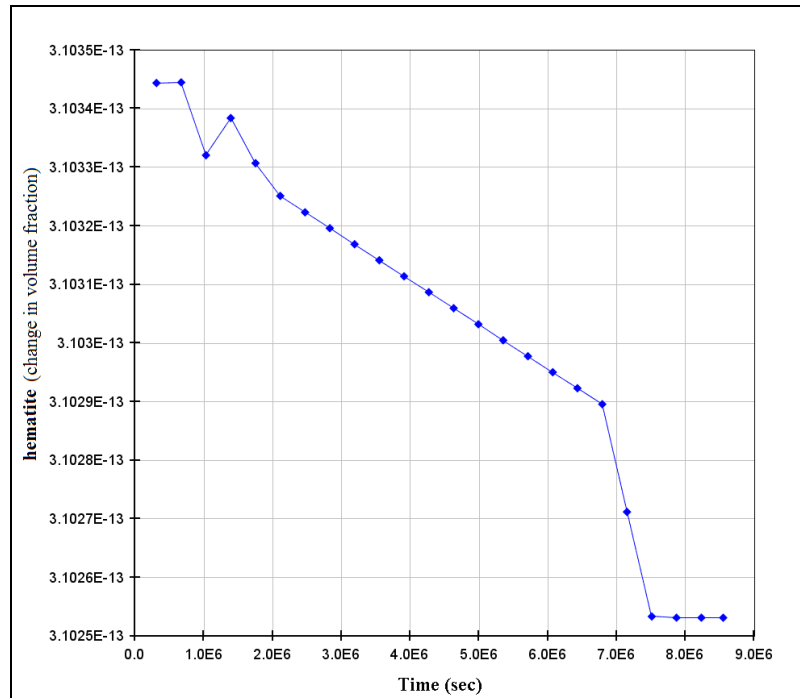


Figure L. 16 Variation in volume fraction of hematite during the 99 day-simulation

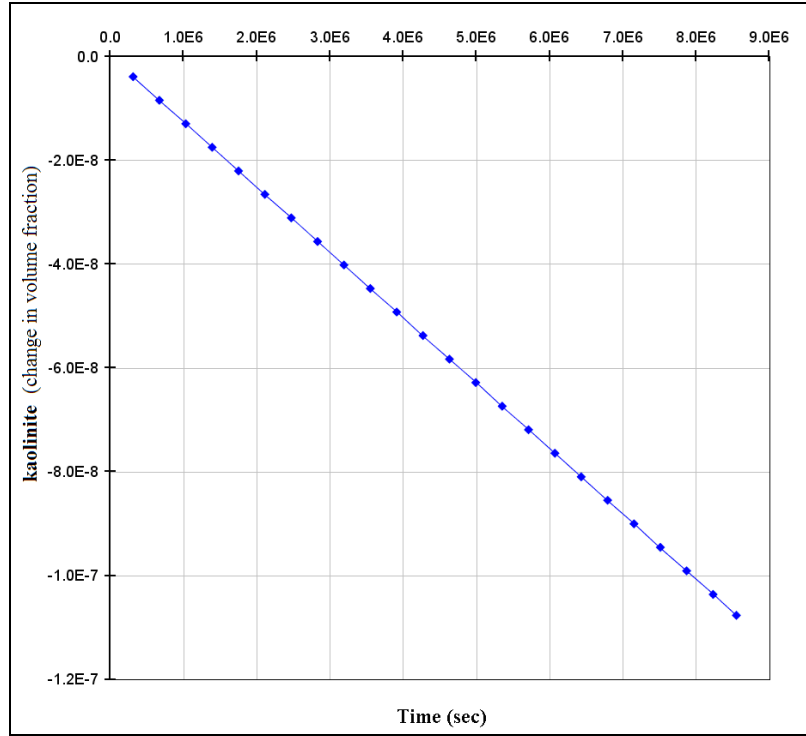


Figure L. 17 Variation in volume fraction of kaolinite during the 99 day-simulation

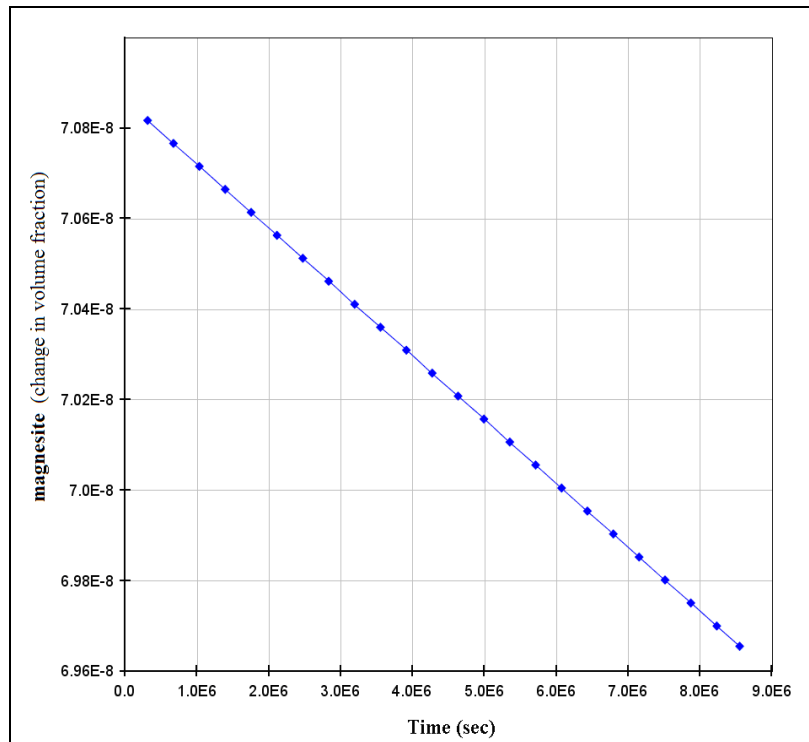


Figure L. 18 Variation in volume fraction of magnesite during the 99 day-simulation

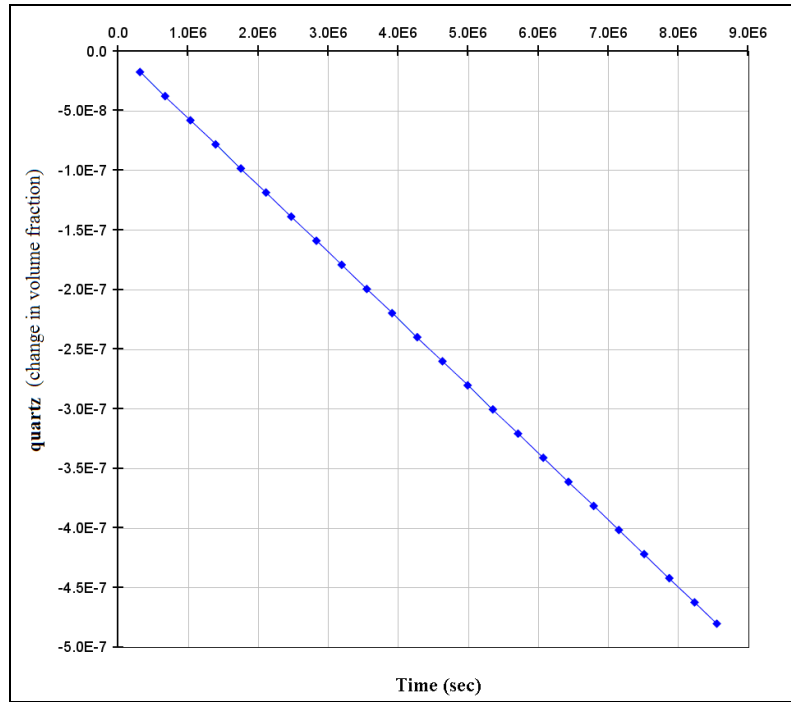


Figure L. 19 Variation in volume fraction of quartz during the 99 day-simulation

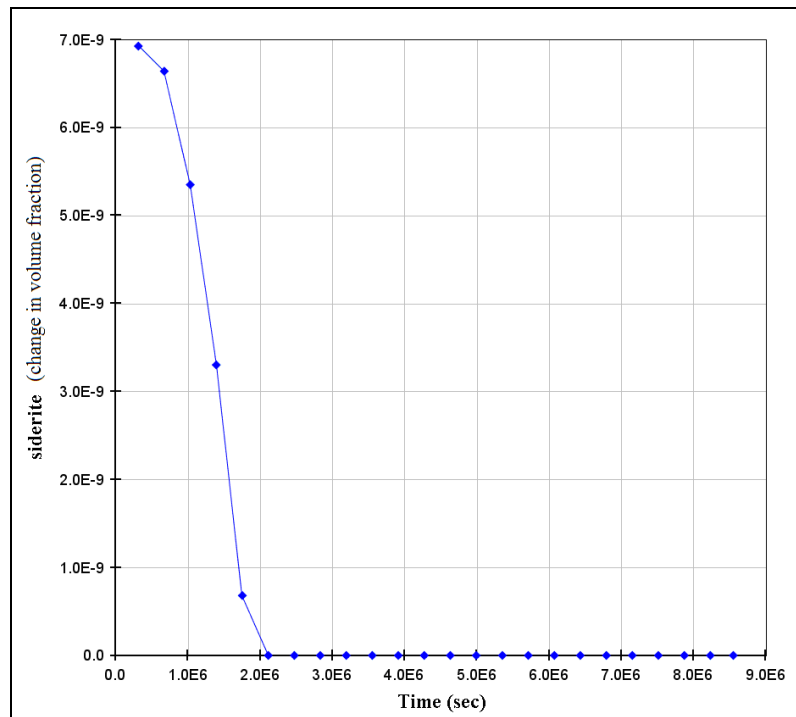


Figure L. 20 Variation in volume fraction of siderite during the 99 day-simulation

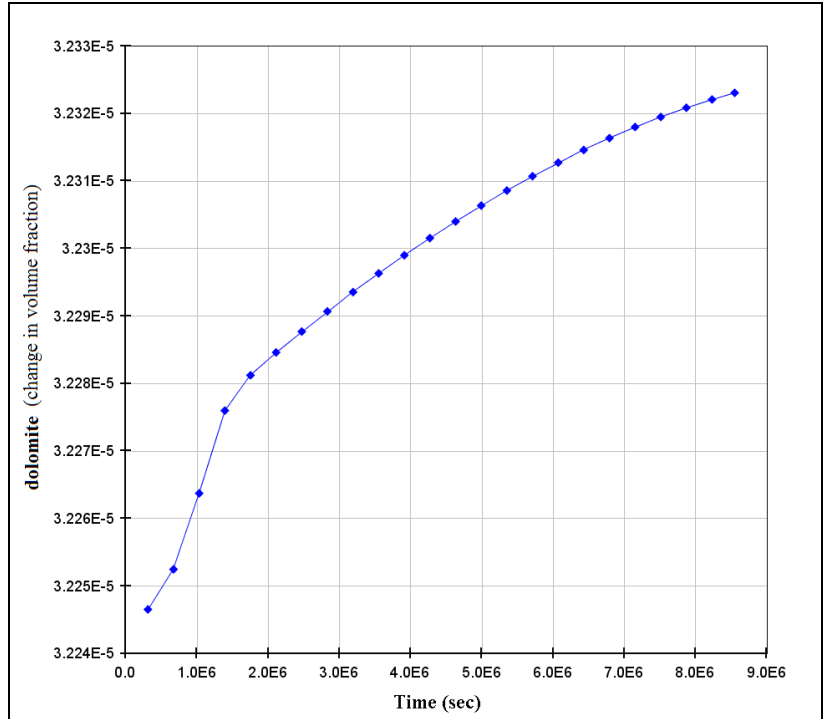


Figure L. 21 Variation in volume fraction of dolomite during the 99 day-simulation

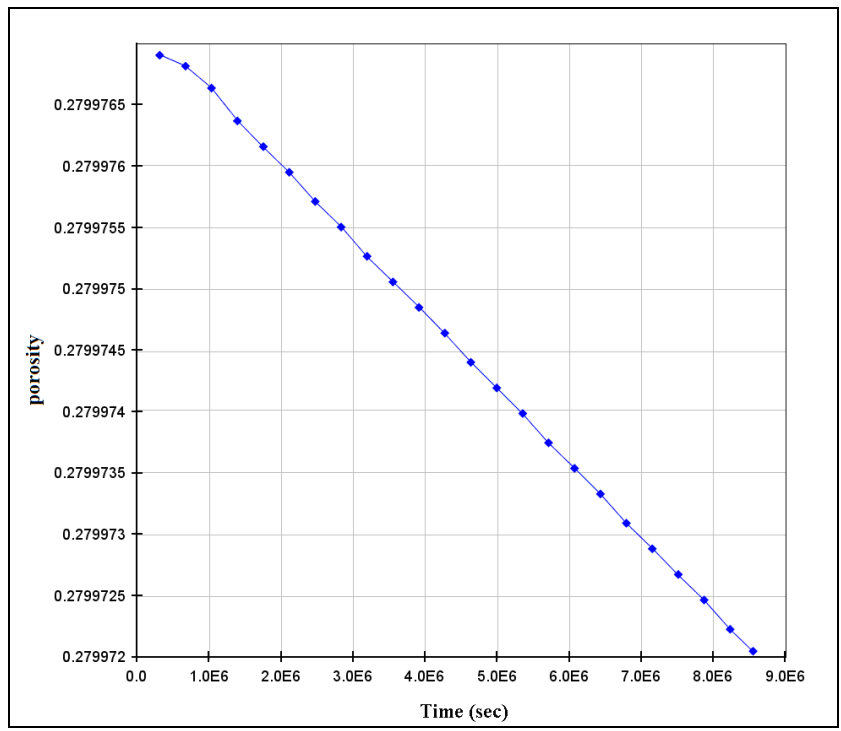


Figure L. 22 Time evolution of porosity during the 99 day-simulation

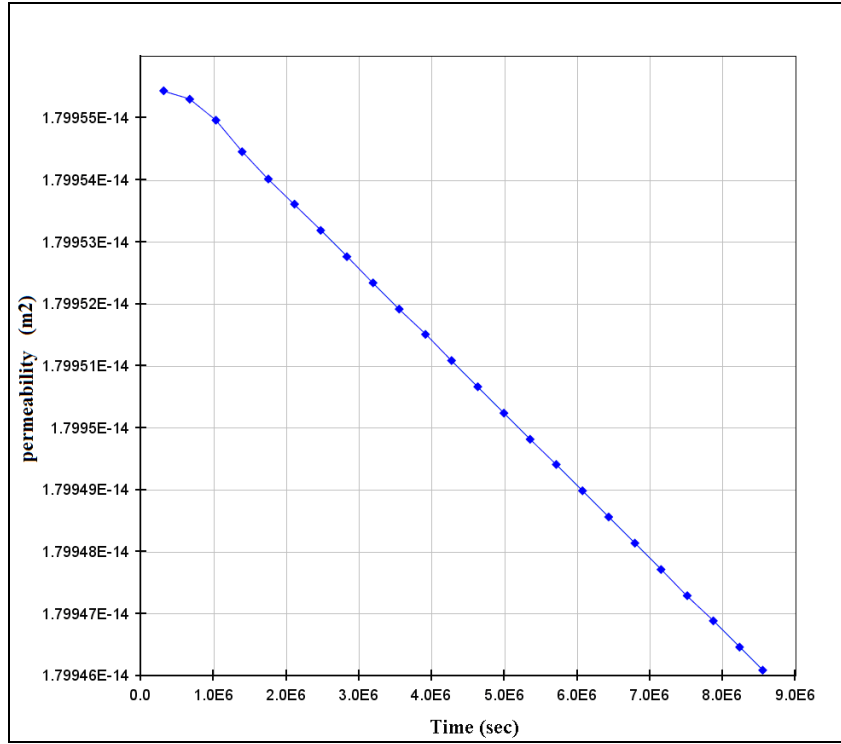


Figure L. 23 Time evolution of permeability during the 99 day-simulation

APPENDIX M

FORMULAS FOR POROSITY AND PERMEABILITY CALCULATIONS IN SIMULATION

Porosity changes are related to the volume changes as a result of mineral precipitation and dissolution, and these changes are taken into account in the calculations. The porosity of the medium is calculated as follows:

$$\phi = 1 - \sum_{m=1}^{nm} fr_m - fr_u$$

where “nm” is the number of minerals, and fr_m and fr_u are the volume fraction of mineral “m” in the rock and the volume fraction of nonreactive rock, respectively. The permeability changes associated with changes in porosity are calculated from the following simplified cubic law:

$$k = k_i * \left(\frac{\phi}{\phi_i} \right)$$

where k_i and ϕ_i are the initial permeability and porosity, respectively (Gherardi et al, 2007).

APPENDIX N

RESULTS OF THE SIMULATION OF 25 YEARS WITHOUT CO₂ INJECTION

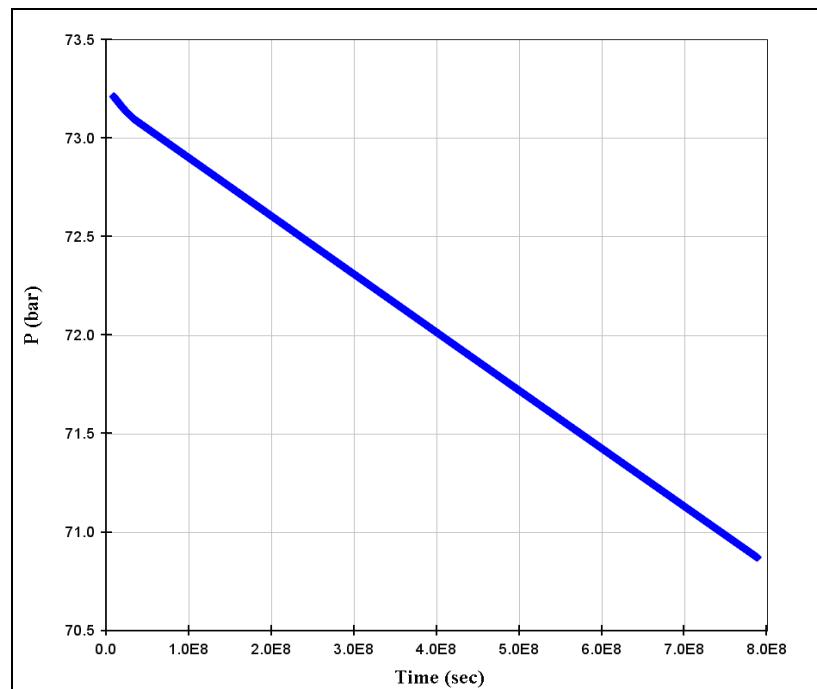


Figure N. 1 Time evolution of pressure during the 25 year-simulation

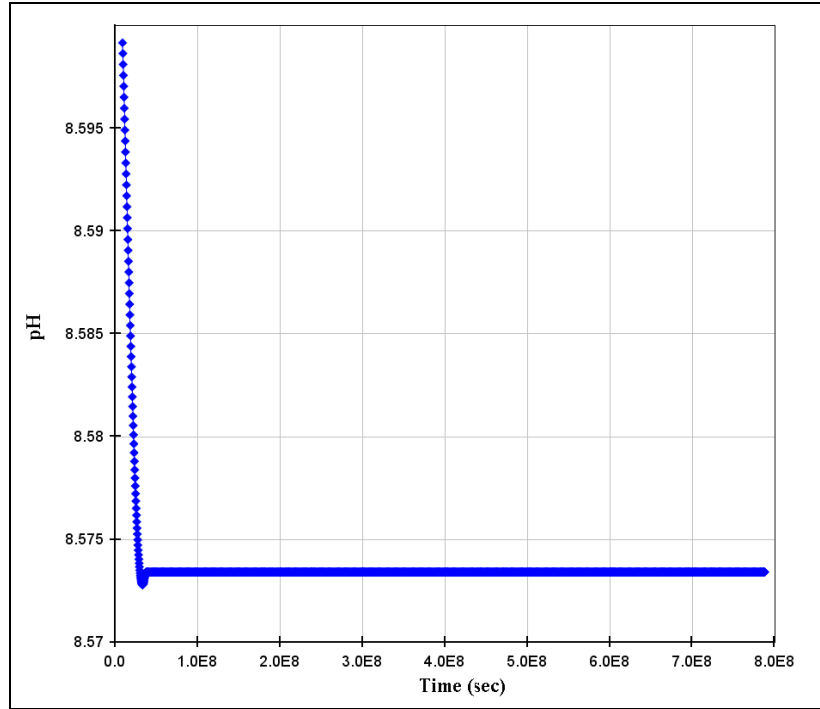


Figure N. 2 Time evolution of pH during the 25 year-simulation

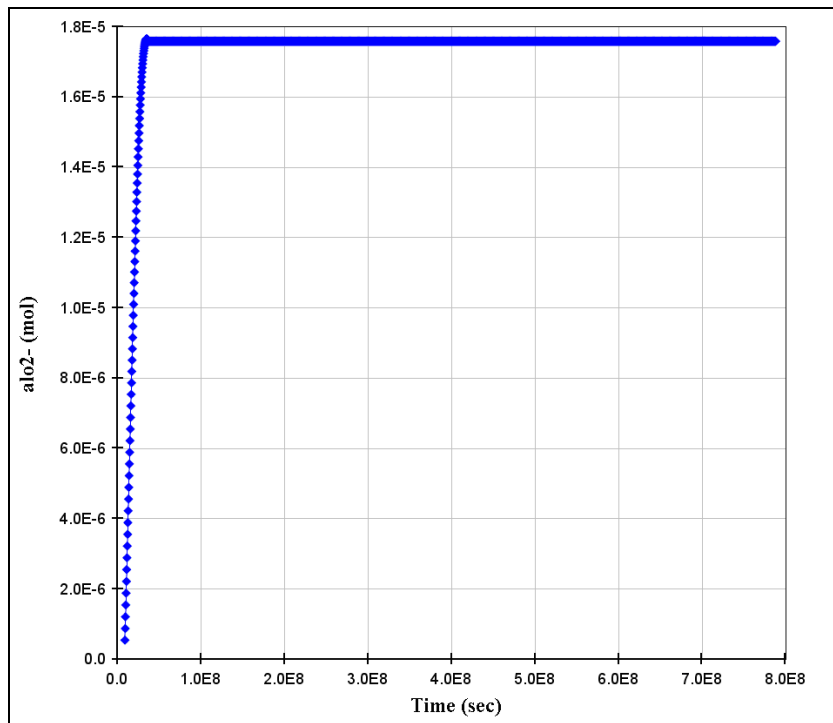


Figure N. 3 Time evolution of AlO₂⁻ during the 25 year-simulation

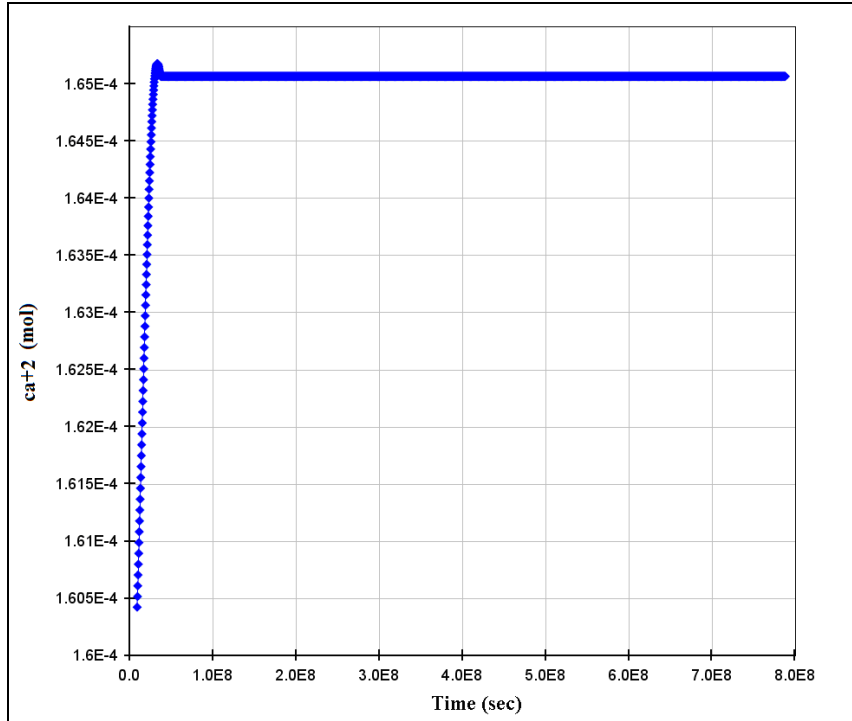


Figure N. 4 Time evolution of Ca^{+2} during the 25 year-simulation

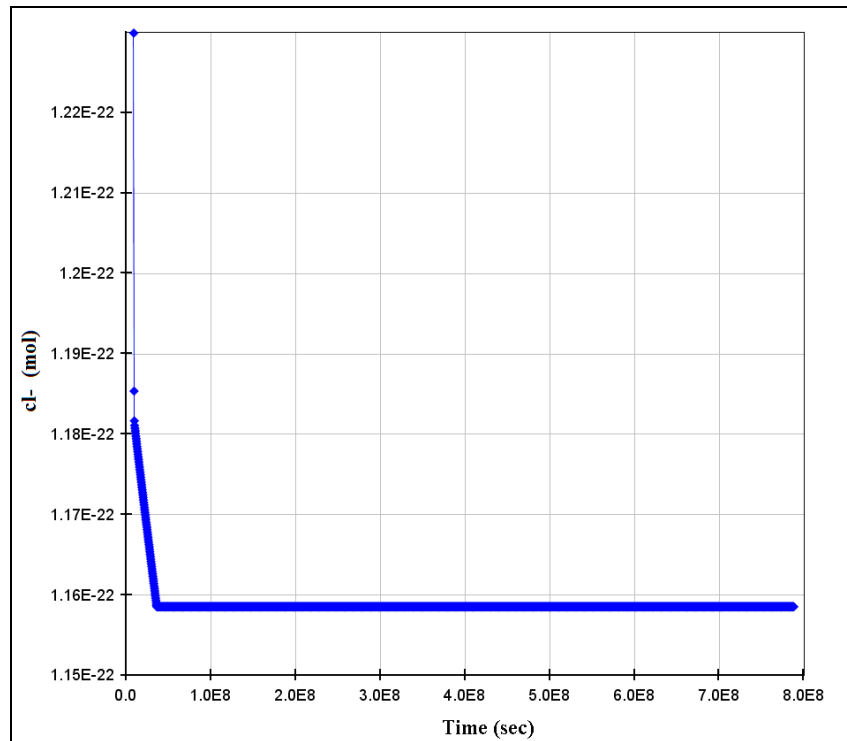


Figure N. 5 Time evolution of Cl^- during the 25 year-simulation

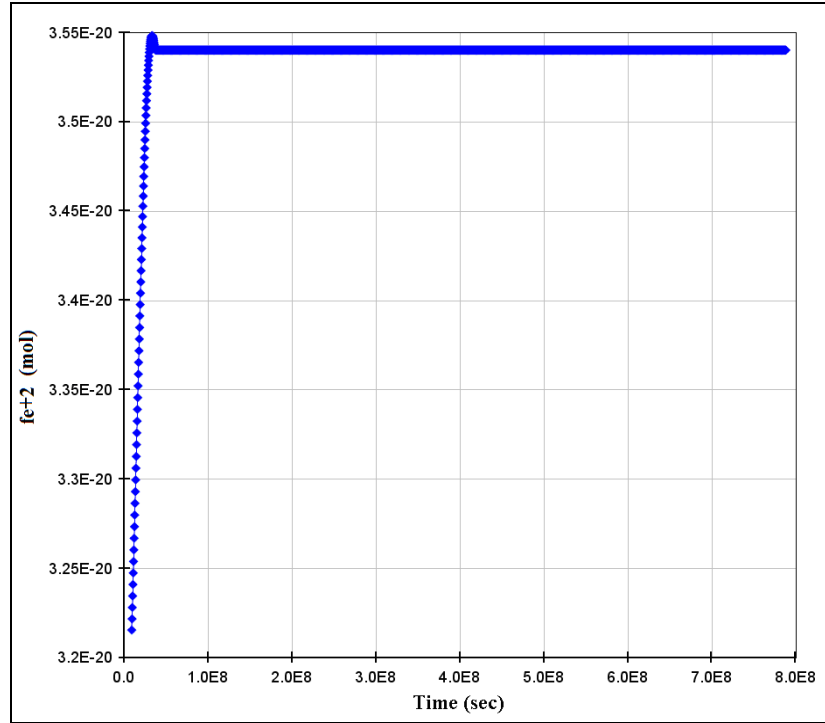


Figure N. 6 Time evolution of Fe^{+2} during the 25 year-simulation

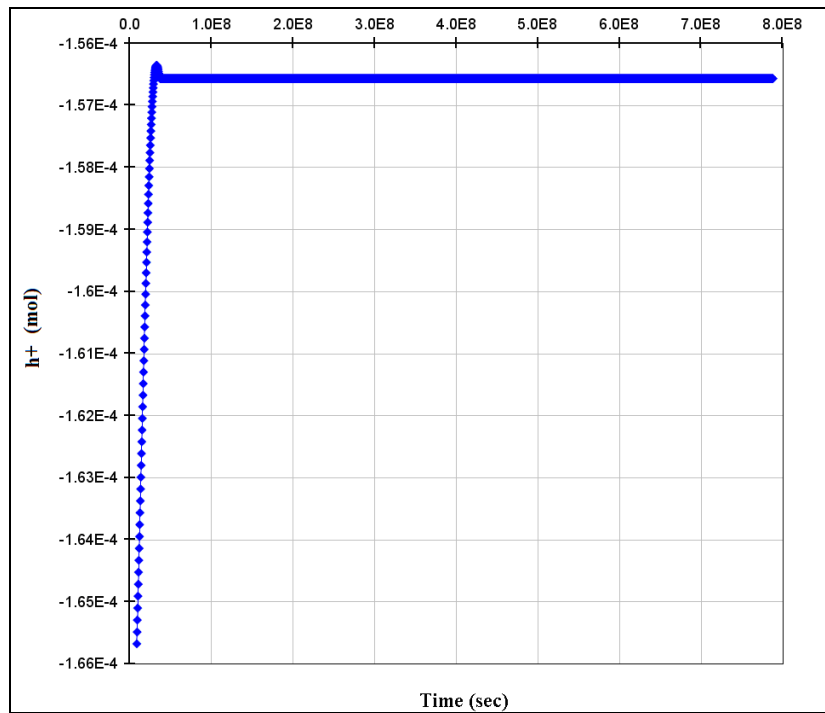


Figure N. 7 Time evolution of H^{+} during the 25 year-simulation

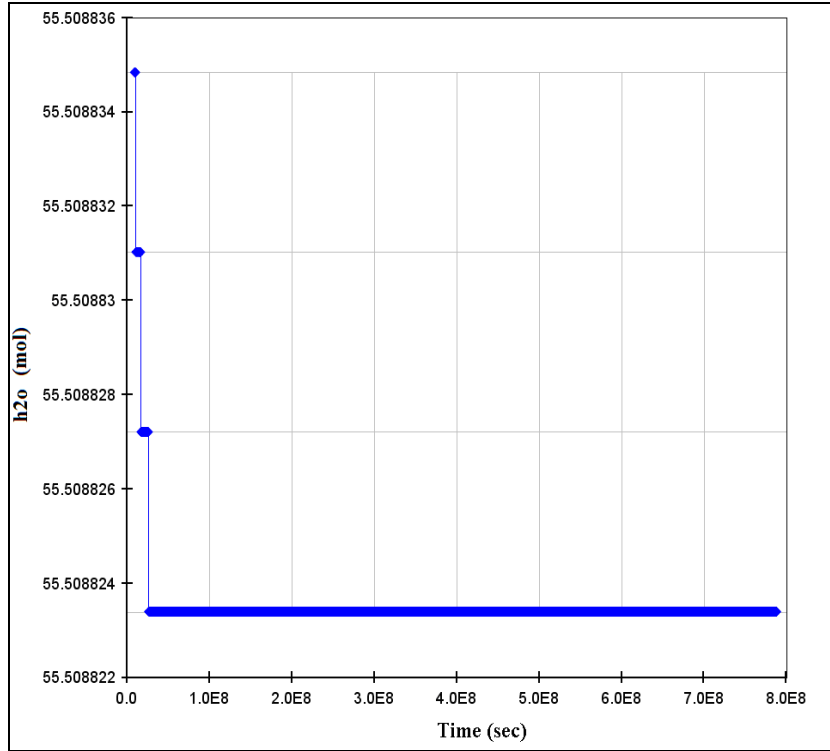


Figure N. 8 Time evolution of H₂O during the 25 year-simulation

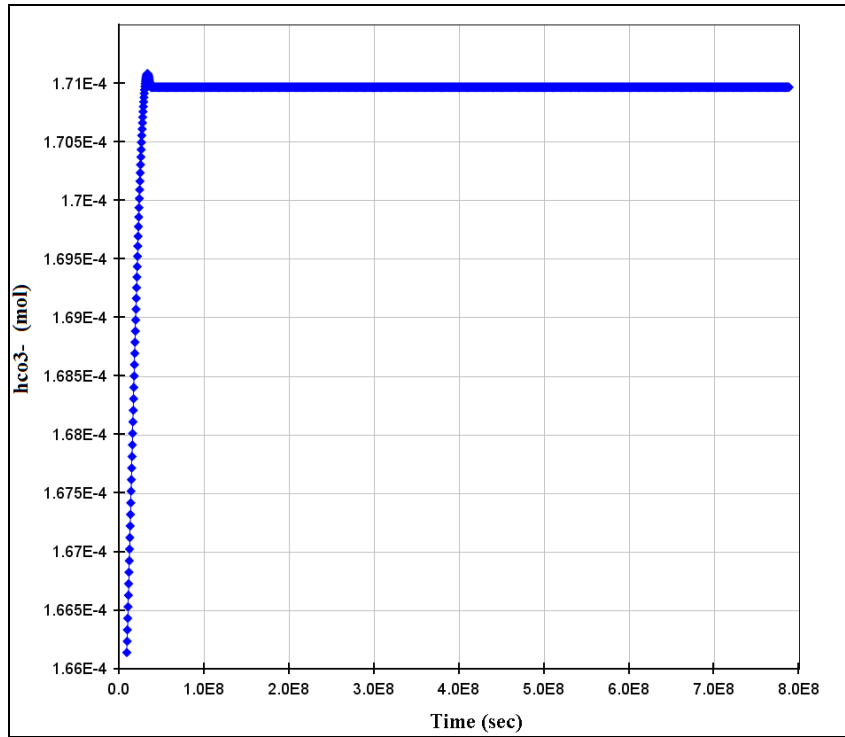


Figure N. 9 Time evolution of HCO₃⁻ during the 25 year-simulation

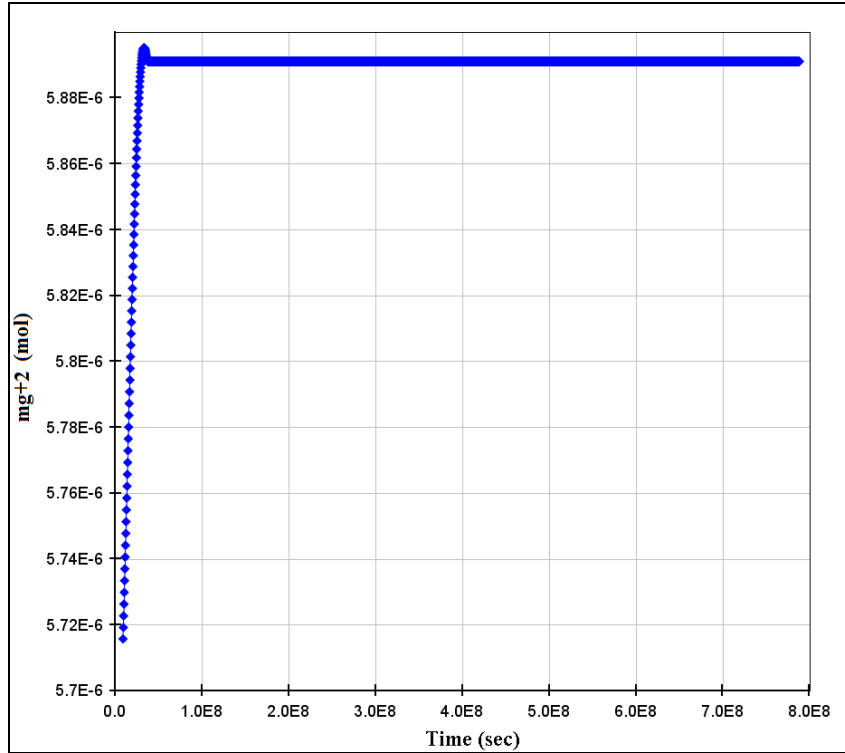


Figure N. 10 Time evolution of Mg^{+2} during the 25 year-simulation

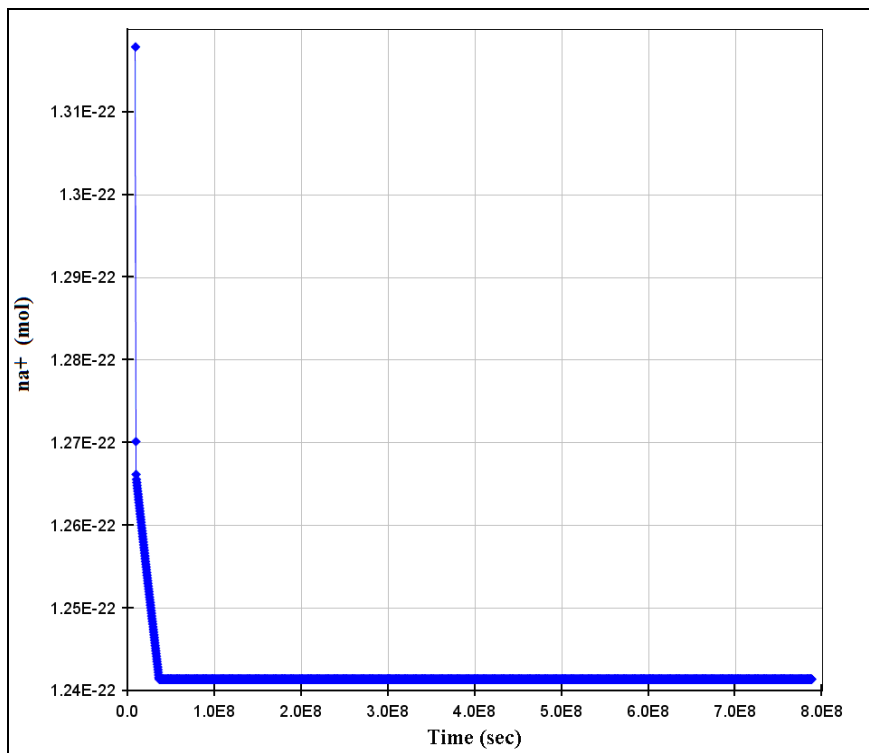


Figure N. 11 Time evolution of Na^{+} during the 25 year-simulation

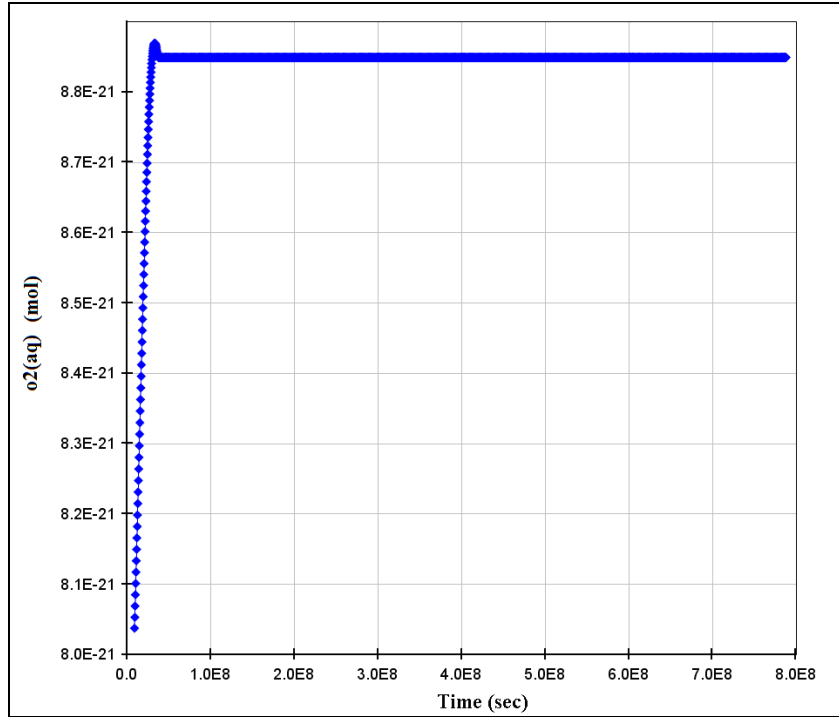


Figure N. 12 Time evolution of $O_2(aq)$ during the 25 year-simulation

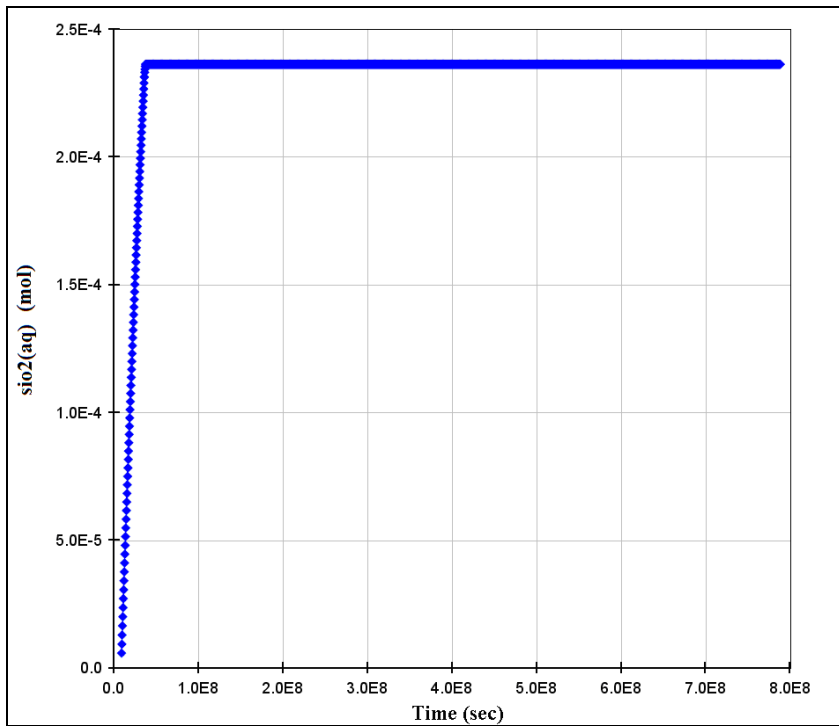


Figure N. 13 Time evolution of $SiO_2(aq)$ during the 25 year-simulation

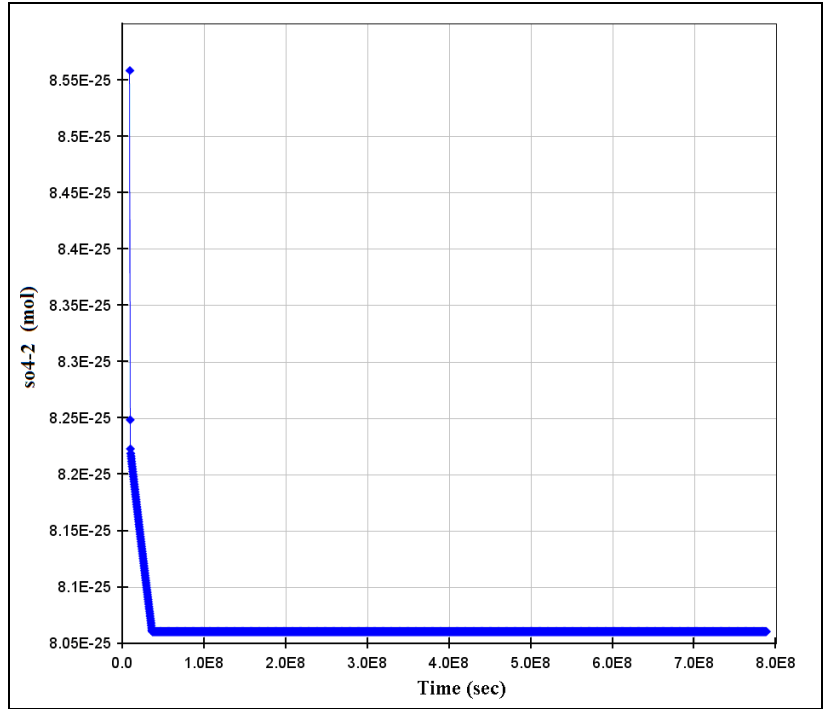


Figure N. 14 Time evolution of SO_4^{2-} during the 25 year-simulation

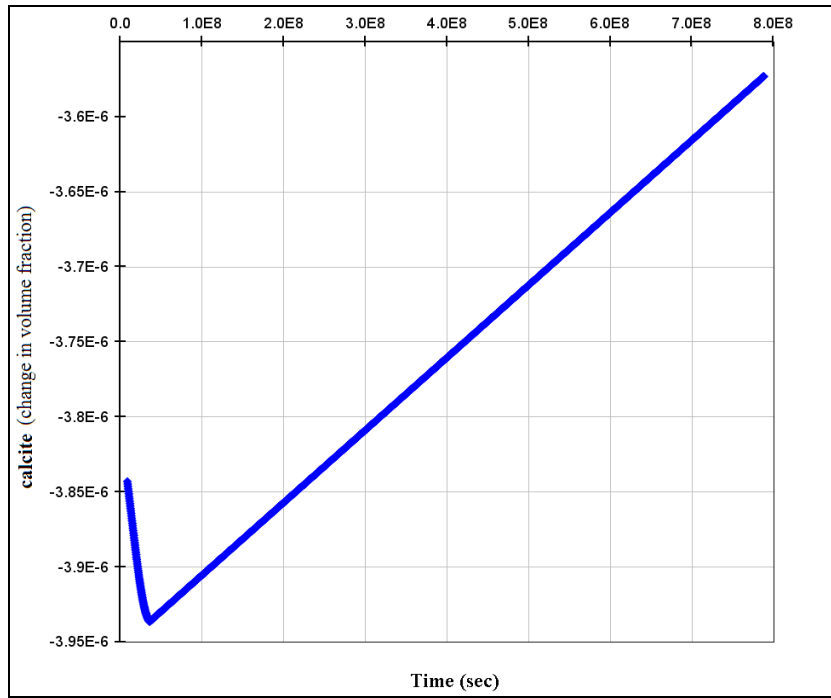


Figure N. 15 Variation in volume fraction of calcite during the 25 year-simulation

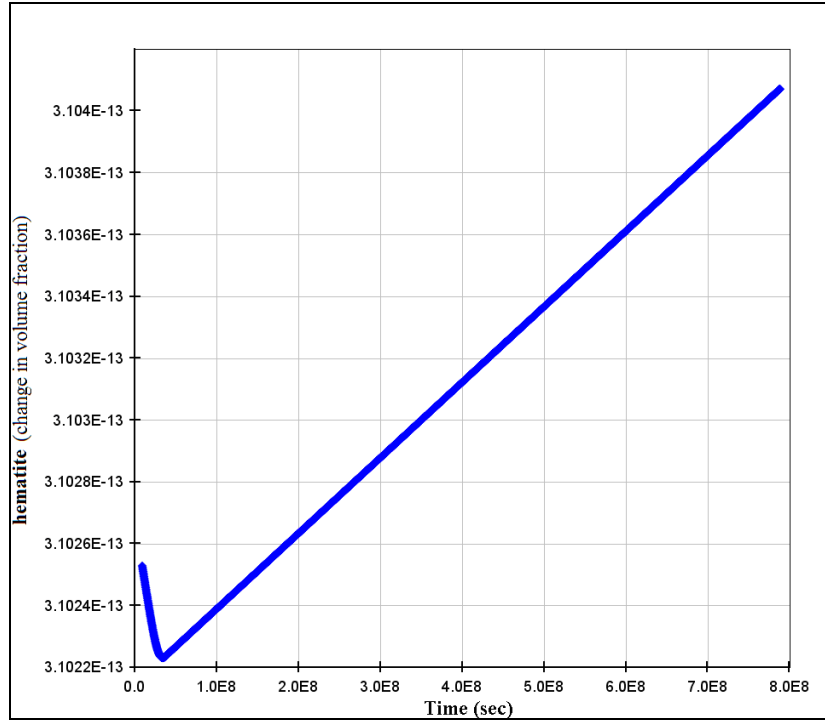


Figure N. 16 Variation in volume fraction of hematite during the 25 year-simulation

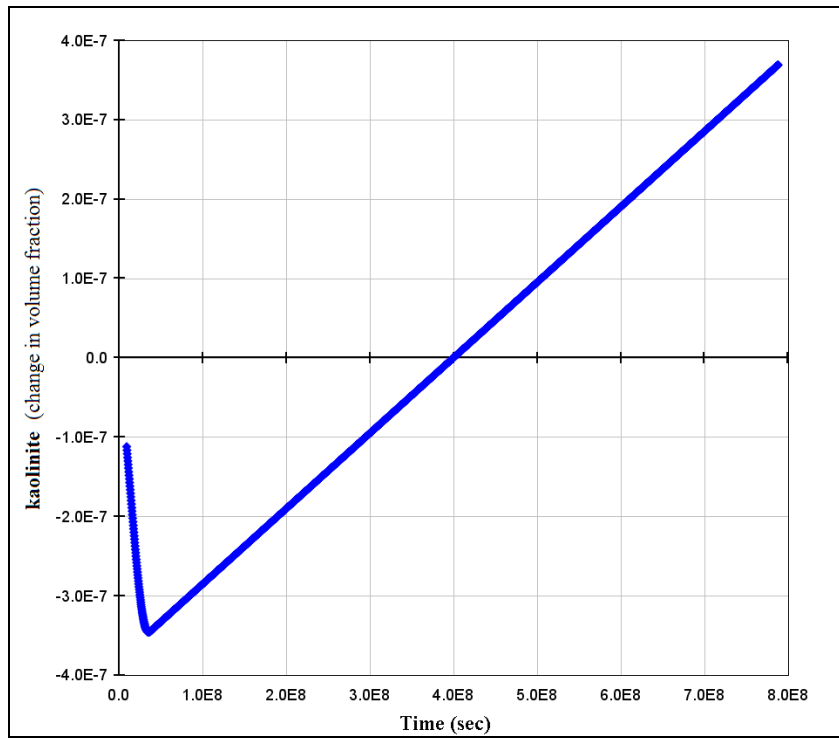


Figure N. 17 Variation in volume fraction of kaolinite during the 25 year-simulation

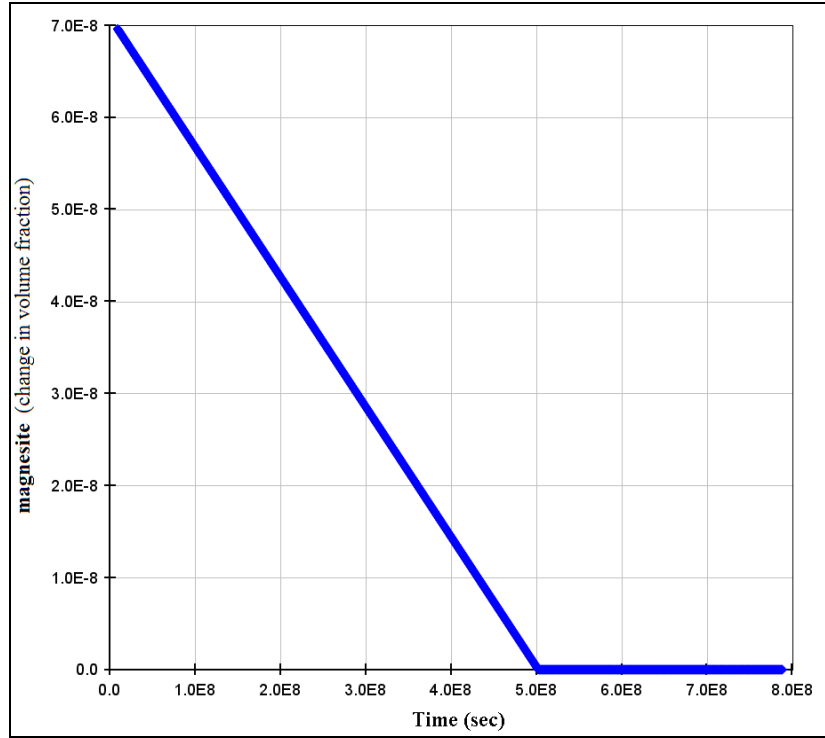


Figure N. 18 Variation in volume fraction of magnesite during the 25 year-simulation

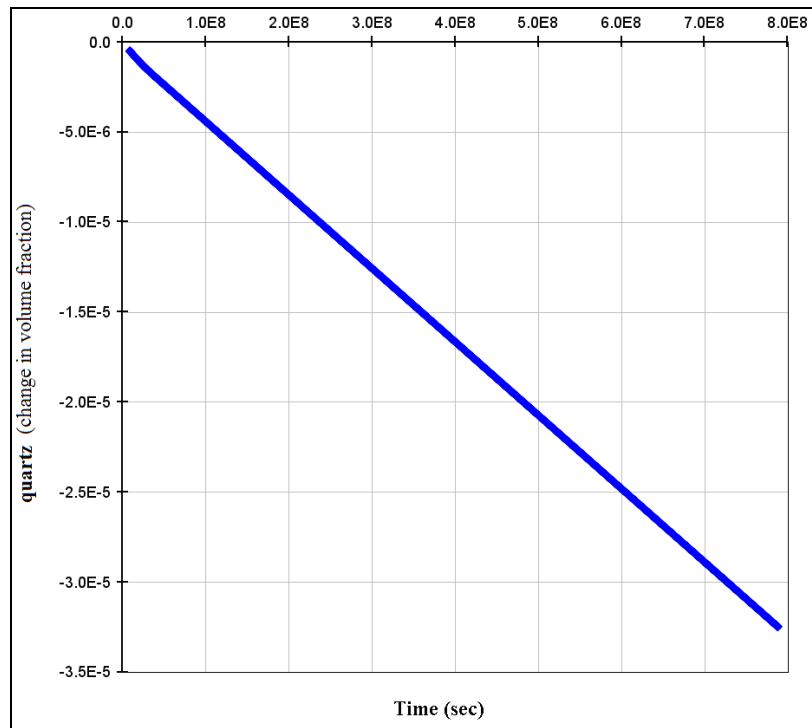


Figure N. 19 Variation in volume fraction of quartz during the 25 year-simulation

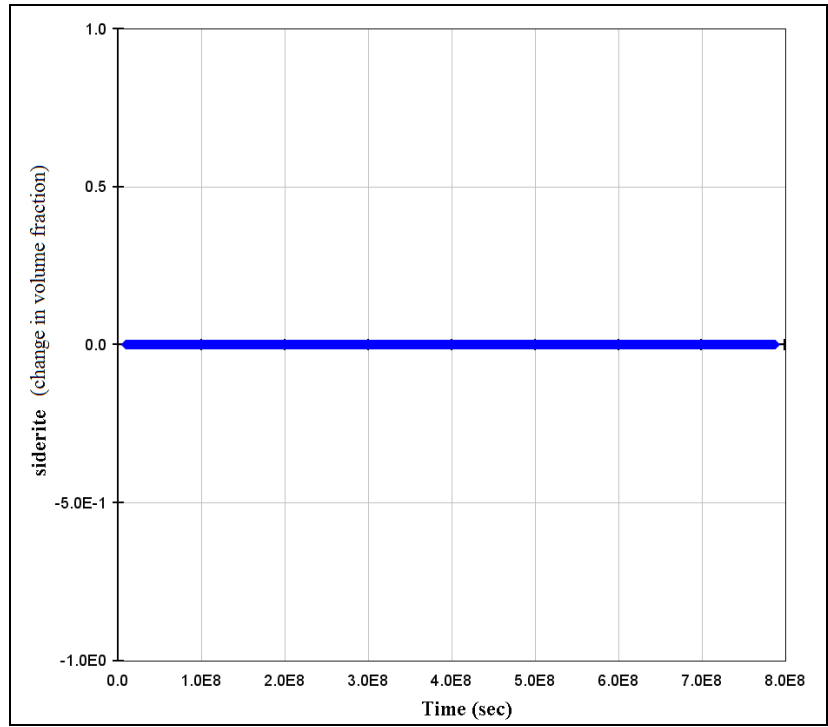


Figure N. 20 Variation in volume fraction of siderite during the 25 year-simulation

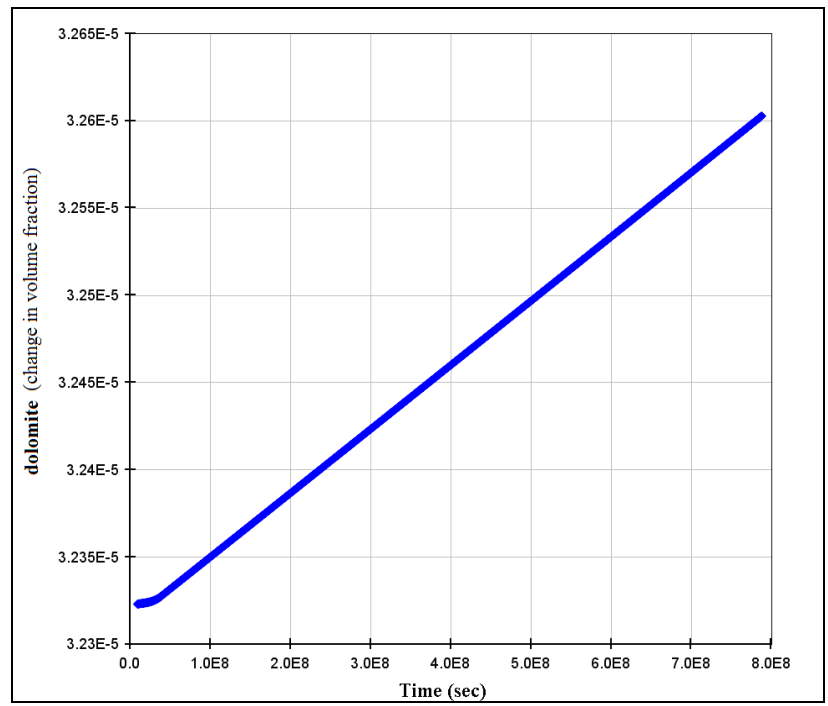


Figure N. 21 Variation in volume fraction of dolomite during the 25 year-simulation

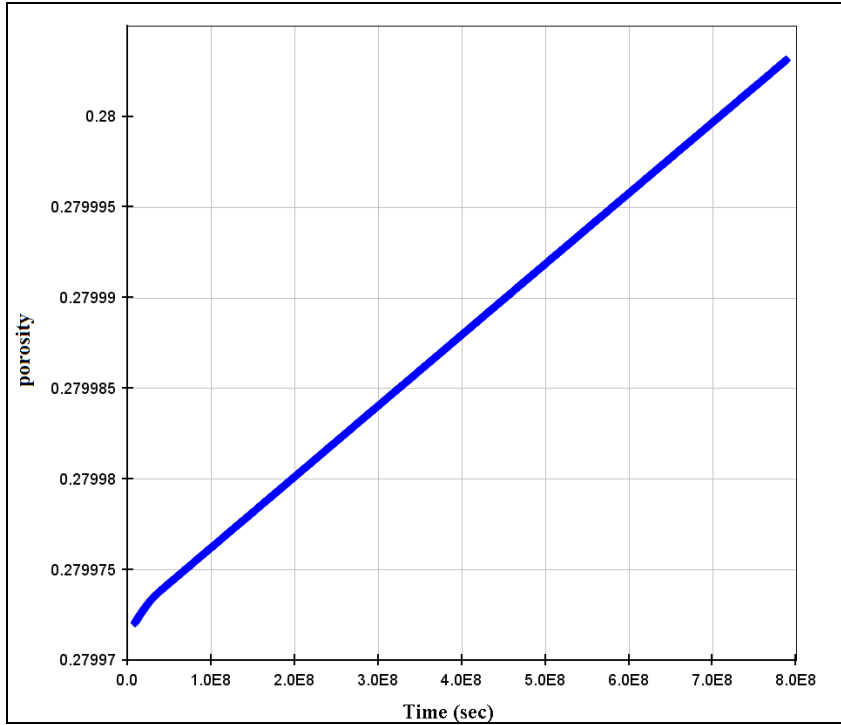


Figure N. 22 Time evolution of porosity during the 25 year-simulation

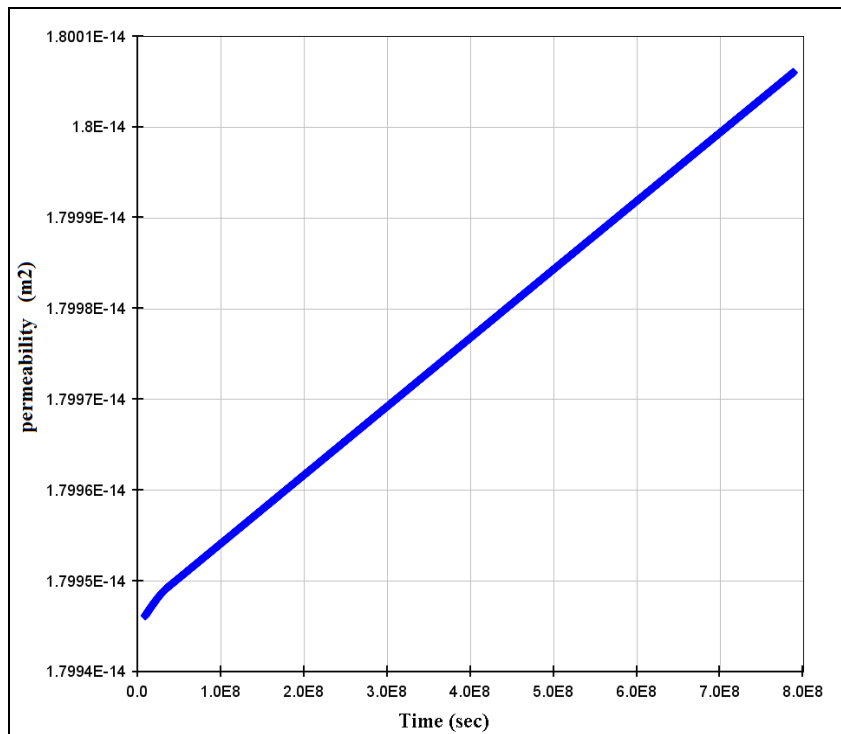


Figure N. 23 Time evolution of permeability during the 25 year-simulation

CURRICULUM VITAE

CHANTSALMAA DALKHAA

Department of Petroleum & Natural Gas Engineering
Middle East Technical University
Inonu Bulvari, 06531, Ankara-Turkey

Tel:+90 535 817 9919
Email: dchantsa@gmail.com

PERSONAL DETAILS

Date & Place of Birth: 6th March 1980, Mongolia
Nationality: Mongolian
Marital Status: Single

EDUCATION

- ✓ 2006-present PhD, Middle East Technical University
Department of Petroleum & Natural Gas Engineering, Ankara./
TURKEY
- ✓ 2003- 2005 Msc, Middle East Technical University
Department of Petroleum & Natural Gas Engineering, Ankara./
TURKEY
- ✓ 1998- 2003 Bs, Middle East Technical University
Department of Petroleum & Natural Gas Engineering, Ankara/
TURKEY
- ✓ 1995-1998 High School 21, Mongolia.

WORK EXPERIENCE

- ✓ 2002 Intern at Perenco, European privately owned Oil
And Gas Exploration and Production Company. Ankara/ TURKEY.
- ✓ 2001 Intern at Turkish Petroleum Cooperation. Adiyaman/ TURKEY

ASSISTED COURSES

- ✓ Pete 352, Well Logging (2007- 2010)
- ✓ Pete 411, Petroleum Property Valuation (2007- 2010)

PROJECTS

- ✓ “Evaluation of CO₂ Emission From Industrial Sectors in Turkey and Determination of Possible CO₂ Storage Sites in Turkey and Modeling & Simulation of CO₂ Sequestration in an Oil Field in Turkey”- funded by the Scientific & Technological Research Council of Turkey (2007- 2009)

THESIS

- ✓ Msc Thesis: Study of Water Saturation Models in Non- Archie Porous Media (2003- 2005)
- ✓ PhD Thesis: Cap rock integrity in CO₂ Storage (2006- 2010)

AWARDS

- ✓ 2003-2004 Graduate Course Performance Award at Middle East Technical University
- ✓ MSc fellowship of Ministry of National Education of Turkey
- ✓ Phd fellowship of the Scientific and Technological Research Council of Turkey

FIELD OF INTEREST

carbon capture and storage, water-rock interaction, geochemical and reactive transport modeling and simulation, coalbed methane gas recovery, reservoir characterization and simulation, fluid flow through porous media, remote Sensing

COMPUTER SKILL

MapInfo and ArcGis, Petrel, Visual C++, Matlab, Tough2, ToughReact, PetraSim, Phreeqc

INTERNATIONAL CONFERENCE & SUMMER SCHOOL

- ✓ 2nd EAGE CO₂ Geological Storage Workshop, 11-12 March 2010, Berlin-Germany
- ✓ Summer School CO₂ReMoVe, 11-16 July 2010, London-UK

- ✓ International Interdisciplinary CCS Summer School, 21-28 August 2010, Svalbard- Norway
- ✓ GHGT 10 International Conference on Greenhouse Gas Control Technologies 19-23 September, Amsterdam-Holland

LANGUAGE SKILLS

- ✓ Mongolian: native, English: advanced, Turkish: advanced, French: intermediate

HOBBIES

- ✓ Books, Tennis, Photography

MEMBERSHIP

- ✓ Member of Society of Petroleum Engineers (SPE)
- ✓ Member of European Association of Geoscientist and Engineers (EAGE)